Wind Turbine Adaptive Blade Integrated Design and Analysis

HUI ZHANG

A Thesis Submitted in Partial Fulfilment of the Requirements of the University of Northumbria at Newcastle for the Degree of Doctor of Philosophy

A Research Undertaken in the Faculty of Engineering and Environment

October 2013

Declaration

I declare that the work contained in this thesis has not been submitted for any other award and that it is all my own work. I also confirm that this work fully acknowledges opinions, ideas and contributions from the work of others.

Name: Hui Zhang

Signature:

Date: 30 October 2013

Abstract

This project aims to develop efficient and robust tools for optimal design of wind turbine adaptive blades. In general, wind turbine adaptive blade design is an aero-structure coupled design process, in which, the evaluation of aerodynamic performance cannot be carried out precisely without structural deformation analysis of the adaptive blade. However, employing finite element analysis (FEA) based structural analysis commercial packages as part of the aerodynamic objective evaluation process has been proven time consuming and it results in inefficient and redundant design optimisation of adaptive blades caused by elastic-coupled (bend-twist or stretch-twist) iteration. In order to achieve the goal of wind turbine adaptive blade integrated design and analysis, this project is carried out from three aspects. Firstly, a general geometrically linear model for thin-walled composite beams with multi-cell, non-uniform cross-section and arbitrary lay-ups under various types of loadings is developed for implementing structural deformation analysis. After that, this model is validated by a simple box-beam, single- and multi-cell wind turbine blades. Through validation, it denotes that this thin-walled composite beam model is efficient and accurate for predicting the structural deformations compared to FEA based commercial packages (ANSYS). This developed beam model thus provides more probabilities for further investigations of dynamic performance of adaptive blades. Secondly in order to investigate the effects of aero elastic tailoring and implanting elastic coupling on aerodynamic performance of adaptive blades, auxiliary software tools with graphical interfaces are developed via MATLAB codes. Structural/material characteristics and configurations of adaptive blades (i.e. elastic coupling topology, layup configuration and material properties of blade) are defined by these auxiliary software tools. By interfacing these software tools to the structural analysers based on the developed thin-walled composite beam model to an aerodynamic performance evaluator, an integrated design environment is developed. Lastly, by using the developed thin-walled composite beam model as a search platform, the application of the decoupled design method, a method of

design of smart aero-structures based on the concept of variable state design parameter, is also extended.

Acknowledgements

Firstly, I would like to express my sincere gratitude and appreciations to my principal supervisor Dr. Alireza Maheri for his conscientious, generous guidance and support throughout my three-year postgraduate programme.

Secondly, I would also like to extend my appreciation to the second and third supervisors Dr. Ali Daadbin and Dr. Phil Hackney and other colleagues who gave me great help in the past three years.

Thirdly, I would sincerely thank the Faculty of Engineering and Environment at Northumbria University and Synchron Technology LTD of UK for financial support of this project.

Fourthly, I would also like to extend my deepest gratitude to my wife Mrs. Lu Wang for her continuous support, encouragement, love and care in all aspects of my life. Without her encouragement in the pasted three years, I would not finish my project on time.

Last but not the least I am grateful to my mother-in-law Gui Zhi Zhang and my parents for their love, companionship and support spiritually throughout my three-year research.

Table of Contents

List of Figures

List of Tables

Nomenclature

C	Blade chord length
$[C_{ij}]$	Stiffness matrix under principle coordinate system
$[\overline{C}_{ij}]$	Stiffness matrix
$[\widetilde{C}_{ij}]$	Reduced stiffness matrix
$\vec{e}_n$, $\vec{e}_t$	Unit vectors along n- and s-direction
F_z, Q_x, Q_y	Resultant forces
E_{11}, E_{22}, E_{33}	Young's moduli under principal coordinate system
$\widetilde{G}$	Conveniently chosen shear modulus
G_{12}, G_{13}, G_{23}	Shear moduli under principal coordinate system
G_{sz}	Shear modulus under $s-z-n$
h	Thickness of the shell
$\widetilde{h}(s)$	Modulus-weighted thickness
$\vec{i}$, $\vec{j}$	Unit vectors in x- and y-axis
$[K_{ij}]$	Stiffness of beam cross-section
M_x, M_y, M_z	Resultant moments
N	The number of cell for multi-cell beams
o_p	Origin of plane system of coordinates $(x_p - y_p - z_p)$
O_g	Origin of global system of coordinates $(X_g - Y_g - Z_g)$
P_i	The i^{th} patch on the beam
$pitch$	Pitch angle
q_{ij}	Shear flow in common wall between i^{th} and j^{th} cell
q_R	Shear flow in R^{th} cell
r	Radius of blade
$\vec{r}$	The position vector of general point on the middle surface
$\vec{R}$	The position vector of general point off the middle surface

R_{hub}	Radius of hub
R_{rotor}	Radius of rotor
$(s-z-n)$	System of coordinates $(s-z-n)$
s_0	Origin of coordinate of s
$span$	Length of the blade
S	The coordinate of s off the centre line
S_0	Origin of S
$[s]$	Flexibility matrix
$[S]$	Compliance matrix
t	Time
t_{aero}	Thickness at $x_{p,w}$ and y_p location
$[T(\theta)]$	Transformation tensor of stress
$[\tilde{T}(\theta)]$	Transformation tensor of strain
u , v , w	Displacements of a general point on cross-section
U_n, U_t	Displacement components
V_w, V_{rel}	Wind velocity and relative wind velocity
w_0	The longitudinal displacement of origin of s
W	Displacement along z-axis of point off the centre line
W_0	The longitudinal displacement of origin s off the centre line
$(x-y-z)$	Global coordinates system
$(x_l-y_l-z_l)$	Local coordinates system
(x_{pole}, y_{pole})	Coordinates of pole
$(x_p-y_p-z_p)$	Plane coordinates system of patches
$(X_g-Y_g-Z_g)$	Global coordinates system of patches
$x_{p,w}$	x-coordinate of the web under $(x_p-y_p-z_p)$
x_{twist}	Distance from leading edge to the origin of local coordinated system
$z_{lower\ surface}$	z-coordinate at lower surface $x_{p,w}$ and y_p location

Greek Symbols

α	Angle of attack
β	Total twist
β_e	Elastic twist
β_0	Pre-twist
β_p	Perimeter enclosed by the centre line of the beam cross section
γ_{yz}, γ_{xz}	Shear strains under $x-y-z$
γ_{zn}, γ_{sz}	Shear strains under $s-z-n$
γ_{sz}^{i}	Shear strain of i^{th} cell
$\gamma_{sz}^{i,j}$	Shear strain at common shell between i^{th} and j^{th} cell
ε_{zz}	Normal strain of general point on beam cross-section
θ	Fibre angle
θ_x , θ_y	Rotation angle along x and y-axis
$\sigma_{ss}, \sigma_{zz}, \sigma_{nn}$	Normal stresses under $s-z-n$
$\tau_{zs}, \tau_{ns}, \tau_{sz}$	Shear stresses under $s-z-n$
$\nu_{12}, \nu_{13}, \nu_{23}$	Poisson ratios of orthotropic material
ϕ	Rotation angle along z-axis of blade
φ	Inflow angle
ω	Angular velocity of blade rotor
Ω	Area inside the centreline of the cross-section for single cell beam
Ω_R	Area inside the centreline of the R^{th} cell

Subscripts

$aero$	Aero
hub	Hub of the rotor blade
$rotor$	Rotor
$lower\ surface$	Lower surface
$pole$	Pole

1 Introduction

1.1 Structure of the Thesis

This thesis consists of five chapters. Chapter 1 is devoted to the background review of power and load control system of wind turbines; particularly it describes the adaptive blade at various aspects from the concept, history of development, aerodynamic performance analysis, and potentials in enhancing energy output, potentials in blade load alleviation, manufacturing and design. Chapter 2 starts with a comprehensive literature review on thin-walled composite beam models, and then describes the development of a general thin-walled composite beam model; lastly, proposed beam model is validated through a simple box-beam, single- and multi-cells adaptive blades. Chapter 3 describes three auxiliary software tools with graphical interfaces developed by MATLAB$^{@}$ for defining structural/material characteristics and configurations of adaptive blades (i.e. elastic coupling topology, layup configuration, material properties of adaptive blades and simulation of elastic coupling induced twist). Chapter 4 starts with describing the decoupled design method of adaptive blades developed by other authors and then it extends the application of this method to the general case of span wise varying structural characteristics. Chapter 5 summarises the research carried out, the results obtained and highlights the achievements, it also includes a section on the critical appraisal of the work and suggestions for future work.

1.2 Power and Load Control in Wind Turbines

Wind turbines are designed to extract energy with highest efficiency. However, one of the basic requirements for wind turbines is to have a control mechanism in place to ensure: (i) that the rotor does not produce power excess to the rated value for a safe operation of the generator, and (ii) that the aerodynamic load on the blade does not exceed the design load. Power and load control systems used in wind turbines can be classified as conventional and nonconventional. Figure (1.1) shows various power/load control systems.

The simplest conventional control method is stall regulation that uses the characteristics of the aerofoils (such as the difference of the coefficient of lift or drag at various angle of attack) to stall in high winds and regulate the power production of the rotor. Stall regulation is mechanically the simplest power

control method because it does not use any active or moving mechanical parts. The pitch of each blade is adjusted only once when the wind turbine is erected. In order to achieve power control at appropriate wind speeds, the wind turbine blades should operate closer to stall angle. This method is suitable for constant speed rotors. Stall controlled rotors become popular in 1980s and 1990s with the advent of designer aerofoils (Klimas, 1984; Tangler & Somers, 1995) that enhance the stall regulation of a wind turbine at lower power levels with the associated reduced cost of produced energy. These aerofoils have been quite successful in reducing the maximum power output allowing the rotor diameter to be increased without increasing plant capacity. The larger rotor then produces more net energy without proportional increases in system cost.

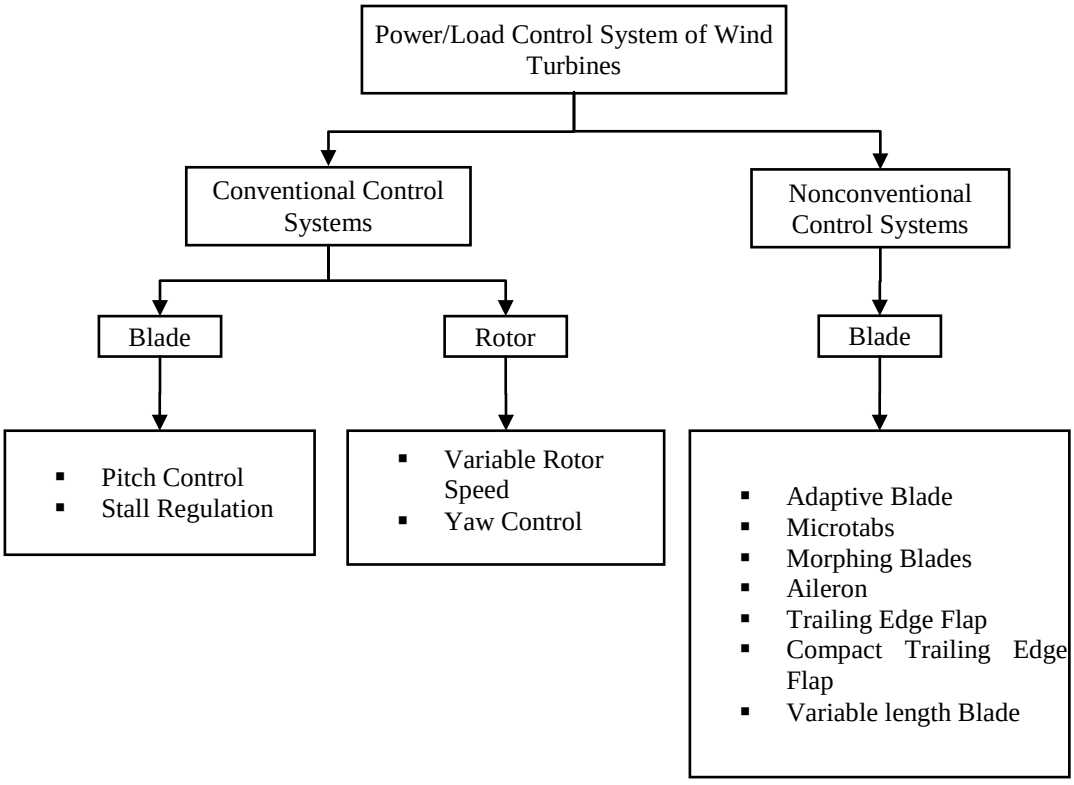

Figure 1.1- Conventional and nonconventional power and load control systems

It is well known that the most effective way of influencing the aerodynamic performance of the wind turbine blades is by mechanical adjustment of the blade pitch angle. Pitch control system, another conventional control method, is more efficient as it adjusts the blade pitch angle and then the blade aerodynamic

characteristics at any operation condition. Individual pitch control system, a particular form of pitch control system in which the pitch angle of each blade is controlled separately, not only works for the power control it also works for load alleviation. Johnson (1982) first introduced the concept of individual pitch control for helicopter rotor blades. Individual pitch control systems have been successfully developed and utilised to alleviate low frequency fluctuating loads by pitching the blades individually (Caselitz, 1997; Bossanyi, 2003; van Engelen, 2006; Larsen, 2005; Lovera, 2003). Since the response time of individual pitch control systems is not fast enough for high frequency load fluctuation, it is limited on large-scale application for wind turbine blades with lower rotor speeds (Lovera 2003).

Another method of regulating the output power is by changing the rotor speed. In variable-speed wind turbines, the rotor speed is changed by varying the output electrical load from the generator. When the wind speed is below its rated value, generator torque is used to control the rotor speed in order to capture as much power as possible. The most power is captured when the tip speed ratio is held constant at its optimum value (typically 6 to 8). That is, as wind speed increases, rotor speed increases proportionally. The difference between the aerodynamic torque captured by the blades and the applied generator torque controls the rotor speed.

The yaw system of wind turbines is the component responsible for adjusting of the orientation of the wind turbine rotor with respect to the wind direction. Another, less common, method of power control is to use the yaw system to face wind turbine at an angle with wind at high wind speeds to reduce the output power. Using yaw mechanism as a power control system is not efficient and increases unbalanced aerodynamic load on blades.

With the increasing size of modern wind turbines, blade load alleviation has become the main challenge for large wind turbines (Nijssen, 2006; Johnson, 2008). In addition to the conventional control methods, many advanced technologies have been investigated for the purpose of power control or load

alleviation, amongst them adaptive blades, trailing edge microtabs, morphing aerofoils, ailerons, trailing edge flaps and telescopic blades.

Most of the early attempts for loads alleviation were relied on pitching the blades to feather to reduce the power output and loads. NorthWind 4kW (Currin, 1981) had a system for passively adjust in the blade pitch for both power and load control. Hohenemser and Swift (1981) studied a design for alleviating the high loads due to yaw control by cyclic pitch adjustments.

Microtabs were described by Baker and Mayda (2005), Chow and van Dam (2007) as small aerodynamic control surfaces with deployment height of order of magnitude of one percent of local chord length. Microtabs work for aerodynamic loads alleviation by fixing these small surfaces close to the trailing edge of the blade. Microtabs have been shown to be effective in alleviating high-frequency loads caused by wind turbulence.

Morphing technologies are currently receiving significant interest from the wind turbine community because of their potential high aerodynamic efficiency, simple construction and low weight. The concept of morphing is that a blade adapts its geometry to changing flow conditions by changing its shape (Stuart et al, 1997; Farhan & Phuriwat, 2008; Barlas & van Kuik, 2010). The morphing concept includes a wide spectrum of shape adaptations, such as variation in camber of the aerofoil, blade twist, blade span, plan form area of blade and segmented span element.

Aileron is another active device and the concept of aileron is borrowed from aerospace industry. It has been used for aerodynamic breaking in the past. Results of a recent research on ailerons via simulating the behaviour of a wind turbine in turbulent wind indicates that aileron load control can assist in power regulation and reduce root flap bending moments during a step-gust and turbulent wind situation (Migliore, 1995; Stuart, 1996; Enenkl, 2002).

Trailing edge flap follows the same principle as aileron, but by deflecting the trailing edge portion of the aerofoil to change the aerodynamic characteristics of

the blade in high-wind conditions and turbulent wind (Troldborg, 2005; Buhl & Guwiaa, 2005; Andersen, 2006). Compact trailing edge flaps made of smart materials is another concept under investigation for load alleviation. Results of a recent research demonstrate large reduction (50 -90%) in vibratory load (Barlas & van Kuik, 2010).

Variable length blades are fitted with a tip that automatically extends outwards in response to light winds and retract in stronger winds. This action allows higher energy capture in low wind conditions, while minimising mechanical loads in high wind conditions (DOE, 2005; GE Wind Energy, 2006; Pasupulapati et al, 2005; Shrama & Madawala, 2007).

Among nonconventional control approaches, adaptive blades, as another advanced technology for power enhancement and loads alleviation, are investigated in this project.

1.3 Adaptive Blades: Control Concept

Karaolis (1988, 1989) and later Kooijiman (1996) and Lobitz and Veers (1996) suggested the shift from the conventional control methods by aeroelastic tailoring of fibre reinforced composite blades. In adaptive blades, a controlled and limited torsional deformation is produced because of elastic coupling in the blade, it responses to changes in wind speed. This approach, also known as smart blades, employs the blade itself as the controller to sense the wind velocity or rotor speed variations and adjust its aerodynamic characteristics to affect the wind turbine performance.

Blade aerodynamic performance is highly under influence of the angle of attack along its span. The angle of attack depends on the inflow angle, pre-twist, elastic twist and the pitch angle as expressed by Equation (1.1) and shown in Figure (1.2).

$$\alpha = \varphi - \beta_e - \beta_0 - pitch \tag{1.1}$$

Inflow angle (φ) depends on wind turbine run conditions (i.e. wind speed) which is out of the control, thus it cannot be treated as a controlling parameter. Pre-twist also is fixed because it has been embedded in the blades geometry in the blade design process. For pitch angle, it can be fixed or actively controlled depending on whether the pitch control system is applied or not. In adaptive blades, it is intended to treat the elastic twist (β_e) as a controlling parameter affecting the angle of attack passively in response to changes in aerodynamic forces.

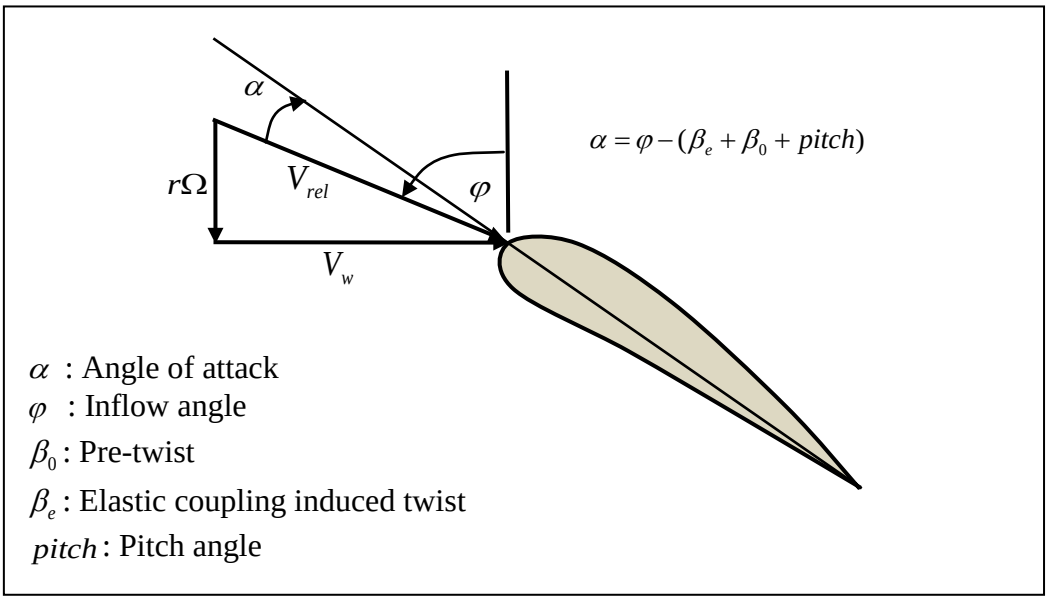

Figure 1.2-Flow kinematics diagram at a typical span location r

In conventional wind turbine blades, the elastic twist is due to pitching moment only and has little effect on the blade aerodynamic performance. In order to treat elastic twist as a controlling parameter, its effect should be magnified by making it a stronger function of aerodynamic or centrifugal forces, which have significantly higher values compared to the pitching moment. This is achievable by two methods as explained below.

1.4 Adaptive Blades: Sweptback Type

Geometric type adaptive blades, rather than a straight axis have a distinctive gently curving tip or sweep with curvature towards the trailing edge. Theoretically, this increases the pitching arm of the outer parts of the blades producing higher pitching moment. This, consequently, allows the blade to respond to changes in aerodynamic forces, for example, due to wind turbulence.

Aerodynamic forces applied to this curved profile generate twist, which further affects the dynamic performance of the blade. In nature, a similar sweep profile can be seen in the wing shape of birds and in the characteristic profile of cetacean tails and dorsal fins. Knight and Carver group (Ashwill, 2010) developed a sweep-twist adaptive rotor blade with reduced operating loads for Sandia National Laboratories, in order to seek for a larger and more productive rotor blade. They successfully designed, fabricated, tested and evaluated this prototype blade through laboratory and field tests. It showed that this sweep-twist blade met the engineering design criteria and economic goals for the program. The effort demonstrated that the sweep-twist technology could improve significantly greater energy capture about 5%-8% without higher operating loads on the turbine.

1.5 Adaptive Blades: Elastically Coupled Type

Composite laminates can be designed to exhibit unique structural responses that which are not possible with isotropic materials. Specific layup configurations produce various elastic couplings. Figure (1.3) is a simple illustration showing how using unbalanced configurations in a blade skin makes the internal forces elastically coupled. As shown in this figure, different layup configurations can be used to achieve different types of couplings. A mirror layup generates bend-twist coupling in which the bending moment also produces the torsional deformation. A helical layup makes the blade a stretch-twist coupled structure in which the axial load produces the torsional deformation. By implanting bend-twist or stretch-twist elastic coupling in a blade, the elastic twist becomes a function of the aerodynamic forces (lift and drag) or axial forces (weight and centrifugal inertia forces). That is, we can have a significantly higher elastic twist depending on wind speed, rotor speed and blade azimuth position. This twist is also called induced twist, as it is the result of the induced torsional deformation due to implanted elastic coupling in the blade.

Different levels of elastic coupling can be achieved in the blade by changing the ply angle in the layers. For helicopter blades and small wind turbines with fast rotor speed, the centrifugal forces are dominated, thus it is suitable for stretch-twist. Conversely, bend-twist is suitable for large wind turbines because the rotor

speed is slow and the bending moment will be dominated compared with centrifugal forces.

The term adaptive blade in this project refers to the second type: elastically coupled adaptive blades.

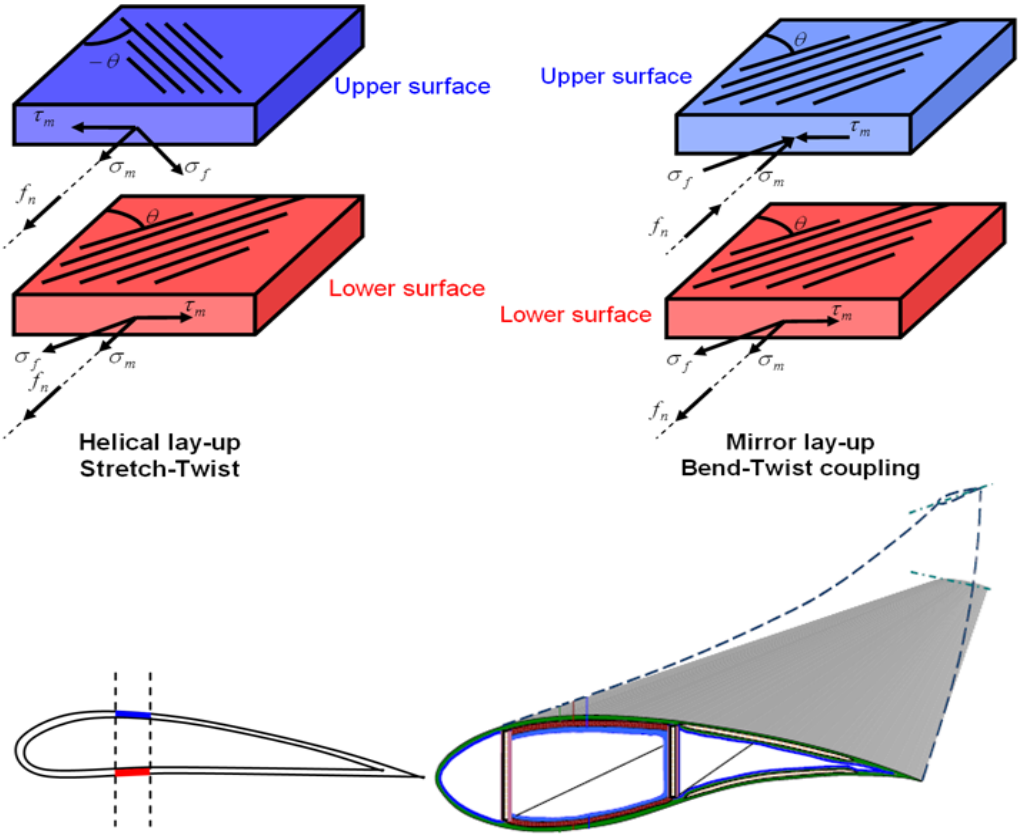

Figure 1.3- Two types of elastic couplings: stretch-twist and bend-twist

1.6 Wind Turbine Adaptive Blades, a Concept Borrowed from Helicopter Industry

Modest blade twist produced by the elastic coupling implanted in the blade itself without any additional mechanisms or devices has been investigated in helicopter industry long time ago. The earliest studies by Hong and Chopra (1985) and then Panda and Chopra (1987) on the aeroelastic behaviour of composite blades showed that the elastic couplings could have a powerful influence on aeroelastic stability, blade stresses and loads. Smith and Chopra (1991) and later Chandra and Chopra (1991, 1992) used Vlasov theory to extend composite blade modelling to include composite beams of arbitrary sections, including open sections and closed

multi-cell sections. These models were integrated into a comprehensive aeroelastic code (Bir et al, 1990) and used as a starting point for all the subsequent investigation on the aeroelastic tailoring of helicopter blades. Friedman et al (1992) were also involved in the development of an aeroelastic tailoring capability for composite straight and swept-tip blades and demonstrated that elastic couplings can significantly influence rotor vibration and stability. Ganguli and Chopra (1993, 1994) were the first persons to apply a systematic optimisation approach to composite tailoring of helicopter blades. The analytical formulation of sensitivity derivatives, a key step in the optimal tailoring process, was extended to cover composite blades. Ganguli and Chopra (1997) extended aeroelastic-tailoring research to simultaneously minimise both hub and blade loads.

Jeon et al (1998) investigated the aeroelastic instability of a composite rotor blade in a hover using a finite element method. The results showed that the instability of the blade was significantly improved.

Büter and Breitbach (2000) investigated effect of actively controlled tension-torsion-coupling of the blade structure by integrating actuators within the helicopter blade. It was shown that this method has high potential in suppressing noise, reducing vibration and increasing the overall aerodynamic efficiency.

1.7 Potentials of Adaptive Blades for Increasing Power Output

The earliest investigations of adaptive blade in wind turbines by use of asymmetric fibre reinforced laminates for active and passive aeroelastic power control was introduced by Karaolis et al (1988, 1989). They illustrated how to achieve power control by such smart blade and even provided optimum composite ply structures to provide maximum coupling.

Weber (1995) proposed the implementation of torsional deformation or bend-twist coupling mechanisms in future blade design both in relation to power performance and stability aspects is very useful for larger wind turbines.

Kooijman (1996) studied the bend-twist coupling in details. He showed that the bend-twist coupling created at outer 60% of the blade span by a hybrid laminate

lay up of carbon and glass epoxy, can give a potential increase in annual energy yield of several percentages.

Lobitz et al (1996) also investigated bend-twist coupling effects on annual energy production of a nominally 26-meter diameter stall regulated turbine by using PROP software (Tangler, 1987) and answered the question "How much energy production can be gained by adaptive blades twisting to stall". In this work, the blades were assumed to twist to stall, reducing maximum power. The rotor diameter was then increased to bring maximum power back up to the initial level. Induced twist was prescribed as a function of wind speed and spanwise location on the blade in either a linear or quadratic fashion, as well as twist proportional to power was used. These twisting scenarios promoted stall in such a way to capture extreme energy can be instead by extending the blade length, without an increase in maximum power output. It was discovered that the details of spanwise variation (or how the twist varied with wind speed or power) had only minor impacts. The twist-coupled blades increase power in the important middle-range of wind speeds, while power in high winds remains the same. Annual energy was increased by about 5% for one-degree tip twist and for two degrees, about 10%. This study also suggested that those substantial increases in annual energy capture could be achieved if the blades can be made to twist towards stall with increasing applied load. The twisting schedule and the average wind speed are not crucial to achieving a significant increase in annual energy capture. It should be noted that their assumptions was challenged later in 2010 (Maheri & Isikveren, 2010).

Eisler and Veers (1998) carried out research on the potentials of adaptive blades to enhance the performance of horizontal axis wind turbines. They investigated whether enhanced stall regulation can achieve substantial benefits in a fixed-pitch, variable-speed rotor by a gradient-based parameter optimisation method without increasing the blade size. The results showed that adaptive pitch changes can compensate for constrained rotor speed operation in the regimes covered in their study to improve average annual power output.

Maheri et al (2006a) developed an algorithm for modifying an ordinary blade into a bend-twist adaptive blade, showing potential benefits of utilising adaptive blades on stall regulated wind turbines. They continued by carrying out an optimal design of the topology of an adaptive blade using a genetic algorithm (Maheri et al, 2007). The results showed a significant improvement in the energy capture capabilities of a stall-regulated wind turbine. They also showed the adaptability of the bend-twist adaptive blades not only makes the blades more efficient but also allows designing longer blades optimally without changing the design rotor speed.

Rachel (2007) and Nicholls-Lee (2009) have even applied the torsion coupling design idea of wind turbine to the design of tidal turbine blade as to improve the annual power capturing capability of the tidal turbine, approaching the Betz limit. The research showed that the adaptive blades of tidal power generation could also improve the annual power capturing capability, as well as reduce the load-carrying capability to enhance the reliability of the blade.

1.8 Potentials of Adaptive Blades for Load Alleviation

Lobitz and Laino (1999) examined the effects of bend-twist coupling on alleviation of aerodynamic loads by use of ADAMS-WT, AeroDyn (Hansen, 1998), and SNLWIND-3D (Kelley, 1993) software. The results showed that for lower fatigue damage estimates for twist towards feather, maximum loads decreased modestly and average power increased due to elevations in the power curve in the stall region. Moreover, extra test was carried out by altering the pitch angle for a bend-twist (towards to feather) coupling blade to bring the power curve into agreement with that of the uncoupled blade. They discovered that fatigue damage levels remain at the same reduced levels while differences in maximum load and average power are reduced. Results also showed that twist toward stall produces significant increases in fatigue damage and instability of structure, and for a range of wind speeds in the stall regime apparent stall flutter behaviour was observed. There was evidence in the power curve that pitching the bend-twist coupled blade may reduce overall energy capture. However, they suggested that twist-coupled blades should be carefully designed to minimise this

reduction. In addition, the use of coupling along with active turbine power control could better take advantage of the increased energy capture while maintaining the fatigue load mitigation.

A further investigation was carried out by Lobitz et al (2001) for load mitigation with bend-twist blades by using modern control strategies. In their report, ADAMS software was used to undertake the simulation. The twist coupling coefficient for the blades was set at $\alpha = 0.6$ (twisting toward feather), and the blades were pre-twisted toward stall to match the constant speed power curve for an uncoupled blades. Three different strategies namely, constant speed stall-regulated, variable speed stall regulated, and variable speed pitch-controlled were employed. Turbulent wind simulations were made for testing fatigue effects. In most cases, significant fatigue damage reductions (20-80%) were exhibited by the twist-coupled rotor. For the constant speed and variable speed rotors that employed stall-control, significant damage reductions were observed at the higher material exponents for the 8 m/s average wind speed where the rotor operates primarily in the linear aerodynamic range. For the variable speed pitch-controlled rotor, significant reductions were observed at the higher wind speeds as well due to its ability to continue to operate in the linear aerodynamic range even at the higher wind speeds. For this bend-twist blade, substantial fatigue damage reductions prevail for the rotor in variable speed operation as in the case for constant speed, and with no loss in power output. Maximum loads for the bend-twist blades were also reduced, especially for the variable speed pitch-controlled one. For the variable speed pitch-controlled rotors, elastic coupling would substantially decrease fatigue damage as well as the maximum loads over all wind speeds without reducing average power.

1.9 Static and Dynamic Stability of Adaptive Blades

Whenever the wind turbine blade becomes aeroelastically “active,” that is, the elastic deformations play a role in the aerodynamic loading, dynamic stability will be affected. Lobitz and Veers (1998) addressed two of the most common stability constraints, namely flutter and divergence. Flutter is the condition where the phasing between the aerodynamic load fluctuations and elastic deformations are

such that a resonant condition is achieved. Every wing will have a flutter boundary at some speed; for wind turbines, the boundary is defined at the rotational speed (typically determined in still air) at which the blade will flutter. The stability margin is the difference between the flutter speed and the normal operating speed. Divergence is a quasi-static condition where the blade twists in response to increasing load in a direction that further increases the load. If this condition exists on a blade, there will be an operating speed at which the increase in loads caused by the deformation exceeds the ability of the blade to resist the load, called divergence.

Kooijman (1996) reported that in case of producing induced twist towards stall, the dynamic stability of the blade is reduced, while twist towards feather improves the blade stability.

Lobitz and Veers (1999) also investigated the aeroelastic behaviour of bend-twist adaptive blades. They noted that when the bend-twist elastic coupling was introduced into the blade design, it influenced the aeroelastic stability. This stability was investigated by classical flutter and dynamic divergence as a function of the coupling coefficient. For flutter, the first torsional mode showed that the damping coefficient is increasing with rotor speed before they fall off to negative values which indicate instability and showed extreme coupling coefficient (toward to stall) would make rotor speed have broad range. It also denoted that divergence occurs at lower rotor speeds as the coupling coefficient increases (toward to stall), with the coupling coefficient decreasing to negative (toward feather), it is increasingly difficult to get the blade to diverge. However, it would make the blade flutter easily. This investigation showed that the bend-twist blade is less stable when it twists toward to stall due to the divergence caused by the increasing aerodynamic loads. Conversely, the blade is less stable toward to further due to flutter.

1.10 Implementing Elastic Coupling in Adaptive Blades

Although there are potential benefits from aeroelastic tailoring, it does not mean that the blades can be manufactured to produce the necessary coupling. There are

limits to the amount of coupling that can be achieved with asymmetric fibre layups. The best direction and the maximum coupling are a function of the fibre and matrix properties. Karaolis et al (1988, 1989) figured out the best combinations of two direction layups to maintain strength and produce twist coupling in an aerofoil shape. The results indicated that the best coupling could be achieved with the off-axis fibres oriented at about 20 degrees to the longitudinal axis of the blade. Kooijman (1996) also recommended 20 degree reinforcement, suggested that the coupling is maximised by avoiding 45 degree layups in the rib.

Tsai and Ong (1998) indicated that stiffer fibre materials would result in the higher coupling levels, with maximum coupling for flat plates, the coupling coefficient is below 0.8 for a graphite epoxy system and coefficient is below 0.6 for a glass-epoxy system. The carbon system achieves maximum coupling with all the fibres at about 20 degrees to the axis of bending while the glass maximum is at about 25 degrees. These theoretical maxima, however do not account for the need for off-axis strength and toughness nor do they apply directly to cross sections other than flat plates. Tsai and Ong (1998) also obtained the same result for the D-spar shape. Their results indicated that graphite-epoxy D-spar have maximum couplings around coupling factor of α = 0.55 while glass-epoxy D-spar around α = 0.4. Interestingly, hybrid glass and graphite layups, using the graphite to get the coupling and the glass to provide the off-axis strength, do just as well as all graphite.

Manufacturing process will depend on the type of coupling to be produced. Fibre winding is well suited to producing stretch-twist coupling in a spar while clam-shell construction with the top and bottom skins manufactured separately is best suited to bend-twist coupling.

1.11 Adaptive Blades Integrated Design

Maheri (2006b) showed that simulation of wind turbines utilising bend-twist adaptive blades is an iterative coupled-aero-structure process. Because of this, the traditional design methods for conventional blades are not applicable to the design of bend-twist adaptive blades.

In simulation of the aerodynamic performance of a wind turbine with ordinary blades, only the aerodynamic characteristics of the blades are involved. Therefore, the aerodynamic design of ordinary blades can be performed without direct participation of the material properties and structure configurations of the blade. The aerodynamic and structural design phases of traditional wind turbine blades take place sequentially. In case of adaptive blades, for aerodynamic simulation of wind turbine, structural characteristics of the blade must be also known. Therefore, the aerodynamic and structural design phases are integrated in nature (See Figures (1.4) and (1.5)).

Lobitz and Veers (1999) showed that an induced twist at the tip of the blade as small as one degree could have significant effect on the performance of wind turbine. Therefore, the evaluation of the induced twist accurately becomes the main concern in analysis and design of adaptive blades. Maheri et al (2006c, 2006d, and 2007b) developed a standalone software tool for aero-structure analysis of adaptive blades. Aiming at minimising the computational time, while maximising the accuracy of the structural analysis, they developed a wind turbine simulator with a built-in FEA-based structural analyser and an adaptive mesh generator. In a further step towards reducing the computational time, they developed a hybrid analytical/FEA method for simulation and design of adaptive blades (Maheri et al, 2007c, 2007d). This approach brings in the induced twist distribution and the flap bending moment at the hub of the blade predicted via a FE-based structural simulation at a reference run condition of an adaptive wind turbine to define the wind turbine performance at other run conditions. Running a FE-based structural analysis only once thus, this method reduces the computational time significantly and makes the aerodynamic simulation of bend-twist adaptive blades more efficient.

Further work on integrated design of adaptive blades using FE-based methods can be seen in Maheri (2012) and Nicholls-Lee (2013). Nicholls-Lee et al (2013) developed a fluid-structure coupled tool for the design of passively adaptive, composite horizontal axis tidal turbine blades. The structural analysis was carried out by FEA and it was coupled with a fluid dynamic model for performance a full

fluid-structure interaction analysis. The results compared well to the previous studies by Nicholls-Lee and Turnock (2007), and indicated that decrease C_T and an increase C_{Pow}, that could be achieved using properly designed bend-twist coupled blades.

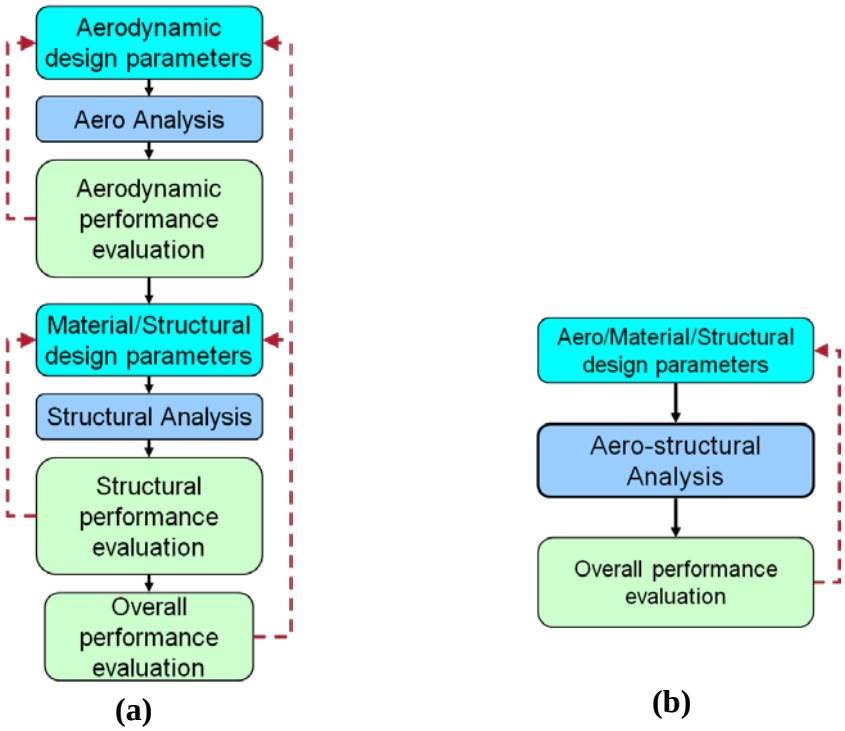

Figure 1.4-(a) Sequential versus (b) Integrated design

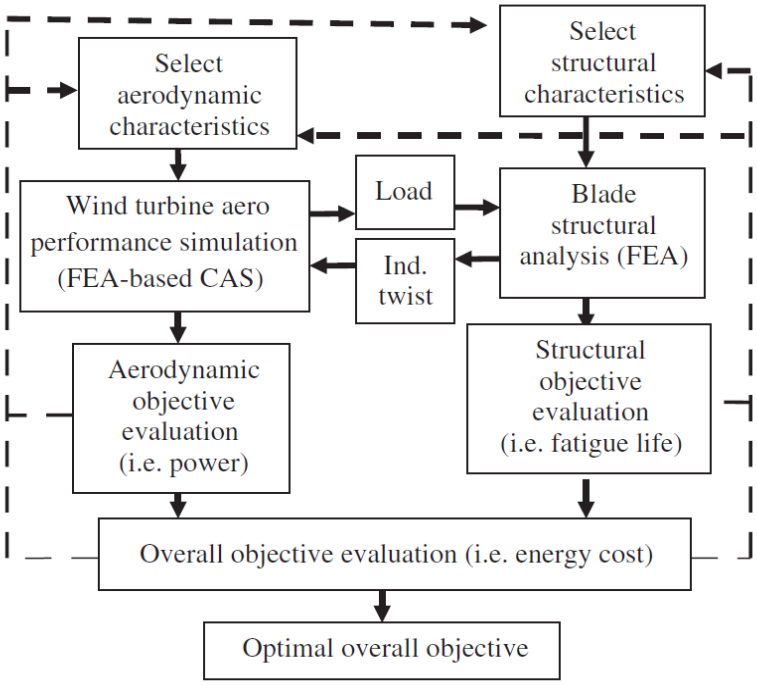

Figure 1.5-Adaptive blade integrated design process (Maheri, 2007a)

1.12 Adaptive Blades Decoupled Design

Maheri et al (2007a) argued that integrated design of adaptive blades using FEA-based structural analyser is inefficient. They pointed out that performing a coupled aero-structure design process for adaptive blades has two main drawbacks. Firstly, simulation of wind turbines with bend-twist adaptive blades is a CAS process, in which in order to obtain reliable results for the induced twist of the blade, the structural analyser must be based on FEA. Employing a FE-based code, as a part of a design objective evaluator, makes the aerodynamic objective evaluation very time consuming. Secondly, in aerodynamic objective evaluation part, in addition to the aerodynamic parameters many structural and material parameters are also involved in. This increases the number of parameters producing the design space and consequently the number of required evaluations grows exponentially.

Decoupled design approach (Maheri, 2007a) was based on the concept of "variable state design parameters" (Maheri, 2008). In the decoupled design approach, the induced twist is considered as an aerodynamic design variable whilst its dependency on the structural characteristics of the blade is taken into

account by imposing a proper constraint on the structure design. It separates the aerodynamic design from structural design by treating the inducted twist as a variable state design parameter. The main advantage of this method is the significant reduction in evaluation time by replacing a FEA-based coupled-aero-structure simulation in the aerodynamic objective evaluation by a non-FEA-based coupled-aero-structure simulation. Maheri et al (2009) also developed a GA-based optimisation tool particularly designed for decouple design of adaptive blades. This design method, at its status, could be used to design adaptive blades with non-varying structural characteristics along the span of the blade.

1.13 The Overall Aim and Objectives of the Present Research

Maheri et al (2007a) suggested that two approaches could make a design process efficient and practical:

- To run an integrated design process by employing an efficient and robust structural analysis tools. It is well recognised that in interdisciplinary problems, an integrated design, where possible, provides superior results compared to sequential design methods. However, as mentioned previously, using FEA-based structural analysers makes the integrated optimal design of adaptive blades very time-consuming and therefore inefficient. Using analytical beam models instead of FEA-based analysis saves time and makes the analysis computationally efficient. However, none of the available beam models have been claimed or shown to be accurate enough for our purpose here. In order to make integrated design of adaptive blades practical, a robust structural analysis tool based on an accurate beam model for thin-walled, multi-cell, non-uniform composite beams is required.
- To decouple the coupled-aero-structure design. Decoupled design method has been shown to be highly efficient in design of adaptive blades. However, more investigation must be carried out to develop models in which the effect of the spanwise variations of the shell thickness and fibre angle are taken into account (Maheri, 2010).

Aim: The overall aim of this project is to develop efficient and robust tools and methods for optimal design of wind turbine adaptive blades.

In order to achieve the overall aim of this project the following objectives are defined:

Objective 1: To develop a general thin-walled composite beam model that is suitable for deformation analysis for beams with arbitrary lay-ups, no uniform cross-section, and single/multi-cell cross-section under various types of loadings. The accuracy of the beam model must be verified.

Objective 2: To develop a set of auxiliary software tools for defining structural/ material characteristics of adaptive blades and interfaces to the in-house aerodynamic performance simulator and design optimisation packages.

Objective 3: To extend the application of the decoupled design method and using this extended method for design of adaptive blades with spanwise varying structural characteristics.

In order to expand the application of decoupled design a search platform correlating the structural behaviour of adaptive blades to their structural/material characteristics is required. The beam model from Objective 1, developed for integrated design, can be used to produce a search platform for enhancing the models used in the decoupled design method.

2 A Beam Model for Deformation Analysis of Multi-cell Thin-Walled Unbalanced Composite Beams

2.1 Introduction

In adaptive blades design process, in cooperation with structural analysis by use of FEA based software is highly time-consuming and inefficient as mentioned before. That is, however, the only method currently available for accurate deformation analysis of thin-walled composite beams.

On the other hand, wind turbine rotor blades, as high-aspect-ratio structures, can be modelled as thin-walled closed beams and thus owns much simpler governing equations compared to massive bodies, plates and shells. To take the advantage of this geometric feature without loss of accuracy, one has to capture the behaviour associated with the eliminated two dimensions (the cross sectional coordinates). Classical thin-walled beam theories can be found in pioneering monographs Umansky (1939) and Vlasov (1940, 1961).

Fibrous composite materials as anisotropic materials have been broadly used in civil and aerospace engineering, so far, numerous number of thin-walled composite beam models have been proposed through various methods during the past two decades. These models, however, usually put some constraints, which partly model thin/thick-walled composite single/multi-cell beams with uniform cross-section or only for simple geometries.

This is mainly due to non-classical effects in thin-walled composite beams, such as restrained warping, transverse shear effect, 3-D strain effect, and non-uniform shear stiffness. These effects have been identified as having significant influences on the prediction accuracy of the beam models.

This chapter is devoted to the development of thin-walled composite beam model for deformation analysis of wind turbine adaptive blades as thin-walled composite beams. Following this introduction, Section 2.2 elaborates on different beam theories, which have been developed recently. Section 2.3 introduces basic definitions, including different elastic-coupling topologies that can be used for adaptive blades and the definition of different systems of coordinates used for driving equations. The 2.4 and 2.5 sections give the details of the beam model for single-cell and multi-cell unbalanced composite beams. In Section 2.6, the

evaluation of the model is carried out for cases: box-beams made of isotropic material, single-cell box-beam made of unbalanced composite materials, and adaptive blades with single/multi-cell. The predicted results are compared with theoretical (where available), experimental (where available) and numerical results.

2.2 Structural Analysis of Unbalanced Thin-Walled Composite Beams

Thin-walled beam models can be classified into two classes. The first class is concerning the so-called free warping of the cross-section in which warping (including primary and secondary warping) refers to the displacement of the cross-section out of its flexural plane without boundary constraint at both of ends. The second class is concerned with constrained warping of the cross-section that occurs when the ends of the beam are prevented from warping displacement by boundary conditions. Constrained warping effects are significant in short beams or in narrow boundary layers at the ends of long beams where the kinematic restraint is imposed.

The problem of thin-walled composite beam under free or constrained warping can be analysed by either stiffness (also called displacement formulation) or flexibility (also called stress formulation). The stiffness method is based on a suitable approximation to the displacement field of the beam cross-section, then the assumed displacement field is used to compute the strain energy of the beam, and the beam stiffness relations are obtained by introducing associated energy principles. The stiffness method is quite straightforward and easy to apply. However, the warping component of the axial displacement is pre-assigned independent of material properties, thus the drawback of the displacement formulation follows from that of the shear flow (resultant shear stress tangent to the contour) and is found from the constitutive equation and is proportional to the shear stiffness of the laminate. This restricts the application of this formulation to a beam whose shear stiffness does not depend on the contour coordinate, or to beams with slowly varying shear stiffness in the contour coordinate.

In contrary to the displacement method, the stress formulation method is well known for isotropic beams and then is extended to composite beams by Vasilier (1993). In this method, the shear flow is determined from an equilibrium equation by integration, and the wall stiffness can vary along the cross-sectional contour and the associated warping directly from the equilibrium equations of the shell wall. Thus the flexibility method provides a systematic method to determine the warping functions and generally leads to better correlation with experimental test data and then leads to a closed-form solution and suitable for design problems.

The beam element method, another effective approach to solving the problem of composite beams, has been widely used due to its versatility and efficiency. The other methods of beam analysis such as variational asymptotic beam section analysis (VABS) (Cesnik & Hodges, 1997) and stiffness and flexibility mixed method and other form of formulation are also reviewed as follows.

2.2.1 Stiffness Method

The stiffness method has been used by many researchers, among them, Rehfield et al (1990), Smith and Chopra (1991), Chandra and Chopra (1992), Kim and White (1996, 1997), Bhaskar and Librescu (1995), Song (1990), Song and Liberscu (1993, 1997), Liberscu and Song (1991, 1992) and Qin & Librescu (2002), Liberscu & Song (2006). The earlier work with the contour-based cross sectional analysis methods was conducted by Vlasov (1961) and Gjelsvik (1981). They presented an isotropic beam theory identified with plate segments of the beam. The plate segment displacements were related to the generalised beam displacements through geometric considerations, where the plate stresses were connected to the generalized beam forces via the principle of virtual work. In addition, this theory was lately employed by other authors to calculate potential energy for thin-walled composite beams.

Smith and Chopra (1991) employed a stiffness-based approach that took into account only the membrane part of the shell wall to obtain a 6 by 6 stiffness matrix and the bending shell measures were neglected in their analysis. Chandra and Chopra (1992) developed the closed form solutions for uniform I-beams

under torsional moment and tested against experimentally determined results. The study showed that unlike isotropic beams, composite beams with large aspect ratios are strongly affected by warping restraints. They also incorporated the warping restraint effects in their displacement-based formulation by extending the Vlasov (1961) theory to thin-walled composite beams with two-cell sections, in constitutive relations, the in-plane strain and curvature were assumed as zero in the shell wall.

The first refined thin-walled beam theory based on Extended Galerkin Method (EGM) originally was developed by Song (1990) and Librescu and Song (1991) without considering 3-D strain effect and non-uniform of membrane shear stiffness along the mid-line contour in that model. However, for the walls composed of different layups leading to different shear stiffness, and then the assumption of uniform shear stiffness along section contour is no longer valid. Then the beam theory was modified by Bhaskar and Librescu (1995) to account for non-uniform shear stiffness for geometrically non-linear beam theory based on previous refined thin-walled beam theory.

The non-uniform membrane shear stiffness and the 3-D strain effect demonstrated by Smith and Chopra (1991), Bhaskar and Librescu (1995), Kim and white (1996, 1997), Wu and Sun (1992), Jung, Nagaraj and Chopra (2002), have a significant effect on static response predictions. Within the framework of an existing anisotropic thin-walled beam model by Song (1990) and Librescu & Song (1991), Qin & Librescu (2002) developed a shear-deformable beam theory based on the Extended Galerkin Method (EGM). They also investigated the non-classical effects such as 3-D strain effect, non-uniform shear stiffness effect and shear deformation effect on the static responses and natural frequencies of composite thin-walled beams. This work is the first attempt to validate a class of refined thin-walled beam model.

Kim and White (1996, 1997) developed an analytical method by setting up forces equilibrium of cross-sections to account for 3D elastic effects for both thin- and thick-walled composite box-beams considering transverse shear effects and

primary and secondary torsional warping by equilibrium of section forces. The results showed that this method can predict twist and coupled twisting deformations of box-beam accurately considering primary and secondary warping effects, also showed that the contribution of the secondary warping was small for a thin-walled box beam. However, secondary warping became significant as the thickness of the beam wall increased. Both primary and secondary warping tended to decrease torsional and torsion-coupled beam stiffness.

Librescu and Song (2006) systematically summarised previous works (Librescu & Song, 1991, 1992, 1993, 1996a, 1996b, 1997, 1998a, 1998b, 1998c, 1998d, 2000, 2001, 2003; Song & Librescu, 1990, 1993) and also employed research results from other authors about thin-walled composite beams, and developed a set of thin-walled composite beam theories. In their work, the focus was on the formulation of the dynamic problem of laminated composite thin- and thick-walled, single-cell beams of arbitrary cross-section and on the investigation of their associated free vibration behaviour. At present, the basic of refined beam theory has been extensively used for the study of dynamic response, structural feedback control and static aeroelasticity considering a number of non-classical effects such as non-uniform shear stiffness along contour, shear deformation, warping constraint, second warping effect etc.

Kim et al (2006) developed a numerical method to evaluate the exact element stiffness matrix for the thin-walled open-section composite beams subjected to torsional moment. Through introducing Vlasov's assumption and the equilibrium equations and the force–deformation, relations are derived from the energy principle. Applying the displacement state vector consisting of 14 displacement parameters and the nodal displacements at both ends of the beam, the displacement functions are derived exactly. This systematic method determines Eigen modes corresponding to multiple zero and non-zero Eigen values and derives the exact displacement functions for displacement parameters based on the undetermined parameter method. The exact element stiffness matrix may be easily determined using the member force–deformation relationships. Through the numerical examples, it demonstrated that the results by this study using only a

single element have shown to be in an excellent agreement with the closed-form solutions, the finite element solutions and the results by ABAQUS shell elements.

Furthermore, Kim and Shin (2009) used the same method for thin-walled composite beams with single- and double-celled sections by introducing fourteen displacement parameters. Consequently, it was judged that the present numerical procedure provides a simple but efficient method for not only the numerical evaluation of exact stiffness matrix of thin-walled composite box beams but also general solutions of simultaneous ordinary differential equations of the higher order.

Lee, Kim and Hong (2002) studied the lateral buckling of a laminated composite beam with doubly symmetric and mono symmetric I-sections by use of the displacement- based finite element method. Maddur and Chaturvedi (1999, 2000) modified first-order shear deformation theory considering shear deformation of open profile section without violating the assumption of zero mid-plane shear strain. And then, they simplified their theory for I-beams as a special case and evaluated the rotation and warping deformations for cross ply laminated graphite epoxy cantilevered I-beam subjected to only torsional load at free end based on finite element procedure by using Lagrange interpolation function for the geometric coordinate variables and Hermitian interpolation function for the unknown functions.

Lee and Lee (2004) and Lee (2005, 2006) developed analytical models for studying the flexural–torsional behaviour, without considering shear deformation and flexural behaviour and with shear deformation consideration. They worked on I-section composite beams with arbitrary laminate stacking sequence and solved it by displacement-based finite element method through expressing the generalised displacements as a linear combination of the 1-D Lagrangian interpolation function for axial displacement and the Hermite-cubic interpolation function for lateral displacements and twist angle.

Vo and Lee (2007) extended the open cross-section beam model generated by Lee and Lee (2004) to a closed cross-section beam model subjected to vertical and

torsional loads. This model was based on the classical lamination theory, accounting for the coupling of flexural and torsional responses for arbitrary lamination schemes without considering the shear deformation effect and a one-dimensional displacement-based finite element method is employed. The results showed that the assumption that stress flow in the contour direction vanishes ($\sigma_s = 0$) seems more appropriate than the free strain assumption in the contour direction.

Vo and Lee (2008) improved their previous beam model by considering shear-deformable effect and the results showed that the shear effects become significant for lower span-to-height ratio and higher degrees of orthotropic of the beam. Based on previous work (Vo & Lee, 2007, 2008, 2009a, 2009b, 2010a, 2010b, 2011, 2012) they developed geometrically nonlinear theory considering various non-classical effects.

Shadmehri et al (2007) investigated the flexural-torsional behaviour of thin-walled composite beams with closed cross-section based on the beam theory from Librescu and Song (2006), they mainly investigated the effect of circumferentially asymmetric stiffness (CAS) configurations on twist, deflection and natural frequencies by a box-beam. Piovan and Cortinez (2007) developed a general model for composite thin-walled beams derived by applying the linearised principle of virtual works. Fatmi and Ghazouani (2011) developed a higher order composite beam theory that can be viewed as an extension of Saint-Venant's theory. It is based on a kinematics built from the exact form of Saint-Venant displacement.

Kim and Lee (2013) developed the improved torsional analysis of the laminated box beams with single- and double-celled sections subjected to a torsional moment by introducing 14 displacement parameters and solved by transforming the higher order simultaneous differential equations into first order ones. It showed that by this method, using a minimum number of elements would agree well with the solutions using large number of beam elements by finite element program.

2.2.2 Stress Formulation Method

The stress formulation has been used by Johnson et al (2001) and Patil and Johnson (2005). Johnson, Vasilier and Vasiliev (2001) developed a complete thin-walled anisotropic beams theory with closed cross-sectional contours by use of the flexibility method. The advantage of the stress formulation is the exact satisfaction of the equilibrium equations and without introduction of assumptions concerning the form of the warping function, then stress formulation provides more accurate results for beams whose stiffness coefficients depend on the contour coordinate. Patil and Johnson, (2005) extended the work of Johnson, Vasilier and Vasiliev (2001) by including embedded strain actuation for cross-sectional analysis of anisotropic thin-walled, closed section beams by using the same method.

2.2.3 Mixed and Other Methods

Jung, Nagaraj and Chopra (2002); Jung and Park (2005a, 2005b) used a mixed beam approach by combining both the stiffness and flexibility methods to analyze the coupled composite blades with closed two-celled cross-sections. Jung, Park and Shin (2007) based on their previous work a developed mixed beam theory to analyse the elastically-coupled composite beams with closed cross-sections and solved by using Hermite polynomials (FEA method). It was used to examine rigidity of cross-section associated with elastic coupling. The analysis model includes the effects of elastic couplings, shell wall thickness, torsion warping, and constrained warping. The Reissner's semi-complementary energy functional was used to derive the beam force–displacement relations. Numerical results showed the importance of shell bending measures were presented for coupled composite box beams.

Loughlan and Ata (1995) solved constrained torsional response of the open-section beams for Z and channel sections by simple engineering theoretical analysis. Subsequently Loughlan and Ata (1997a) presented a simple analytical procedure for determining the constrained torsional response of a cantilevered box beams subjected to torque at the free end and the torsional and warping rigidities

of the composite box sections were determined using the appropriate equivalent engineering elastic constants of the individual thin-walled composite walls.

Loughlan and Ata (1997b) extended their theoretical approach to the torsional analysis for thin-walled open-section composite beam. Some detailed attention was paid to the effects of primary and secondary warping restraint on the torsional response of open-section beams. Furthermore, Loughlan and Ata (1998a, 1998b) developed an experimental test for purpose of understanding the constrained torsional response of open-section and single-cell closed-section composite beams and then examined the constrained torsional response by using the simple engineering theoretical approach. It indicated that the shear flow due to primary warping restraint in open-section beams plus the St. Venant shear flow serves to equilibrate the applied torque on the beam. The warping shear flow in a closed-cell box is completely self–equilibrating and thus the applied torque on the box is equilibrated by the Bredt-Batho shear flow.

Swanson (1998) reviewed an existing solution for the problem of torsion of orthotropic laminated rectangular bars and then extended to the case of laminated cross sections with high aspect ratio by a set of formulas that are used to calculate the stiffness and shear stress in torsion of laminated, orthotropic thin rectangular sections. It showed that the specialization to thin sections is important, as it can be applied to laminated rods with general open cross-sections.

Loughlan and Ahmed (2008) examined the structural performance of multi-cell carbon fibre composite box beams when subjected to constrain torsional loading by a simplified analytical procedure for determining the constrained torsional response of a specific class of multi-cell carbon fibre composite box beams. The resulting approach is shown to be able to predict the structural response of the multi-cell composite beams with a considerable degree of accuracy and comparisons between the theory and the results from finite element numerical modelling.

Wu et al (2002) developed a set of calculation formulas, which are capable of analysing the torsional behaviour of composite box-beam under torsional load

without external restraint. This method was based on the theory of composite laminated plates and was deduced by means of the free torsional theory of thin-walled beams, which made the produce simple and practical.

Toutanji and Dempsey (2001) discussed the benefits of using FRP composites and provided a theoretical model with stress expressions and circumferential stress curves showing the interaction between the different stresses exerted on pipe walls and the effects of FRP composite sheets on the circumferential stresses of damaged pipe wall.

Cesnik and Hodges (1997) developed a method: variational asymptotic beam section analysis (VABS), which partitions the model into 2D FE analysis of an arbitrary cross-section and a 1D non-linear beam analysis and it has shown to be quite accurate for stress/strain results. Latterly, Yu et al (2002) and Yu et al (2005) validated this method, used this method for modelling initially curved, twist composite beam, and set up a generalized Vlasov theory for composite beams.

Ferrero et al (2001a) proposed an analytical theory based on variational asymptotic method, which allowed the box beams to be dimensioned with extreme accuracy and without using complicated calculations based on a weak hypothesis on the field of deformation without considering warping effects. Moreover, Ferrero et al (2001b) presented an analytical theory that enabled simple identification of the stress caused by the twisting moment for a thin-walled structure with mid-plane symmetry and available for warping definition.

Kollar and Pluzsik (2002) presented a beam theory for thin-walled open and closed section composite beams with arbitrary layups that neglects the effect of restrained warping and transverse shear deformation, and developed expressions for the stiffness matrix.

Volovoi and Hodges (2000, 2002) developed closed-form expressions for the stiffness matrix by using the variational-asymptotic approach. The shell bending strain measures as well as constraint conditions were not taken into account in

their literature. They used the variational-asymptotic beam approach to derive a 4 by 4-stiffness matrix and the zero hoop-stress-flow condition for the constitutive relations was derived by asymptotic procedure.

Salim and Davalos (2005) derived a general solution for a fixed composite box beam under tip torsional loads and investigated the effect of warping-torsion on the torsional stiffness of the beam. In their paper, the transverse shear deformations are included in the formulation in order to overcome the overestimation of stiffness by the often assumption of negligible tangential stress, the laminate resultant force and moment are instead set to zero. The analytical model predictions agree closely with the experimental results and finite element results.

2.2.4 Beam Models by Use of FEA Method

In addition to beam theories, many beam elements have been developed for buckling, static and dynamic FEA of anisotropic, open and closed cross-section composite thin-walled-beams with general stacking sequences and arbitrary states of initial stresses and off-axis loadings. Stemple and Lee (1989) developed a FEA method, which can be used to model combined bending, torsional and extensional behaviour of composite helicopter rotor blades. The warping effects are incorporated by assuming warping displacements superimposed over cross-sections normal to the beam axis in the deformed configuration of a shear flexible beam and the Newton–Raphson method was used to solve the non-linear equilibrium equation resulting from the finite element approximation. This method yielded accurate results but required too many degrees of freedom to be practical for aeroelastic analysis.

Floros and Smith (1997) developed a finite element that was capable of modelling the kinematic boundary conditions associated with mixed torsion to capture the span-wise torsion-related warping restraint effects in composite I-beam. Cardoso et al (2009) developed a finite element model for structural analysis of composite laminated thin-walled beams with geometrically nonlinear behaviour and torsion warping deformation. Herein the structural discretisation was performed

throughout three-dimensional two-node Hermitean finite beam elements, with seven degrees-of-freedom per node. The influence of the lamina orientation on the structural behaviour as well as on the critical load of composite laminated beams has been studied. As one expected, the critical load of laminate composite beam is strongly dependent on the lamina orientation, hence this orientation is a fundamental parameter to these structures.

Back and Will (2008) presented a first order shear-deformable finite element for the flexural and buckling analyses of thin-walled composite I-beams. Vo and Thai (2011) developed three general geometrically nonlinear models for thin-walled composite beams for open cross-section beam under vertical loading and torsion loads, closed cross-section beam without considering shear deformation and considering shear deformation effect under various types of loadings respectively. In their models, a displacement-based one-dimensional finite element model that accounts for the geometric nonlinearity was developed in these models. General nonlinear governing equations were derived from the principle of the stationary value of total potential energy and solved by means of an incremental Newton–Raphson method.

As mentioned earlier, most of the above-mentioned beam models have been developed for beams with simple cross sections, or are based on particularly assumptions, which lead to inaccurate results when it is applied to a wind turbine adaptive blade with multi-cell, variable spanwise geometry and unbalanced layups.

2.3 Definitions and Key Assumptions

2.3.1 Elastic Coupling Topology

As mentioned earlier in Chapter 1 and shown in Figure (1.3), mirror and helical layup configurations on opposite surfaces of a fibre reinforced composite structure produce bend-twist and stretch-twist elastic couplings. Figure (2.1) shows various types of elastic-coupling topologies. Figures (2.1.a) to (2.1.d) show exemplar locations on the cross section and Figures (2.1.e) and (2.1.f) show exemplar locations along the span of the blade that can be used for implanting elastic coupling. In Figure (2.1.a) the entire of the section of the blade is made of

composite materials with unbalanced layup, while in Figures (2.1.b) to (2.1.d), only part of the cross section is made of unbalanced layup. In Figure (2.1.e) the entire of the blade is elastic coupled structurally, while in the blade of Figure (2.1.f) only the inboard section is made of unbalanced layup.

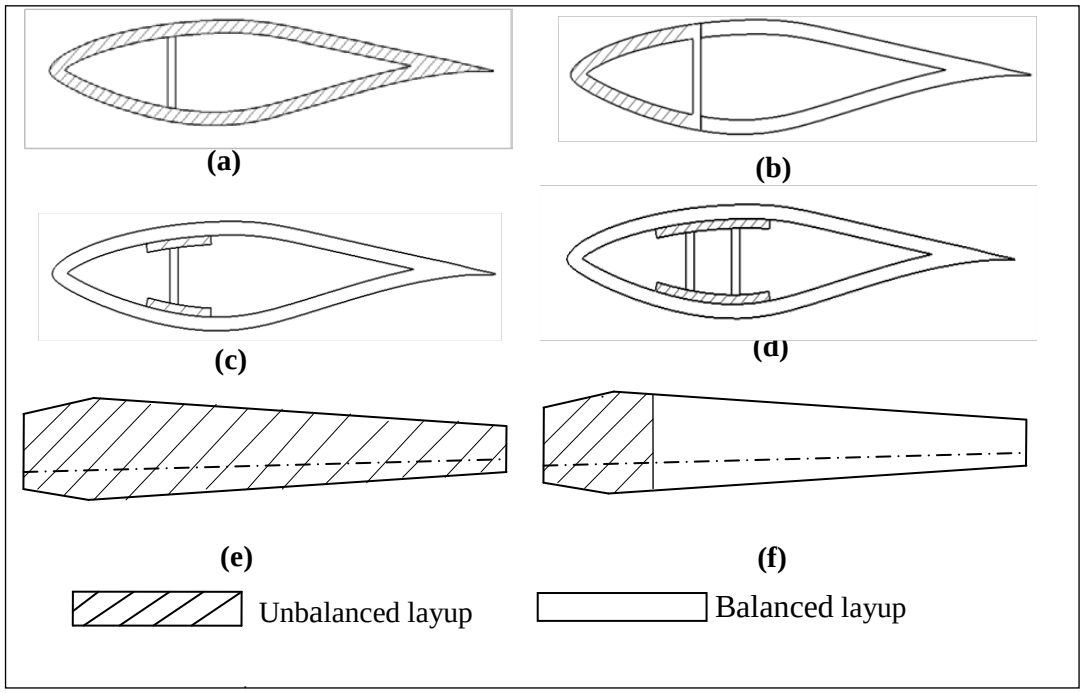

Figure 2.1-Examples of different elastic coupling topologies

2.3.2 Definition of Coordinate of Systems

The coordinate of systems required for analysing the kinematics of the beam, namely, Cartesian ($x-y-z$) and orthogonal curvilinear ($s-z-n$), are shown in Figure (2.2). In both coordinate systems, z-axis is defined along the axis of the beam.

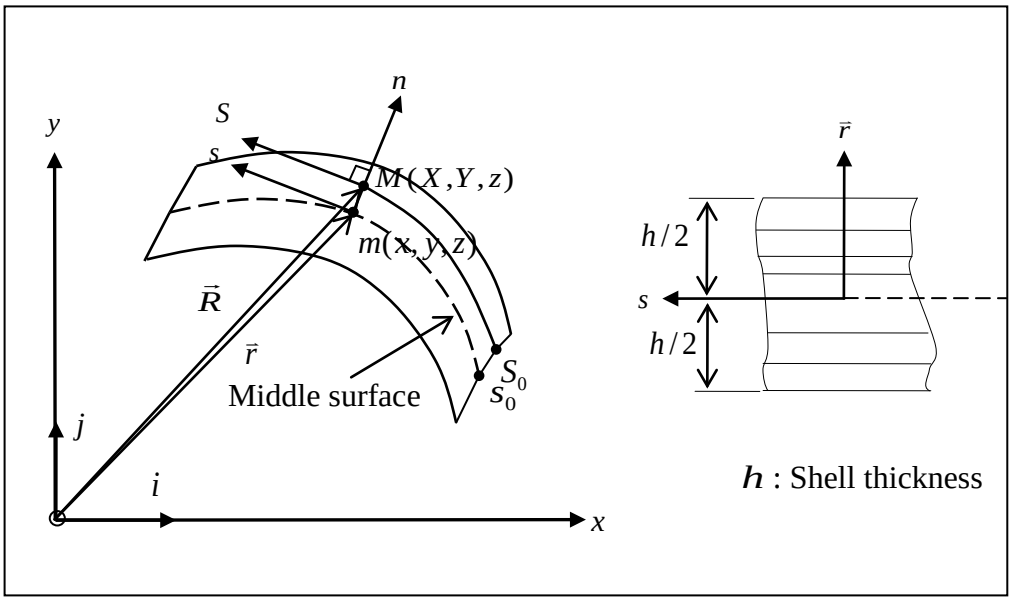

Figure 2.2- Orthogonal curvilinear coordinate of system

The middle surface of thin-walled beams plays an important role and it is defined as the locus of points with equal distances from the upper and lower surfaces of the beam. The middle surface belongs to the class of cylindrical surfaces. The straight lines lying on the middle surface parallel to the beam longitudinal axis are the generators of this surface. The intersection of the middle surface with a plane normal to the generators determines the mid-line of the cross-section contour. Coordinates s and n are respectively, tangent to the middle surface in anticlockwise direction with the origin conveniently chosen on the mid-line contour and perpendicular to the middle surface with the origin on the mid-line contour. The z-coordinate is identical with the z-coordinate of Cartesian system. In order to distinguish between the points located on or off the mid-surface, notations $(x, \mathrm{y}, \mathrm{z})$ and $(X, \mathrm{Y}, \mathrm{z})$ are used respectively.

The position vector of a general point located on the middle surface, $\vec{r}$ in Cartesian system of coordinates is given by:

$$\vec{r}(s,z) = x(s)\vec{i} + y(s)\vec{j} + z\vec{k} \tag{2.1}$$

The position vector $\vec{R}$ of a general point off the mid-surface can be expressed as:

$$\vec{R}(s,z) = \vec{r}(s,z) + n\vec{e}_n \tag{2.2}$$

Using Equations (2.1) and (2.2) one can set up the relationship between the Cartesian and the curvilinear coordinate of systems. The unit vectors in *n* and *s* direction, $\vec{e}_n$ and $\vec{e}_t$, are related to the unit vectors in Cartesian coordinate system by Equations (2.3) and (2.4):

$$\vec{e}_t = \frac{d\vec{r}}{ds} = \frac{dx(s)}{ds}\vec{i} + \frac{dy(s)}{ds}\vec{j} \tag{2.3}$$

$$\vec{e}_n = \vec{e}_t \times \vec{k} = \frac{dy(s)}{ds}\vec{i} - \frac{dx(s)}{ds}\vec{j} \tag{2.4}$$

Figure (2.3) shows the origin of *s*-direction for different cases (no-web, one-web and two-web cases). It should be noted that the ply angle θ here is always measured from the positive *s* -direction at first quadrant of curvilinear coordinate of system.

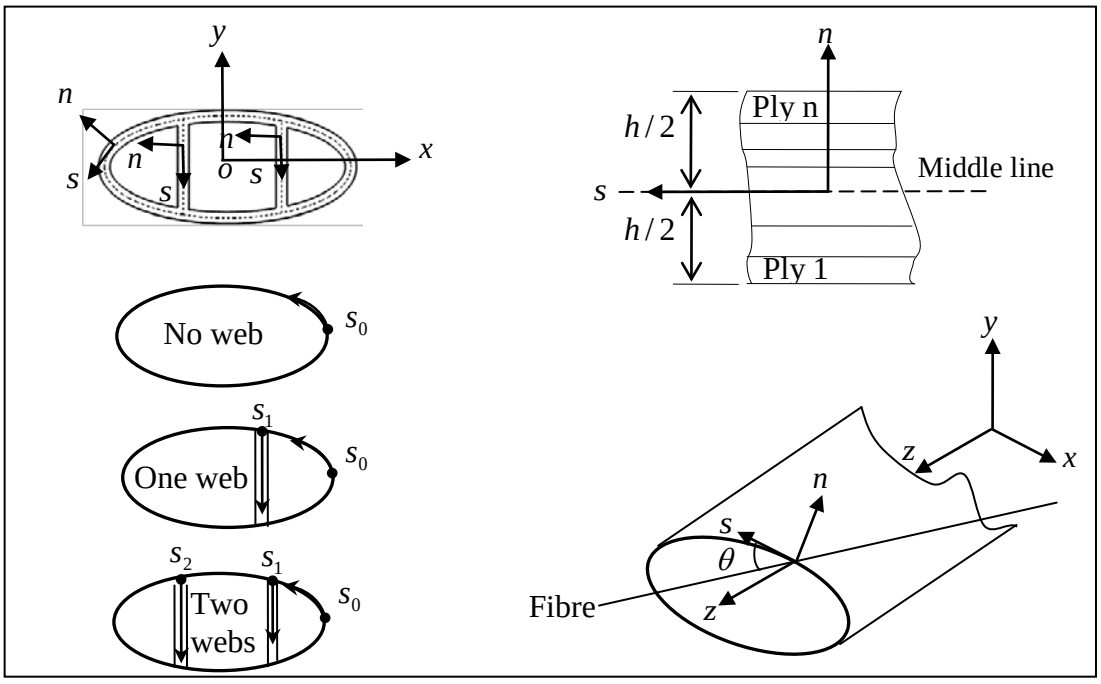

Figure 2.3-$(x-y-z)$ and $(s-z-n)$ coordinate of systems

2.3.3 Thin-Walled Beams: General Assumptions

Thin-walled beams are defined as slender structures whose distinctive geometric dimensions are all of different orders of magnitude. Compared to the cross-sectional dimensions, the thickness is very small and the beam length is

significantly greater. Furthermore, thin-walled beams also can be classified by geometrical features as double symmetric, single symmetric or general cross-section, open or closed cross-section, straight or curved and straight or twisted.

In order to develop the thin-walled composite beam model, the following assumptions, which are valid for case of wind turbine blades, are made:

- The shape of the cross-section and its geometrical dimensions remain invariant in its plane. However, normal deformations are permitted to warp out of their original planes. In case of wind turbine blades, the original cross-sectional shape is always maintained un-deformed in its plane by employing transverse stiffening members (webs). Webs are assumed rigid within their plane but deformable normal to their own plane.
- The transverse shear strains are uniform over the beam cross-section.
- Thin-walled beams are considered only (primary warping considered only).
- For geometrical linear theory, the displacements are assumed as infinitesimal.

2.3.4 Reduced Constitutive Equation of Orthotropic Materials

The distinctiveness between usual isotropic beams and composite beams is laid on the constitutive equation of elements of layers. In adaptive blades, unidirectional fibre-reinforced composite laminate is used as the blade material because of its special tailor characteristic for generating various elastic couplings. An elementary cell of a unidirectional composite lamina can be treated as being made of a fibre embedded in matrix with more than one layers. Thus, the material behaves as an orthotropic material. Orthotropic materials have three mutually orthogonal, symmetry planes. Compliance and stiffness matrixes are given in principal reference system $(1-2-3)$, shown in Figure (2.4), by Equation (2.5).

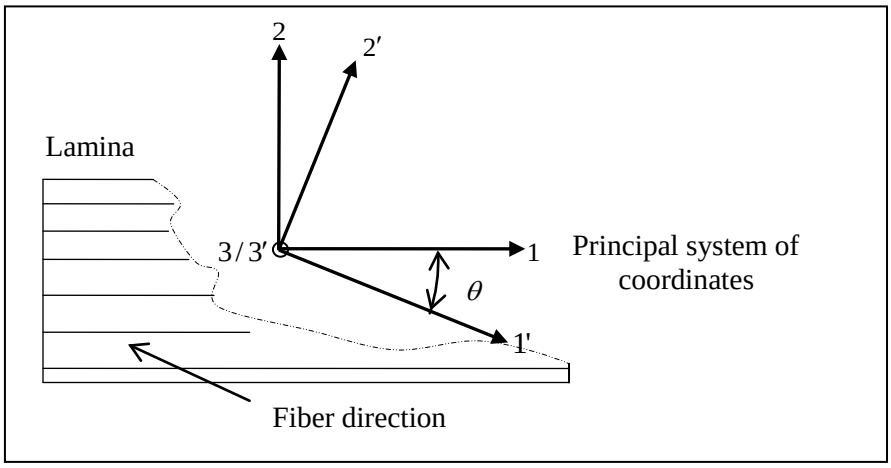

Figure 2.4-Principal (1-2-3) and reference (1'-2'-3) coordinate of systems

$$[S]=\begin{bmatrix} 1/E_1 & -\nu_{12}/E_1 & -\nu_{13}/E_1 & 0 & 0 & 0 \\ -\nu_{21}/E_2 & 1/E_2 & -\nu_{23}/E_2 & 0 & 0 & 0 \\ -\nu_{31}/E_3 & -\nu_{32}/E_3 & 1/E_3 & 0 & 0 & 0 \\ 0 & 0 & 0 & 1/G_{23} & 0 & 0 \\ 0 & 0 & 0 & 0 & 1/G_{31} & 0 \\ 0 & 0 & 0 & 0 & 0 & 1/G_{12} \end{bmatrix} \tag{2.5}$$

$$[C]=[S]^{-1}=\begin{bmatrix} C_{11} & C_{12} & C_{13} & 0 & 0 & 0 \\ C_{12} & C_{22} & C_{23} & 0 & 0 & 0 \\ C_{13} & C_{23} & C_{33} & 0 & 0 & 0 \\ 0 & 0 & 0 & C_{44} & 0 & 0 \\ 0 & 0 & 0 & 0 & C_{55} & 0 \\ 0 & 0 & 0 & 0 & 0 & C_{66} \end{bmatrix} \tag{2.6}$$

Matrix $[C]$ stands for the stiffness matrix. The entries of this matrix are given in Appendix A.

To have layer properties along a different set of axes, the stresses/strains can be calculated by employing the transformation tensor as given by Equations (2.7) through (2.10).

$$\{\sigma'\}=T(\theta)\{\sigma\} \tag{2.7}$$

$$\{\gamma'\}=\tilde{T}(\theta)\{\gamma\} \tag{2.8}$$

$$T(\theta)=\begin{bmatrix} m^2 & n^2 & 0 & 0 & 0 & 2mn \\ n^2 & m^2 & 0 & 0 & 0 & -2mn \\ 0 & 0 & 1 & 0 & 0 & 0 \\ 0 & 0 & 0 & m & -n & 0 \\ 0 & 0 & 0 & n & m & 0 \\ -mn & mn & 0 & 0 & 0 & m^2-n^2 \end{bmatrix} \tag{2.9}$$

$$\tilde{T}(\theta)=\begin{bmatrix} m^2 & n^2 & 0 & 0 & 0 & mn \\ n^2 & m^2 & 0 & 0 & 0 & -mn \\ 0 & 0 & 1 & 0 & 0 & 0 \\ 0 & 0 & 0 & m & -n & 0 \\ 0 & 0 & 0 & n & m & 0 \\ -2mn & 2mn & 0 & 0 & 0 & m^2-n^2 \end{bmatrix} \tag{2.10}$$

Where $\gamma_{ij} \equiv \varepsilon_{ij}$ for $i = j$ and $\gamma_{ij} \equiv 2\varepsilon_{ij}$ for $i \neq j$. Here ε_{ij} denote the axial strain components. σ', γ', σ, γ denote the stress and strain tensor in the primed and un-primed reference system; and $m = \cos(\theta)$, $n = \sin(\theta)$, where θ denotes fibre angle between axis 1' and the principal axis 1 measured anticlockwise. The stiffness matrix of an elementary cell of layer in the reference system (1'-2'-3) is given by Equations (2.11) and (2.12).

$$[\overline{C}] = [T(\theta)]^{-1}[C][\tilde{T}(\theta)] \tag{2.11}$$

$$[\overline{C}]=\begin{bmatrix} \overline{C}_{11} & \overline{C}_{12} & \overline{C}_{13} & 0 & 0 & \overline{C}_{16} \\ \overline{C}_{12} & \overline{C}_{22} & \overline{C}_{23} & 0 & 0 & \overline{C}_{26} \\ \overline{C}_{13} & \overline{C}_{23} & \overline{C}_{33} & 0 & 0 & \overline{C}_{36} \\ 0 & 0 & 0 & \overline{C}_{44} & \overline{C}_{45} & 0 \\ 0 & 0 & 0 & \overline{C}_{45} & \overline{C}_{55} & 0 \\ \overline{C}_{16} & \overline{C}_{26} & \overline{C}_{36} & 0 & 0 & \overline{C}_{66} \end{bmatrix} \tag{2.12}$$

The constitutive equation for an element in one layer of a laminate is expressed in curvilinear system of coordinates by Equation (2.13). The entries of matrix $[\overline{C}]$ are listed in Appendix A.

$$\begin{Bmatrix} \sigma_{ss} \\ \sigma_{zz} \\ \sigma_{nn} \\ \tau_{zn} \\ \tau_{ns} \\ \tau_{zs} \end{Bmatrix} = \begin{bmatrix} C'_{11} & C'_{12} & C'_{13} & 0 & 0 & C'_{16} \\ C'_{12} & C'_{22} & C'_{23} & 0 & 0 & C'_{26} \\ C'_{13} & C'_{23} & C'_{33} & 0 & 0 & C'_{36} \\ 0 & 0 & 0 & C'_{44} & C'_{45} & 0 \\ 0 & 0 & 0 & C'_{45} & C'_{55} & 0 \\ C'_{16} & C'_{26} & C'_{36} & 0 & 0 & C'_{66} \end{bmatrix} \begin{Bmatrix} \varepsilon_{ss} \\ \varepsilon_{zz} \\ \varepsilon_{nn} \\ \gamma_{zn} \\ \gamma_{ns} \\ \gamma_{sz} \end{Bmatrix} \tag{2.13}$$

Beam cross-sections are rigid without deformations in cross-section plane - one of the basic beam assumptions made in Section 2.1.3- leads to the fact that the stresses σ_{ss}, σ_{nn} and τ_{ns} can be neglected (or $\sigma_{ss} = \sigma_{nn} = \tau_{ns} \approx 0$). Equation (2.13) is thus reduced to Equation (2.14):

$$\begin{Bmatrix} \sigma_{zz} \\ \tau_{zs} \\ \tau_{zn} \end{Bmatrix}_k = \begin{bmatrix} \tilde{C}_{11} & \tilde{C}_{12} & 0 \\ \tilde{C}_{12} & \tilde{C}_{22} & 0 \\ 0 & 0 & \tilde{C}_{33} \end{bmatrix}_k \begin{Bmatrix} \varepsilon_{zz} \\ \gamma_{zs} \\ \gamma_{zn} \end{Bmatrix}_k \tag{2.14}$$

The entries of the reduced stiffness matrix are also given in Appendix A.

2.4 Single-Cell Beam Model

Displacement and strain field for a generic point on the cross-section of thin-walled composite beam with closed section (single-cell) are derived from Librescu and Song's (2006) geometrical linear beam theory (GLBT). This theory considers non-classical effects such as transverse shear and cross-section warping. The deformation analysis of thin-walled beam translates into how to solve six unknown deformations at each cross-section. Kinematics of entire beam is known when six deformations at each cross-section are known.

2.4.1 Displacement Field

Referring to the key assumption stated in Section 2.3.3, since the cross-section is un-deformable in its own plane, the only possible motion of the section in its own plane is the rigid body motion. That is, the only possible movements of cross-section are restricted to translations and rotations associated with a reference point in cross-section (Figure (2.5)).

Displacement vector of a generic point on the middle-line of cross-section is given by:

$$\vec{u}(x,y,z) = u\vec{i} + v\vec{j} + w\vec{k} \tag{2.15}$$

in which, u, v and w are displacements along the x, y and z directions respectively.

Displacements u and v can be described in terms of those of a reference point $P(x_{pole}, y_{pole})$, called pole, and of the angle of rotation $\phi(z,t)$ of the cross-section about pole.

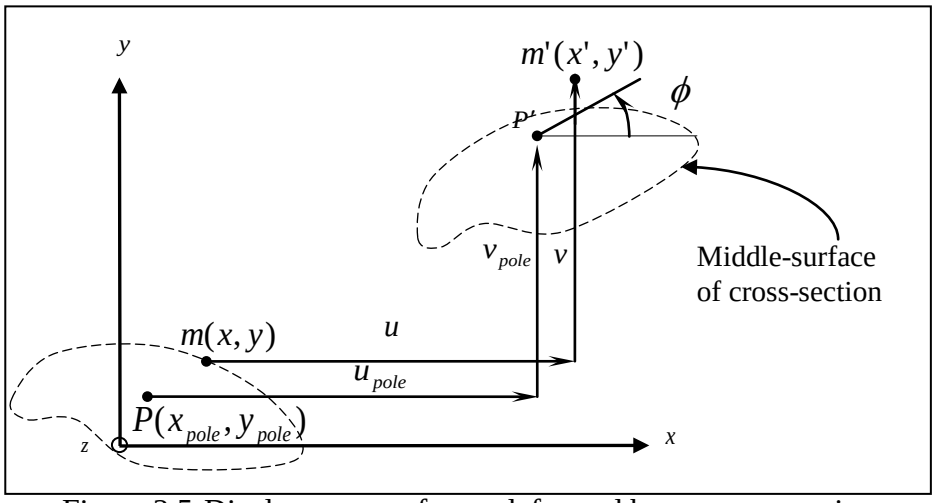

Figure 2.5-Displacements of a un-deformed beam cross-section

Assuming small rotation of the cross-section, the transverse displacements of a general point on the middle-line of the cross-section can be represented in terms of pole's displacements and rotation along pole axis:

$$u(x,y,z) = u_{pole}(z) - (y - y_{pole})\phi(z) \tag{2.16}$$

$$v(x,y,z) = v_{pole}(z) + (x - x_{pole})\phi(z) \tag{2.17}$$

In the above kinematic equations, u_{pole} and v_{pole} stand for the transverse displacements of the reference point P (pole).

In order to calculate membrane strains around the contour of the cross-section, it is necessary to transfer displacements from Cartesian system of coordinates to curvilinear system of coordinates. The vector of resultant displacements in curvilinear system of coordinates consists of three components (u_t, u_n, w) and is expressed as:

$$\vec{u}(x,y,z,t) = u_t\vec{e}_t + u_n\vec{e}_n + w\vec{k} \tag{2.18}$$

where, u_t, u_n are in-plane displacements components defined as:

$$u_t = \vec{u}\cdot\vec{e}_t = u\frac{dx}{ds} + v\frac{dy}{ds} = u_p\frac{dx}{ds} + v_p\frac{dy}{ds} + r_n\phi \tag{2.19}$$

$$u_n = \vec{u}\cdot\vec{e}_n = u\frac{dy}{ds} - v\frac{dx}{ds} = u_p\frac{dy}{ds} - v_p\frac{dx}{ds} - r_t\phi \tag{2.20}$$

where, r_n, r_t are defined as:

$$r_n(s) = (x - x_{pole})dy/ds - (y - y_{pole})dx/ds \tag{2.21}$$

$$r_t(s) = (x - x_{pole})dx/ds + (y - y_{pole})dy/ds \tag{2.22}$$

For the points off the middle-line of cross-section, the displacements vector is defined as in Equation (2.23) with its in-plane components U_t and U_n defined by Equations (2.24) and (2.25).

$$\vec{U}(X,Y,z) = U_t\vec{e}_t + U_n\vec{e}_n + w\vec{k} \tag{2.23}$$

$$U_t = \vec{U}\cdot\vec{e}_t = u_p\frac{dX}{dS} + v_p\frac{dY}{dS} + R_n\phi \tag{2.24}$$

$$U_n = \vec{U}\cdot\vec{e}_n = u_p\frac{dY}{dS} - v_p\frac{dX}{dS} - R_t\phi \tag{2.25}$$

where,

$$R_n = r_n + n \tag{2.26}$$

$$R_t = r_t \tag{2.27}$$

$$dS = (1 + \frac{n}{r_n})ds \tag{2.28}$$

Normal displacement of generic points on and off the middle-line on cross-section is derived from definition of γ_{sz}. Assuming that the closed beam is subjected to external shear, bending moment and torsional loads. Incorporating transverse shear effects and assuming that the shear stresses induced in the 3-D medium of the beam exhibit a linear variation in the thickness direction, the net shear strain Γ_{sz} of any point of the beam cross-section can be therefore expressed as (Nishino et al, 1977)

$$\Gamma_{sz} = l\gamma_{yz} - m\gamma_{xz} + n_{sz}/(hG_{sz}) + nN_{sz}/(hG_{sz}) \tag{2.29}$$

Equation (2.29) can be explained as that the net engineering membrane shear strain (Γ_{sz}) of a general point off the middle-line on the cross-section, consists of transverse shear strain (γ_{yz} and γ_{xz}) components projected in tangential direction ($l\gamma_{yz} - m\gamma_{xz}$) caused by shear forces and torsional shear strain $n_{sz}/(hG_{sz}) + nN_{sz}/(hG_{sz})$ in tangential direction caused by torsional moment. Here, $\hat{N}_{sz}$ and $\hat{\hat{N}}_{sz}$ stand for the tangential shear flows in the cross-section evaluated at coordinate $n = h/2$ and $n = -h/2$ respectively. $n_{sz} \equiv (\hat{N}_{sz} + \hat{\hat{N}}_{sz})/2$ and $N_{sz} \equiv (\hat{N}_{sz} - \hat{\hat{N}}_{sz})/h$ indicate the average shear flow and the thickness-wise shear flow respectively; $l = dy/ds$, $m = -dx/ds$. Parameter G_{sz} denotes the tangential shear stiffness of the laminate. Here, n_{sz} and N_{sz} are unknown but later derivation would make it related to rotation angle ϕ.

The mid-line shear strain is expressed by Equation (2.30)

$$\gamma_{sz} = \frac{\partial w}{\partial s} + \frac{\partial u_t}{\partial z} \tag{2.30}$$

The off mid-line counterpart of shear strain is expressed by Equation (2.31)

$$\Gamma_{sz} = \frac{\partial W}{\partial S} + \frac{\partial U_t}{\partial z} \tag{2.31}$$

Substituting for shear strains from Equations (2.30) and (2.31) back into Equation (2.29) one obtains:

$$\frac{\partial W}{\partial S} = (\gamma_{xz} - u'_p)\frac{dX}{dS} + (\gamma_{yz} - v'_p)\frac{dY}{dS} + n_{sz}/(hG_{sz}) + nN_{sz}/(hG_{sz}) - R_n\phi' \tag{2.32}$$

Since W must be continuous around the circumference of the closed cross-section contour, it must satisfy the condition $\oint_S \frac{\partial W}{\partial S} = 0$, in cooperation with Equation (2.32) and considering n_{sz} and N_{sz} are independent on the S-coordinate, one can get

$$n_{sz} = \frac{\oint r_n ds}{\oint \frac{ds}{h(s)G_{sz}(s)}}\phi'(z) \tag{2.33}$$

and

$$N_{sz} = \frac{2\oint ds}{\oint \frac{ds}{h(s)G_{sz}(s)}}\phi'(z) \tag{2.34}$$

Equations (2.33) and (2.34) denote that the shear flow around the cross-section contour and shear flow variation along the thickness wise are only associated with twist angle ϕ and contour shape.

Integrating Equation (2.32) with respect to S-coordinate from a conveniently chosen contour origin $O(X_0, Y_0)$ and substituting for n_{sz} and N_{sz} from Equations (2.33) and (2.34), the normal displacements is obtained as

$$w(s,z,n) = w_0(z) + \theta_y(z)(x + n\frac{dy}{ds}) + \theta_x(z)(y - n\frac{dx}{ds}) - \phi'(z)\int_0^s (r_n(s) - \frac{2\Omega}{h(s)G_{sz}(s)L})ds \quad (2.35)$$

In the kinematic Equation (2.35), z-axis is treated as pole axis through the beam (x_{pole} = y_{pole} =0). Parameter w_0 is the longitudinal displacement of origin of coordinate s marked as s_0 , which is also called the sectorial origin and conveniently chosen on the centreline of the cross-section. Parameters $h(s)$ and $G_{sz}(s)$ are the shell thickness and the shear modulus of the laminate under curvilinear system of coordinates, respectively, both function of s-coordinate. Other parameters are defined as follows: Ω is the area inside the centreline of the cross-section for single-cell beam; $L = \oint \frac{ds}{h(s)G_{sz}(s)}$; θ_x and θ_y the cross-section rotations about x-, y-axis at pole position:

$$\theta_x(z,t) = \gamma_{yz} - v_p' \quad (2.36)$$

$$\theta_y(z,t) = \gamma_{xz} - u_p' \quad (2.37)$$

2.4.2 Strain Field in Curvilinear Coordinates of System

Since unidirectional fibre-reinforced composite materials behave as elastic materials, the same strain-displacement relations are thus valid for them. Strain field $\varepsilon_{zz}, \gamma_{sz}, \gamma_{nz}$ of generic points (on or off mid-line of cross-section) on closed single-cell cross-section under the ($s-z-n$) coordinate of system without considering secondary warping is given as

$$\varepsilon_{zz}(s,z,n) = w_0' + \theta_x'(y - n\frac{dx}{ds}) + \theta_y'(x + n\frac{dy}{ds}) - \phi''(z)\left\{\int_0^s r_n(s)ds - \int_0^s \frac{2\Omega}{h(s)G_{sz}(s)L}ds\right\} \tag{2.38}$$

$$\gamma_{sz}(s,z,n) = [\theta_y(z) + u_{pole}']\frac{dx}{ds} + [\theta_x(z) + v_{pole}']\frac{dy}{ds} + \phi'(z)\left\{\frac{2\Omega}{h(s)G_{sz}(s)L} + \frac{2n\beta_p}{h(s)G_{sz}(s)L}\right\} \tag{2.39}$$

$$\gamma_{nz}(s,z,n,) = [\theta_y(z) + u_{pole}']\frac{dy}{ds} - [\theta_x(z) + v_{pole}']\frac{dx}{ds} \tag{2.40}$$

where, β_p denotes perimeter enclosed by the centre line of the single cell beam cross-section, and $(\,)'$ and $(\,)''$ denote the first and second derivative with respect to z coordinate.

2.4.3 Force-Deformation Equations

Generally, a thin-walled beam can be subjected to complex loadings including biaxial bending, torsional moment, transverse shear and axial force. Furthermore, if the beam is constructed of anisotropic materials, elastic couplings such as bending-twist and stretch-twist are also induced. At a given span location z shown in Figure (2.6), integrating the stress field (keeping in mind that $\sigma_{ss} = \sigma_{nn} = \tau_{ns} \approx 0$) on the cross-section and equating it with internal forces at that span location leads to Equations (2.41) to (2.46):

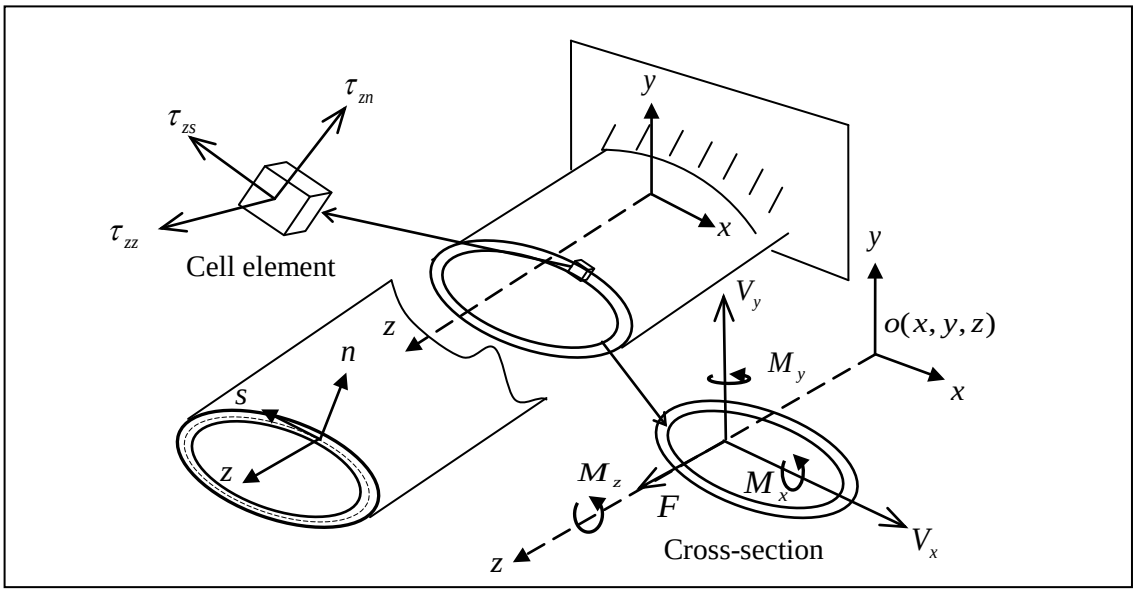

Figure 2.6- Resultant forces of a cross-section

$$F_z(z) = \iint \sigma_{zz} dsdn \tag{2.41}$$

$$Q_x(z) = \iint \tau_{zs} \vec{e_t} \cdot \vec{i}\, dsdn + \iint \tau_{zn} \vec{e_n} \cdot \vec{i}\, dsdn \tag{2.42}$$

$$Q_y(z) = \iint \tau_{zs} \vec{e_t} \cdot \vec{j}\, dsdn + \iint \tau_{zn} \vec{e_n} \cdot \vec{j}\, dsdn \tag{2.43}$$

$$M_x(z) = \iint \sigma_{zz}(y - ndx/ds) dsdn \tag{2. 44}$$

$$M_y(z) = -\iint \sigma_{zz}(x + ndz/ds) dsdn \tag{2. 45}$$

$$\begin{aligned} M_z(z) = &\iint -(\tau_{zs}\vec{e}_t \cdot \vec{i} + \tau_{zn}\vec{e}_n \cdot \vec{i})(y - n\frac{dx}{ds}) dsdn \\ &+ \iint (\tau_{zs}\vec{e}_t \cdot \vec{j} + \tau_{zn}\vec{e}_n \cdot \vec{j})(x + n\frac{dy}{ds}) dsdn \end{aligned} \tag{2. 46}$$

where, $F_z(z)$, $Q_x(z)$ and $Q_y(z)$ denote the resultant axial and shear forces in the z-, x- and y- directions respectively, $M_x(z)$, $M_y(z)$ and $M_z(z)$ denote the resultant moments along the x-, y- and z- axis respectively, $\vec{i}$ and $\vec{j}$ denote the unit vectors

in the x and y directions and $\vec{e}_t$ and $\vec{e}_{\mathrm{n}}$ denote the unit vectors in s- and n-direction respectively.

In deriving the above equation, it is assumed that the bi-moment is zero as explained below. When beams with noncircular cross-sections are subjected to torsion, cross-section warping occurs. In case of thin-walled beams, this cross-sectional warping is caused by internal bi-moments. However, in case of wind turbine blades, the bi-moment can be reasonably neglected as the torque (pitching moment) on wind turbine blade is negligible compared to (flap and edge) bending moments.

Assuming the primary warping has no effect on normal strain, then the terms including second differential of ϕ in the strain field ($\phi''(z)\left\{\int_0^s r_n(s)ds - \int_0^s \frac{2\Omega}{h(s)G_{sz}(s)L}ds\right\}$) can be neglected. Combining Equations (2.14), (2.38), (2.39) and (2.40), and substituting for stresses in Equations (2.41) through (2.46), the force deformation equations can be obtained as:

$$\begin{bmatrix} F_z(z) \\ Q_x(z) \\ Q_y(z) \\ M_z(z) \\ M_x(z) \\ M_y(z) \end{bmatrix} = \begin{bmatrix} K_{11} & K_{12} & K_{13} & K_{14} & K_{15} & K_{16} \\ K_{21} & K_{22} & K_{23} & K_{24} & K_{25} & K_{26} \\ K_{31} & K_{32} & K_{33} & K_{34} & K_{35} & K_{36} \\ K_{41} & K_{42} & K_{43} & K_{44} & K_{45} & K_{46} \\ K_{51} & K_{52} & K_{53} & K_{54} & K_{55} & K_{56} \\ K_{61} & K_{62} & K_{63} & K_{64} & K_{65} & K_{66} \end{bmatrix} \begin{bmatrix} w_0'(z) \\ \theta_y'(z) \\ \theta_x'(z) \\ \theta_y + u_{pole}' \\ \theta_x + v_{pole}' \\ \phi'(z) \end{bmatrix} \tag{2.47}$$

Equation (2.47) defines the relations between the internal forces at each section and the rate of change of deformation, through the stiffness matrix $[K_{ij}]$ (i, j =1 to 6). For a cross-section, magnitude of entries of $[K_{ij}]$ only depends on the shape of the cross-section, the thickness of layers, the material properties and fibre angle of each layer. Entries $[K_{ij}]$ are listed in Appendix B.

2.5 Multi-Cell Beam Model for Deformation Analysis

For multi-cell thin-walled composite beams the transverse displacements u and v of a general point on cross-section are obtained through translations and rotation associated with pole the same as single-cell beams. However, the normal displacement for multi-cell beam is different from single-cell beams. Here, the normal displacement of multi-cell beams is derived through the definition of membrane shear strain and membrane shear stress during torsion with transverse shear effects superposed. Consider a thin-walled beam of arbitrary cross-section, (see Figure (2.7)), it consists of an arbitrary number of cells separated by thin webs, and the cross-sectional distortions during twisting are prevented by transverse stiffening members (ribs or frames), which are considered to be rigid within their plane, but perfectly flexible with regard to deformations normal to their planes.

Equation (2.33) gives relation between shear flow and rate of twist under free warping condition. By defining a modulus-weighted thickness as

$$\tilde{h}(s) = \frac{G_{sz}(s)}{\tilde{G}} h(s) \tag{2.48}$$

where, $\tilde{G}$ is a conveniently chosen shear modulus, and substituting back in Equation (2.33) for $h(s)G_{sz}(s)$ from Equation (2.48), and keeping in mind that $\oint r_n ds = 2\Omega$, the rate of twist can be determined as

$$\phi' = \frac{n_{sz}}{2\Omega\ \tilde{G}} \oint \frac{ds}{\tilde{h}} \tag{2.49}$$

Figure (2.7) shows a multi-cell beam subjected to a pure torque without warping restraint at any cross-section. The rate of twist of the R^{th} cell surrounded by m adjacent cells can be defined as

$$\phi'_R = \frac{1}{2\Omega_R \tilde{G}} (q_R \delta_R - \sum_{r=1}^{m} q_r \delta_{r,R}) \tag{2.50}$$

where, q_R and q_r are the constant shear flow in the R^{th} and other adjacent cells, Ω_R is the area enclosed by the R^{th} cell mid-line contour. δ_R and $\delta_{r,R}$ are defined as: $\delta_R = \oint \frac{ds}{\tilde{h}}$ (line integral along all the walls enclosing the R^{th} cell) and $\delta_{r,R} = \int_{r,R} \frac{ds}{\tilde{h}}$ (line integral along the common wall between the r^{th} - and R^{th} - cell).

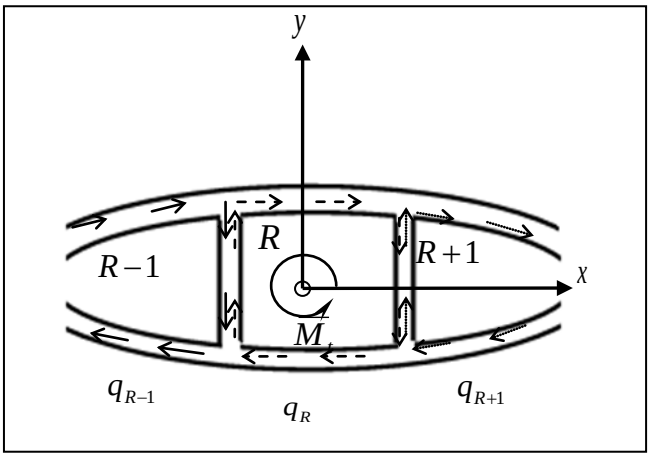

Figure 2.7-Multi-cell beam subjected to a pure torque

For a general closed section with N constituent cells beam, the rate of twist ϕ' for N cells can be expressed as below matrix

$$[\phi'] = [s][q] \tag{2.51}$$

where

$$[\phi'] = \left[\phi'_1, \phi'_2, \cdots \phi'_{N-1}, \phi'_N\right]^T \tag{2.52}$$

$$[q] = \left[q_1, q_2, \cdots q_{N-1}, q_N\right]^T \tag{2.53}$$

$$[s] \equiv \begin{bmatrix} s_{11} & s_{12} & 0 & 0 & \ldots 0 & 0 & 0 & 0 & 0 & 0 & 0 \\ s_{21} & s_{22} & s_{23} & 0 & \ldots 0 & 0 & 0 & 0 & 0 & 0 & 0 \\ \cdots & \cdots & \cdots & \cdots & \cdots & \cdots & \cdots & \cdots & \cdots & \cdots & \cdots \\ 0 & 0 & 0 & & \cdots 0 & s_{R,R-1} & s_{R,R} & s_{R,R+1} & 0 & 0 & 0 \\ \cdots & \cdots & \cdots & \cdots & \cdots & \cdots & \cdots & \cdots & \cdots & \cdots & \cdots \\ \cdots & \cdots & \cdots & \cdots & \cdots & \cdots & \cdots & \cdots & \cdots & \cdots & \cdots \\ 0 & \cdots & \cdots & \cdots & \cdots & \cdots & \cdots & \cdots & 0 & s_{N,N-1} & s_{N,N} \end{bmatrix} \tag{2.54}$$

The entries of flexibility matrix $[s]$ are defined as

$$s_{R,R} = \frac{1}{2\Omega_R \tilde{G}} \delta_R \tag{2.55}$$

$$s_{R,R-1} = \frac{1}{2\Omega_R \tilde{G}} \delta_{R,R-1} \tag{2.56}$$

$$s_{R,R+1} = \frac{1}{2\Omega_R \tilde{G}} \delta_{R,R+1} \tag{2.57}$$

In terms of relation among ϕ_1' to ϕ_N' for an N constituent cells beam ($\phi_1' = \phi_2' \cdots = \phi_{N-1}' = \phi_N' \equiv \phi'$), $[\phi']$ can be expressed as

$$[\phi'] = [\mathrm{I}]\phi' \tag{2.58}$$

where, $[\mathrm{I}]$ is $N \times 1$ unit vector.

Equation (2.51) can be re-written as

$$[q] = \begin{bmatrix} q_1 \\ q_2 \\ \vdots \\ q_N \end{bmatrix} = [s]^{-1}[I]\phi' = [H]\phi' = \begin{bmatrix} H_1 \\ H_2 \\ \vdots \\ H_N \end{bmatrix} \phi' \tag{2.59}$$

where, $[H] = [s]^{-1}[I]$, the shear flows in cells and common walls between two adjacent cells are described as

$$\begin{bmatrix} q_1 \\ q_{1,2} \\ q_2 \\ q_{2,3} \\ \vdots \\ q_N \end{bmatrix} = \begin{bmatrix} H_1 \\ H_2 - H_1 \\ H_2 \\ H_3 - H_2 \\ \vdots \\ H_N \end{bmatrix} \phi' = \begin{bmatrix} H^{1,1} \\ H^{1,2} \\ H^{2,2} \\ H^{2,3} \\ \vdots \\ H^{N,N} \end{bmatrix} \phi' \tag{2.60}$$

in which,

$$H^{i,j} = H_j - H_i \ \ (\ i \neq j \ ) \tag{2.61}$$

$$H^{i,j} = H_i \ \ (\ i = j \ ) \tag{2.62}$$

Therefore, the membrane shear strains γ_{yz} on the cell and the common wall of two adjacent cells caused by pure torque is determined as:

$$[\gamma_{sz}] = \begin{bmatrix} \gamma_{sz}^{1} \\ \gamma_{sz}^{1,2} \\ \gamma_{sz}^{2} \\ \gamma_{sz}^{2,3} \\ \vdots \\ \gamma_{sz}^{N} \end{bmatrix} = \begin{bmatrix} H_1 /(hG_{sz})_{1,1} \\ (H_2 - H_1)/(hG_{sz})_{1,2} \\ H_2 /(hG_{sz})_{2,2} \\ (H_3 - H_2)/(hG_{sz})_{2,3} \\ \vdots \\ H_N /(hG_{sz})_{N,N} \end{bmatrix} \phi' = \begin{bmatrix} \lambda^{1,1} \\ \lambda^{1,2} \\ \lambda^{2,2} \\ \lambda^{2,3} \\ \vdots \\ \lambda^{N,N} \end{bmatrix} \phi' = [\lambda]\phi' \tag{2.63}$$

where [λ] is defined as

$$\lambda^{i,j} = H^{i,j} /(hG_{sz})_{i,j} \tag{2.64}$$

Vectors [γ_{yz}] and [λ] are both $(2N-1)\,by\,1$ vectors. Parameter $(hG_{sz})_{i,j}$ denotes the thickness of cell multiply by shear modulus at the i^{th} cell (or between i^{th}-and j^{th}-cell). Using Equation (2.63) as shear strain induced by pure torque and superposing transverse shear strain, the strain field for thin-walled multi-cell beams can be derived. For multi-cell closed thin-walled beams, the shear strain γ_{sz} of general point on cross-section under curvilinear system of coordinates is defined by strain-displacement relations as Equation (2.31). Consider transverse

shear effect and assume that the shear strain caused by pure torque is no varied along thickness of cell thus shear strain for a general point on cross-section is defined by superposition method as

$$\gamma_{sz} = \gamma_{yz}\frac{dY}{dS} + \gamma_{xz}\frac{dX}{dS} + \frac{H^{i,j}\phi'}{(h(s)G(s))_{i,j}} \tag{2.65}$$

where γ_{yz} and γ_{xz} are unknown uniform distributed shear strain over cross-section caused by internal shear forces. Parameters X , Y , S denote the coordinates of a general point off the mid-line and $dS = (1+n/r_n)ds$. Combining Equation (2.31) with (2.65), the normal displacement component W is developed as below.

$$\begin{aligned}
\frac{\partial W}{\partial S} &= \gamma_{yz}\frac{dY}{ds} + \gamma_{xz}\frac{dX}{ds} + \frac{H^{i,j}\phi'}{(h(s)G_{sz}(s))_{i,j}} - \frac{\partial U_t}{\partial z} \\
&= \gamma_{yz}\frac{dY}{dS} + \gamma_{xz}\frac{dX}{dS} + \frac{H^{i,j}\phi'}{(h(s)G_{sz}(s))_{i,j}} - u_p'\frac{dX}{dS} - v_p'\frac{dY}{dS} - R_n\phi' \\
&= (\gamma_{yz} - v_p')\frac{dY}{dS} + (\gamma_{xz} - u_p')\frac{dX}{dS} + \frac{H^{i,j}\phi'}{(h(s)G_{sz}(s))_{i,j}} - R_n\phi' \\
&= \theta_x\frac{dY}{dS} + \theta_y\frac{dX}{dS} + \frac{H^{i,j}\phi'}{(h(s)G_{sz}(s))_{i,j}} - R_n\phi'
\end{aligned} \tag{2.66}$$

Integrating Equation (2.66) with respect to S from a conveniently chosen contour origin $O(X_o, Y_o)$ (see Figure (2.2)) to an arbitrary point M leads to

$$\begin{aligned}
W &= W_0 + \theta_x Y + \theta_y X + \phi'\int_0^S \left(\frac{H^{i,j}}{(h(s)G_{sz}(s))_{i,j}} - R_n\right)dS \\
&= W_0 + \theta_x Y + \theta_y X + \phi'\int_0^S (\lambda^{i,j} - R_n)dS \\
&= W_0 + \theta_x Y + \theta_y X + \phi'\int_0^s (\lambda^{i,j} - r_n - n)(1+\frac{n}{r_n})ds \\
&= w_0 + \theta_x Y + \theta_y X + \phi'\int_0^s (\lambda^{i,j} - r_n)ds
\end{aligned} \tag{2.67}$$

Here, w_0 and W_0 are interpreted as normal displacement of origin s and S and one can reasonably assume that $W_0 = w_0$ for thin-walled beams. Having found the normal displacement, the strain field for multi-cell beams is determined as follows:

$$\varepsilon_{zz}(s,z,n) = \frac{\partial W}{\partial z} = w_0^{'} + \theta_x^{'}(y - n\frac{dx}{ds}) + \theta_y^{'}(x + n\frac{dy}{ds}) + \phi^{''}(z)\int_0^s \left(\lambda^{i,j} - r_n\right)ds \tag{2.68}$$

$$\gamma_{sz}(s,z,n) = \frac{\partial W}{\partial S} + \frac{\partial U_t}{\partial z} = [\theta_y(z) + u_p{'}]\frac{dx}{ds} + [\theta_x(z) + v_p{'}]\frac{dy}{ds} + \phi^{'}(z)\lambda^{i,j} \tag{2.69}$$

$$\gamma_{nz}(s,z,n) = \frac{\partial W}{\partial S} + \frac{\partial U_n}{\partial z} = [\theta_y(z) + u_p^{'}]\frac{dy}{ds} - [\theta_x(z) + v_p^{'}]\frac{dx}{ds} \tag{2.70}$$

Combining Equations (2.14), (2.68) through (2.70) and (2.41) through (2.46), the force-deformation relations is obtained with the same form as in Equation (2.47). However, in the coefficient matrix $[K_{ij}]$ of Equation (2.49) for multi-cell beams, six entries $K_{16}, K_{26}, K_{36}, K_{46}, K_{56}, K_{66}$, are different from correspondent entries in single-cell beam model respectively (see Appendix B).

To find the deformation of thin-walled composite beams by using the developed beam model, the following steps must be taken:

Step 1. Divide the beam into *n* segments

Step 2. Calculate the internal forces at each cross-section.

Step 3. Compute the entries of stiffness matrix $[K_{ij}]$ at each cross-section using numerical integration along ***s***.

Step 4. Solve the system of Equation (2.47) for the rate of change of deformations, namely, $w_0^{'}(z)$, $\theta_y^{'}(z)$, $\theta_x^{'}(z)$, $\phi^{'}(z)$, $\theta_y + u_{pole}^{'}$ and $\theta_x + v_{pole}^{'}$ at each cross-section.

Step 5. Apply boundary conditions to find $w_0(z)$, $\theta_x(z)$, $\theta_y(z)$ and $\phi(z)$ via numerical integration.

Step 6. Substitute back $\theta_x(z)$ and $\theta_y(z)$ obtained in Step 5 in $\theta_y + u'_{pole}$ and $\theta_x + v'_{pole}$ obtained in Step 4 to find u'_{pole} and v'_{pole}.

Step 7. Apply boundary conditions to find u_{pole} and v_{pole} via numerical integration.

2.6 Validation of Beam Model

In this section, validation of thin-walled composite beam model for single-/multi-cell beams is carried out: (i) by simple box-beams made of isotropic material and comparing the results with analytical results; (ii) by a single-cell box-beam made of composite material with implanted bend-twist and stretch-twist elastic coupling and comparing the results with experimental results and other analytical models; and (iii) by AWT-27 blade with various implanted bend-twist elastic couplings and comparing the results with numerical results obtained by ANSYS®.

2.6.1 Isotropic Box-Beam

Table (2.1) shows the geometric specifications and material properties of the thin-walled box-beam made of isotropic material. Tables (2.2) to (2.4) show the results obtained from analytical equations and the present thin-walled composite beam model for single-/two-/three-cell beams. It can be observed that results from present beam model by use of isotropic material are in good agreement with the analytical results with a maximum error of about only 2%.

Table 2.1-Geometric sand material of the isotropic box-beam

Box–beam geometric specifications		Materials specifications	
Length, l (m)	0.914	Young's modulus, E (GPa)	210
Width, b (m)	0.0242	Density, ρ (kg/m^3)	7800
Depth, d (m)	0.0136	Poisson ration, ν	0.3
Wall thickness, h (m)	0.000762		

Table 2.2-Comparison of the static results of isotropic single-cell box-beam

Single-cell box-beam				
Load	Analytical		Present model	Error (%)
Concentrated lateral load along H, $F_y = 4.45$(N)	Deflection $\delta = F_y L^3/(3EI)$	0.00309	0.00310	-0.32
	Slope $\theta = F_y L^2/(2EI)$	0.00508	0.00506	0.39
Distributed lateral load along H, $f_y = 44.5$(N/m)	Deflection $\delta = f_y L^4/(8EI)$	0.01060	0.01061	-0.09
	Slope $\theta = f_y L^3/(6EI)$	0.01544	0.01543	0.06

Table 2.3-Comparison of the static results of isotropic two-cell box-beam

Two-cell box-beam				
Load	Analytical		Present model	Error (%)
Concentrated lateral load along H, $F_y = 4.45$(N)	Deflection $\delta = F_y L^3/(3EI)$	0.00290	0.00290	0.00
	Slope $\theta = F_y L^2/(2EI)$	0.00476	0.00470	1.26
Distributed lateral load along H, $f_y = 44.5$(N/m)	Deflection $\delta = f_y L^4/(8EI)$	0.00960	0.00980	-2.08
	Slope $\theta = f_y L^3/(6EI)$	0.01451	0.01433	1.24

Table 2.4-Comparison of the static results of isotropic three-cell box-beam

Three-cell box-beam				
Load	Analytical		Present model	Error (%)
Concentrated lateral load along H, $F_y = 4.45$(N)	Deflection $\delta = F_y L^3/(3EI)$	0.00274	0.00270	1.46
	Slope $\theta = F_y L^2/(2EI)$	0.00450	0.00439	2.44
Distributed lateral load along H, $f_y = 44.5$(N/m)	Deflection $\delta = f_y L^4/(8EI)$	0.00939	0.00920	2.02
	Slope $\theta = f_y L^3/(6EI)$	0.01369	0.01337	2.34

2.6.2 Composite Box-Beams with Implanted Elastic Couplings

The present beam model is also validated by comparing the results with single-cell box-beams with bend-twist and stretch twist elastic couplings with the benchmark experimental results reported by Chandra et al (1990) as well as two

other analytical beam models developed by Chandra et al (1990) and Kim & White (1997). In these box beams, three bend-twist elastic couplings (circumferentially asymmetric stiffness (CAS) configurations CAS 1 to CAS 3) and three stretch-twist elastic couplings (circumferentially uniform stiffness (CUS) configurations CUS 1 to CUS 3) are investigated. The geometrical and material properties of the examined box beams are shown in Figure (2.8) and the CAS and CUS configurations are shown in Table (2.5).

Material properties of
AS4/3501-6 graphite/epoxy:
$E_{11} = 141.96GPa$
$E_{22} = E_{33} = 9.79GPa$
$G_{12} = G_{13} = 6.0GPa$
$G_{23} = 4.83GPa$
$\nu_{12} = \nu_{13} = 0.24$
$\nu_{23} = 0.5$
Geometry dimensions
$h = 0.000762m$
$b = 0.0242m$
$d = 0.0136m$
$l = 0.914m$

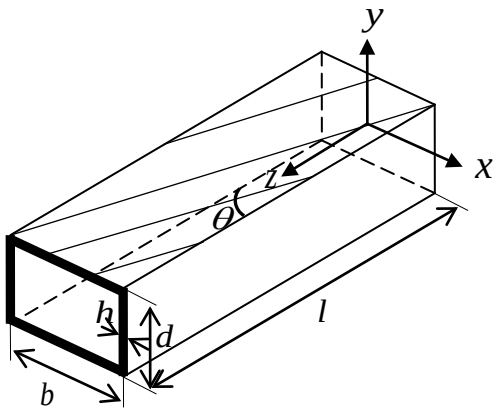

Figure 2.8-Geometry specification and composite material properties of a thin-walled box beam

Table 2.5-Thin-walled box beam layups

Box-Beam		Flanges		Webs	
Layup configurations		Top	Bottom	Left	Right
Bend-twist coupling	CAS 1	$[15]_6$	$[15]_6$	$[15/-15]_3$	$[15/-15]_3$
	CAS 2	$[30]_6$	$[30]_6$	$[30/-30]_3$	$[30/-30]_3$
	CAS 3	$[45]_6$	$[45]_6$	$[45/-45]_3$	$[45/-45]_3$
Stretch-twist coupling	CUS 1	$[15]_6$	$[-15]_6$	$[15]_6$	$[-15]_6$
	CUS 2	$[0/30]_3$	$[0/-30]_3$	$[0/30]_3$	$[0/-30]_3$
	CUS 3	$[0/45]_3$	$[0/-45]_3$	$[0/45]_3$	$[0/-45]_3$

The predicted induced twists by different models are compared with the measured induced twists and are shown in Figures (2.9) to (2.11).

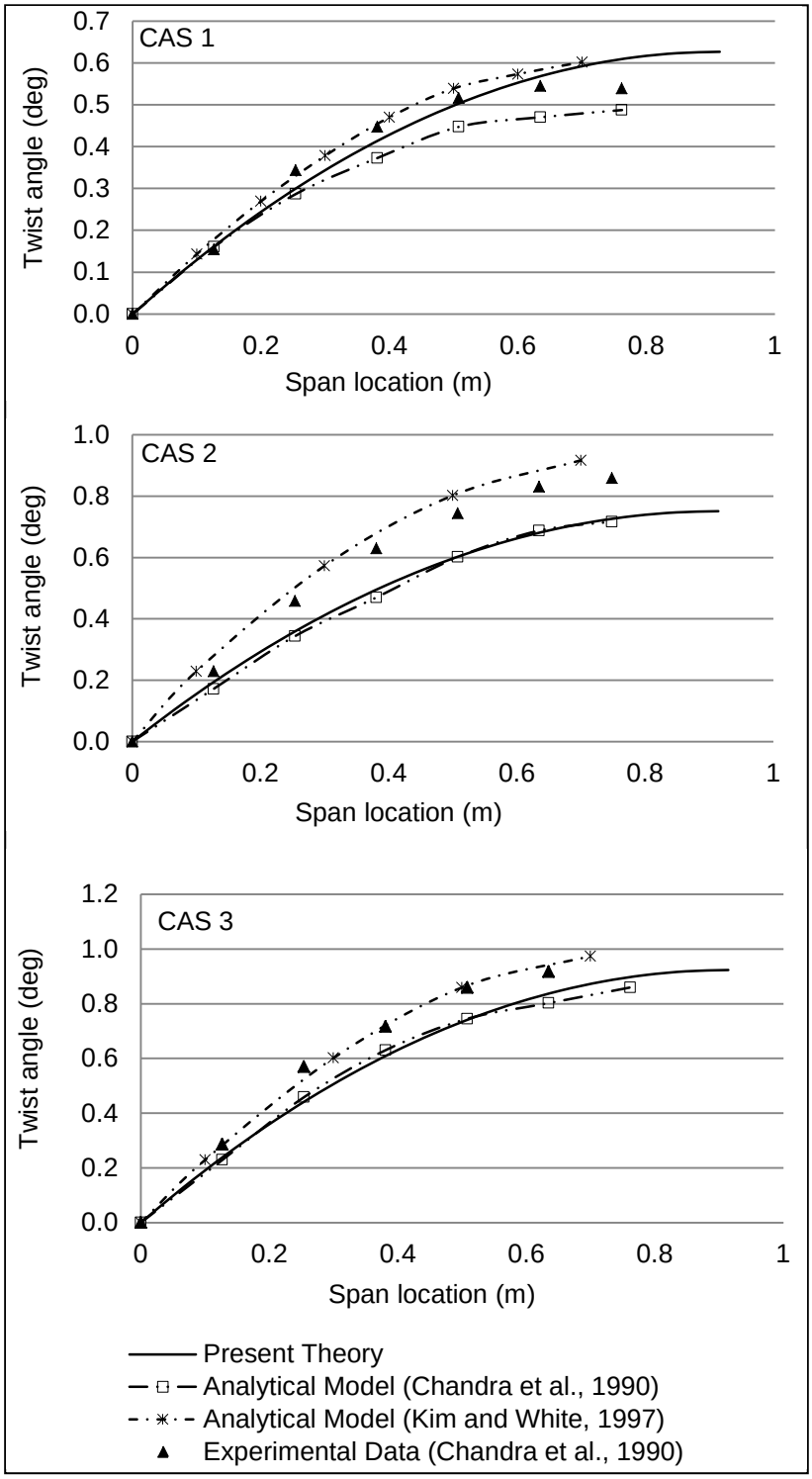

Figure 2.9-Twist angle under tip lateral load (bend-twist coupling)

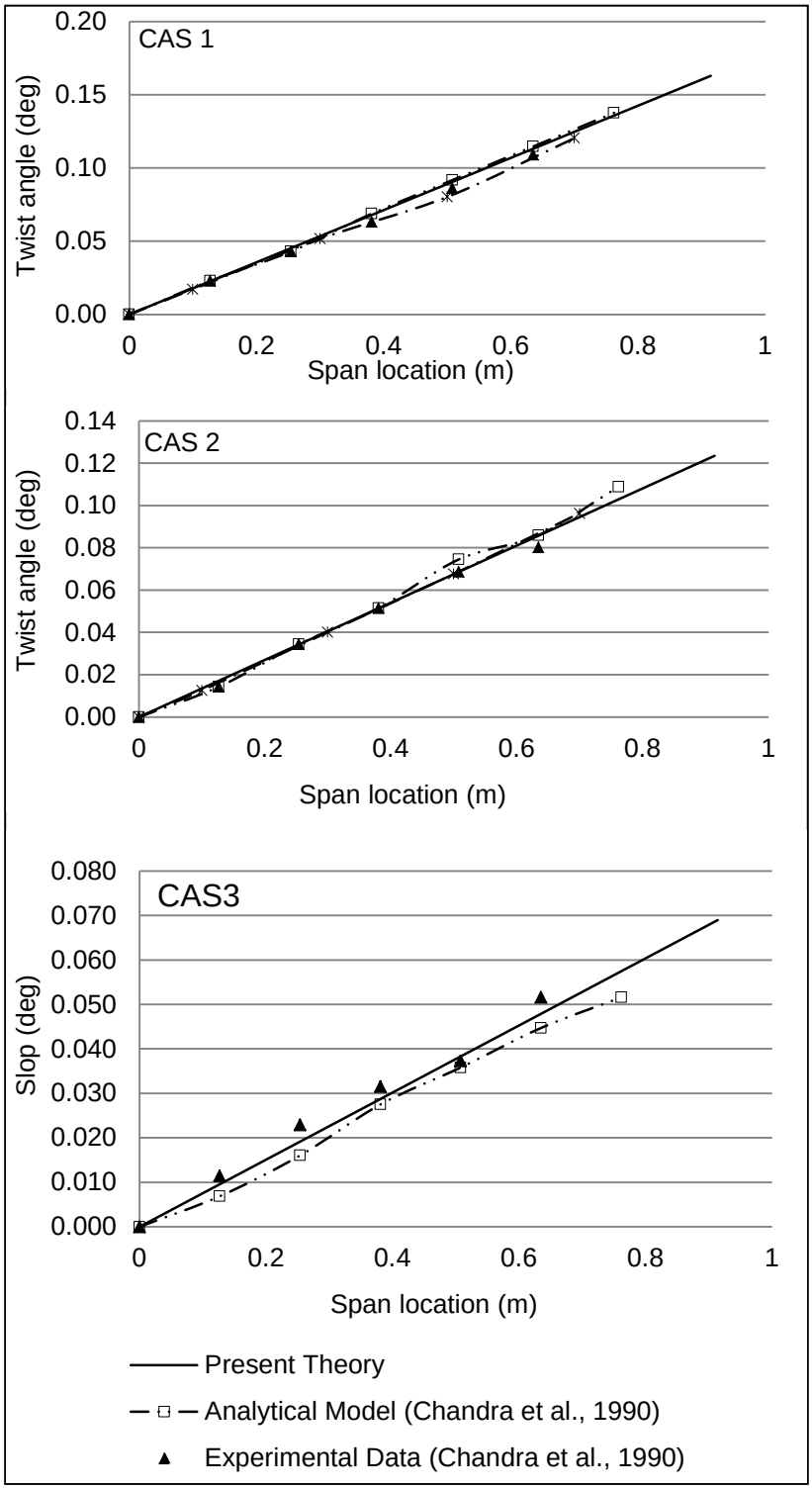

Figure 2.10-Twist angle under tip torsional moment (bend-twist coupling)

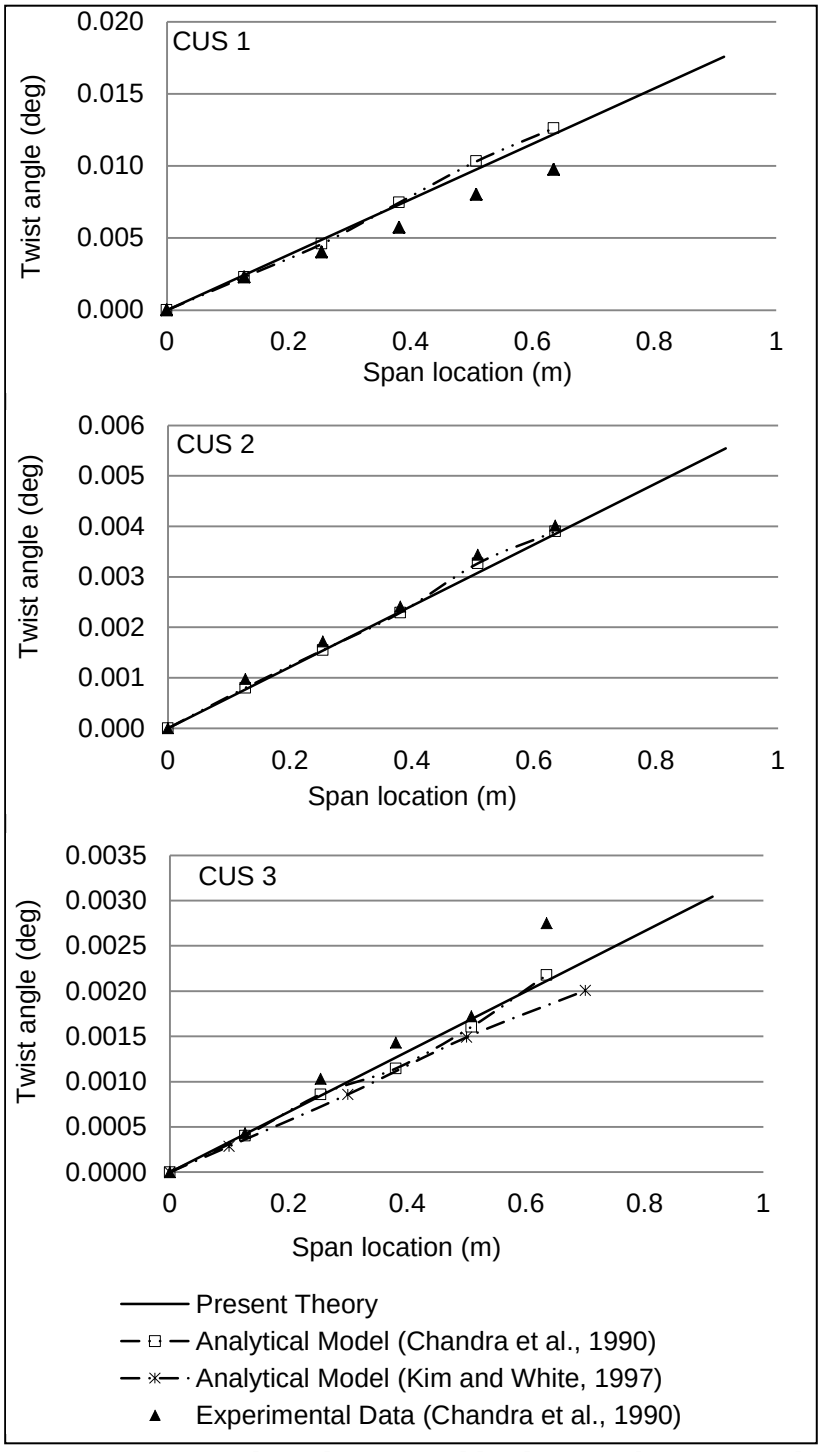

Figure 2.11-Twist angle under tip axial load (stretch-twist coupling)

It can be observed that the predicted results by the developed model are in good agreement with the experimental data. In most of cases, these results are in better agreement with the experimental results compared to the other two models. However, in case of the bend-twist box-beams subjected to the lateral tip load (Figure 2.9), the analytical model of Kim and White (1997) provides better

results. However, it should be noted that the Kim and White model is applicable only to simple geometries such as single-cell box beams.

2.6.3 Wind Turbine Adaptive Blade AWT-27

The blade of 300-kW stall-regulated AWT-27 wind turbine is employed for investigating the accuracy of the developed beam model in deformation analysis of elastic-coupled beams with complex geometries (twisted, variable chord and general cross-section). This blade is assumed to be made of carbon fibre/epoxy, the same material as the material of the box beam of Figure (2.8). The blade has a span length of 12.57m and it is constructed from S800 aerofoils. While aerodynamically, the blade consists of 10 aerofoils, structurally it is constructed from S809 (maximum aerofoil thickness 21%) and S814 (maximum aerofoil thickness 24%) aerofoils, as shown in Table (2.6). In this table c stands for the chord length, $t_{\max}$ is the maximum thickness of the aerofoil, R is the rotor radius and r is the radial location of the aerofoil, measured along the blade from the centre of the rotor.

Table 2.6- AWT-27 blade aerofoil distribution

Normalised span location r/R	Maximum thickness $t_{\max}/c$	Aerofoil #
0.26888	0.24	1
0.36025	0.24	2
0.4517	0.24	3
0.54307	0.24	4
0.63444	0.21	5
0.72581	0.21	6
0.80584	0.21	7
0.86291	0.21	8
0.96344	0.21	9
1	0.21	10

Chord length and pretwisted distributions are shown in Figure (2.12).

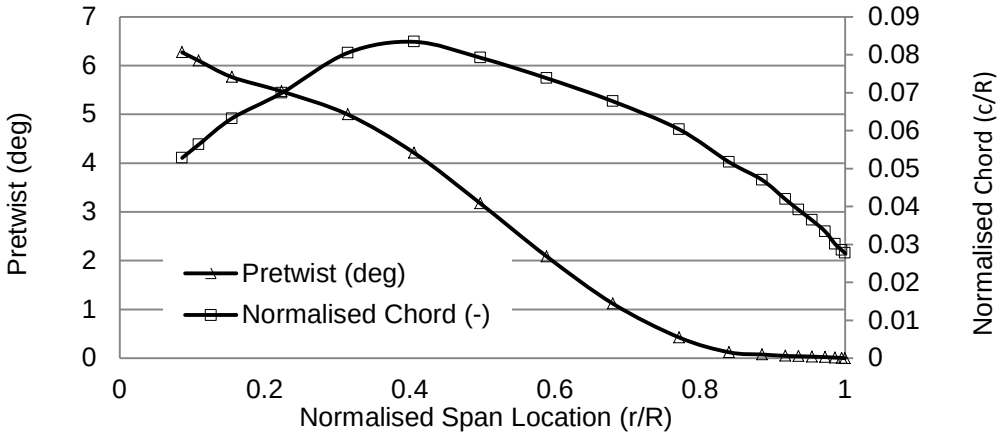

Figure 2.12-AWT-27 chord and pretwist distributions

Figure (2.13) shows the S809 and S814 aerofoil contours.

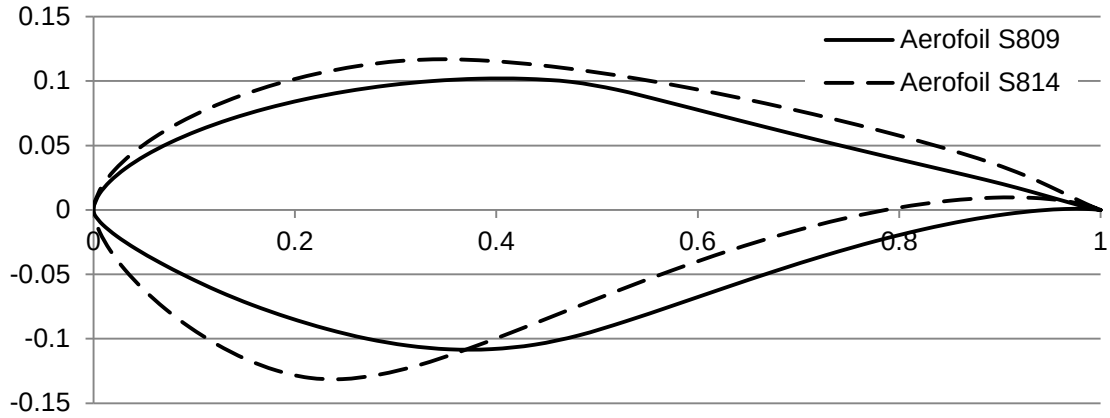

Figure 2.13- S809 and S814 aerofoil contours

WTAero (Maheri 2006a,2006e), an in-house wind turbine aerodynamic performance code, is used to obtain the external aerodynamic forces at operating condition of 10m/s wind speed and 53.3 rpm rotor speed. This software also gives the internal forces at specified number of sections (here 20). Figure (2.14) shows the external lift and drag aerodynamic force distributions. Figure (2.15) presents the internal forces as a function of blade span. It should be noted that the x and y coordinates shown in this figure are the global coordinates identical to the local coordinates at the hub (fixed end) of the blade.

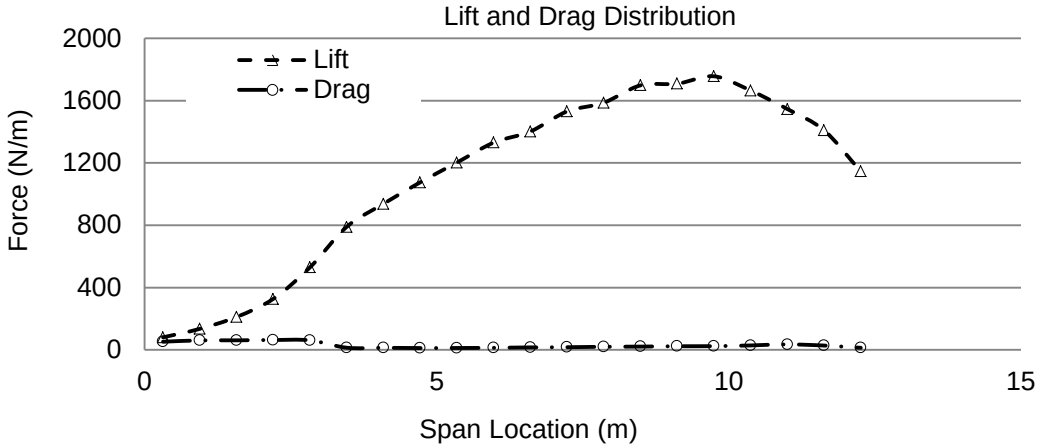

Figure 2.14-Lift and drag distributions along blade span

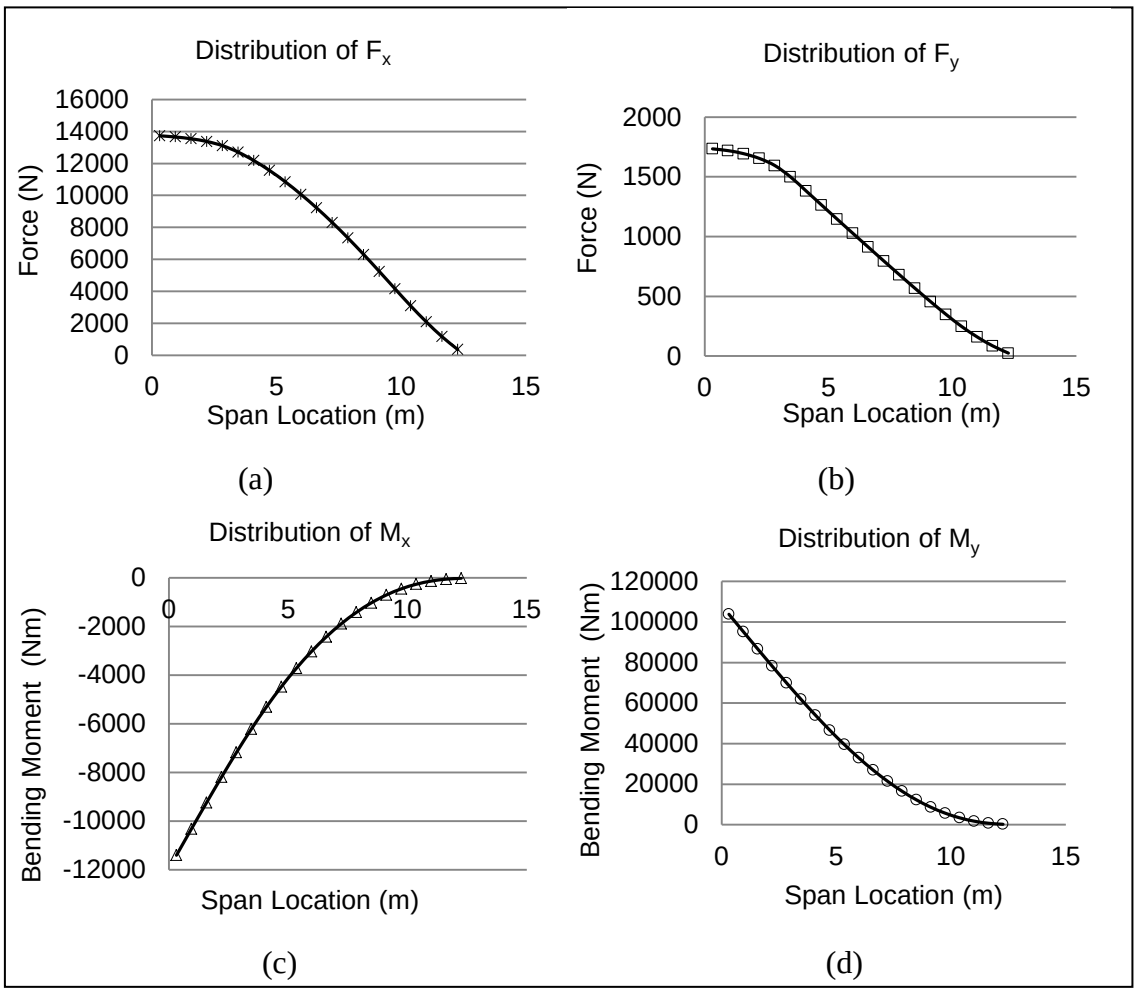

Figure 2.15-Internal forces along the blade span

In order to produce bend-twist elastic coupling, the fibre angle in the layers on the suction side (upper surface) of the blade are assumed to be mirrored with the layers on the pressure side (lower surface) of the blade; for example, $[40]_{20}$ for upper surface and $[-40]_{20}$ for the lower surface. Webs, where applicable, are assumed to be made of balanced layups. Fibre angles are measured from the positive direction of local *s*-coordinate. Using the developed beam model, various layup configurations with various thickness distributions are investigated and the results are compared with the FEA results obtained from ANSYS®.

Table (2.7) and Figure (2.16) show seven different thickness configurations along span wise. Table (2.8) summarises 19 different layup configurations with constant and varied thickness configurations.

Table 2.7- Configurations of variation of thickness along blade span

Thickness Config.	Distribution Style	Thickness Distribution
1	Linear	34mm to 15mm step 1
2		32mm to 13mm step 1
3		29mm to 10mm step 1
4		34mm to 24.5mm step 0.5
5		34mm to 19.75mm step 0.75
6	Quadratic	34.03mm to 15.3mm
7	Third degree	33.99mm to 14.92mm

Table 2.8- Layup configurations for adaptive blade AWT-27

Layup	Upper surface	Lower surface	Web 1 @ $x/c = 0.33$	Web 2 @ $x/c = 0.67$	$t_{shell}(mm)$
1	$[20]_{20}$	$[-20]_{20}$	-	-	20
2	$[30]_{20}$	$[-30]_{20}$	-	-	20
3	$[40]_{20}$	$[-40]_{20}$	-	-	20
4	$[50]_{20}$	$[-50]_{20}$	-	-	20
5	$[20]_{20}$	$[-20]_{20}$	$[45/-45]_{10}$	-	20
6	$[30]_{20}$	$[-30]_{20}$	$[45/-45]_{10}$	-	20
7	$[40]_{20}$	$[-40]_{20}$	$[45/-45]_{10}$	-	20
8	$[50]_{20}$	$[-50]_{20}$	$[45/-45]_{10}$	-	20
9	$[20]_{20}$	$[-20]_{20}$	$[45/-45]_{10}$	$[45/-45]_{10}$	20
10	$[30]_{20}$	$[-30]_{20}$	$[45/-45]_{10}$	$[45/-45]_{10}$	20
11	$[40]_{20}$	$[-40]_{20}$	$[45/-45]_{10}$	$[45/-45]_{10}$	20
12	$[50]_{20}$	$[-50]_{20}$	$[45/-45]_{10}$	$[45/-45]_{10}$	20
13	$[60]_{var}$	$[-60]_{var}$	-	-	Thickness Config. 1
14	$[60]_{var}$	$[-60]_{var}$	-	-	Thickness Config. 2
15	$[60]_{var}$	$[-60]_{var}$	-	-	Thickness Config. 3
16	$[60]_{var}$	$[-60]_{var}$	-	-	Thickness Config. 4
17	$[60]_{var}$	$[-60]_{var}$	-	-	Thickness Config. 1
18	$[60]_{var}$	$[-60]_{var}$	-	-	Thickness Config. 5
19	$[60]_{var}$	$[-60]_{var}$	-	-	Thickness Config. 6

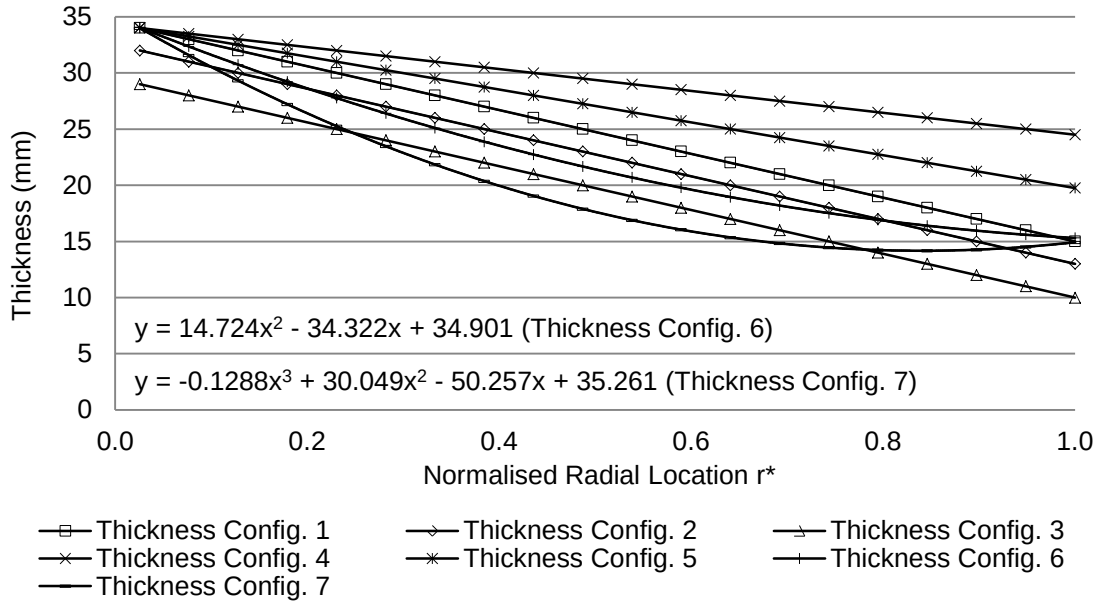

Figure 2.16-Thickness distributions of variation of thickness

The aforementioned geometric data of AWT-27 blade (the aerofoil distribution, pretwist distribution and chord distribution described in Table (2.6) and Figure (2.12)), and material data from composite box-beam shown in Figure (2.8), are used to generate three separate FE models with no web, one-web and two-web for the purpose of evaluating the static performance. These three FE models of the AWT-27 blade were built by SOLIDWORKS® and then they are imported into ANSYS®.

The element of FE models is by 3D SHELL99 quadratic eight-node element. Shell mesh is centred on the mid-surface of the geometry (by default). Particularly, SHELL99 is more suitable for simulating linear performance of shell and it usually has a smaller element formulation time than other element types. SHELL99 also allows up to 250 layers, in each layer, one can define specific material properties, fibre orientation and thickness referred to local coordinate system. SHELL 99 element has six degrees of freedom at each node: translations in the nodal x, y, and z directions and rotations about the nodal x, y, and z-axes.

One FE model of AWT-27 with two-web is showed in Figures (2.17) in which, the blade is divided into twenty segments purposely in span direction in order to apply for varied thickness configurations conveniently. The aerodynamic forces: lift and drag obtained from WTAero (Maheri 2006a, 2006e), which was based on blade element momentum theory (BEMT). For each blade element (or segment), the aerodynamic forces are treated as concentrated forces and they are applied at the centre of each element (or segment) on twist axis of blade. For introducing proper elastic twist, therefore, it needs to make sure, that the fibre orientation that refer to x-axis of local coordinate system at top and lower shell must be mirror or helical layup (both cause elastic coupling). Thus, it is necessary to define individual local coordinate system for top and lower surface of blade. The global coordinate of blade is shown in Figure (2.17) and boundary conditions are shown in Figure (2.18).

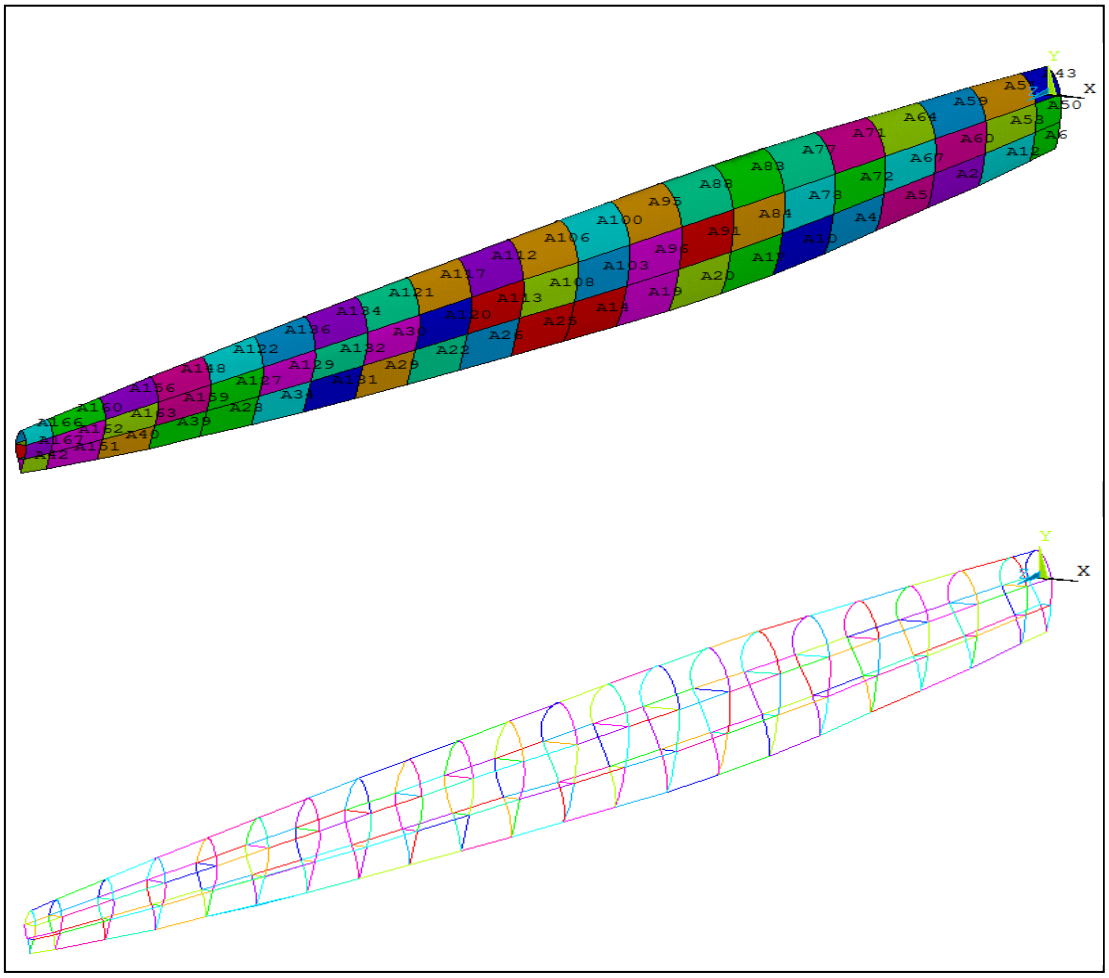

Figure 2.17- AWT-27 model with two-web and twenty segments

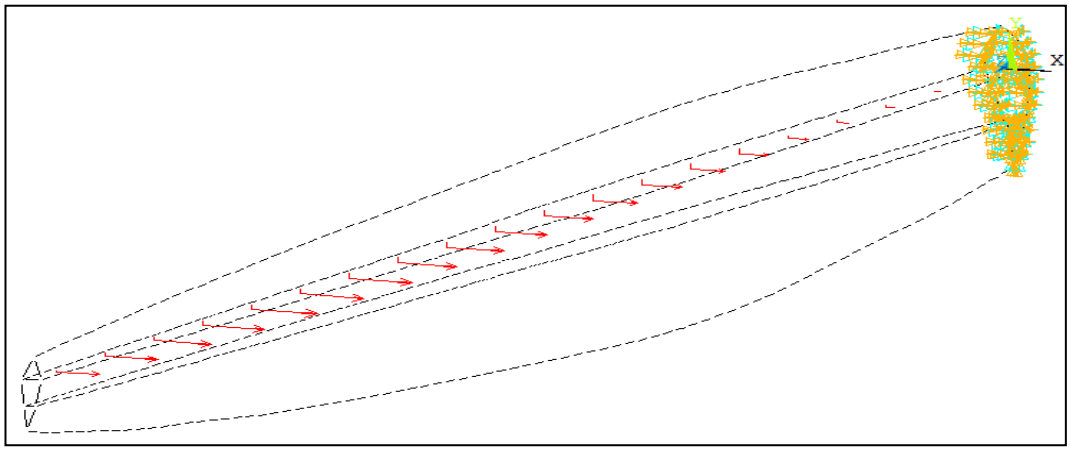

Figure 2.18-Boundary conditions of AWT-27 blade

Besides, the sensitivity of element size was checked in order to make the simulation more realistic and accurate. Quadratic eight-node SHELL 99 element

was chosen and the element size and equivalent to total element, total node and total DOF was listed in Table (2.9). Layup configuration 10 of blade was chosen for checking sensitivity of element size. It reflected that reducing element size did not always yield significant changes in results from Figure (2.19). Thus, it was assumed that accuracy of FE model was not compromised by this issue in future investigation.

Table 2.9- Element size and related element, node and DOF

Element Size (mm)	Total Element	Total Node	Total DOF
250	980	2540	15240
150	1854	5102	30612
100	3339	9453	56718
80	5333	15265	91590
60	9062	26274	157644

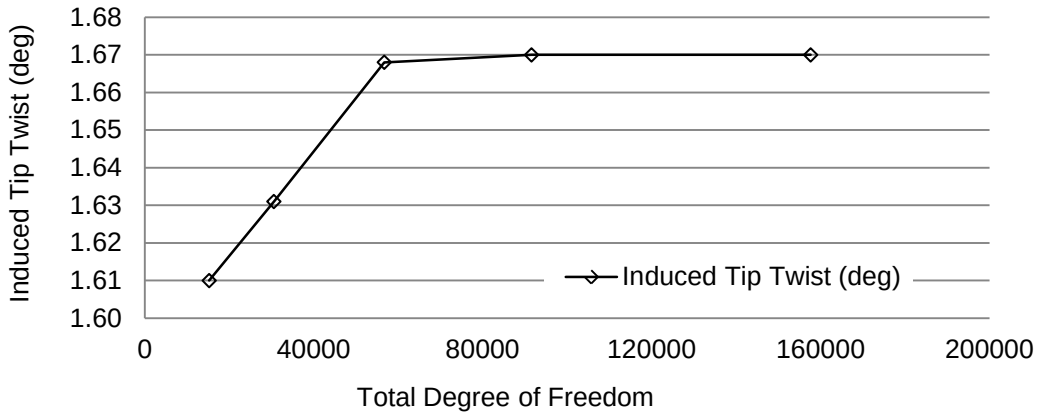

Figure 2.19-Sensitivity test of DOF

The results from present thin-walled composite beam model and FEA are showed in Figures (2.20) through (2.23).

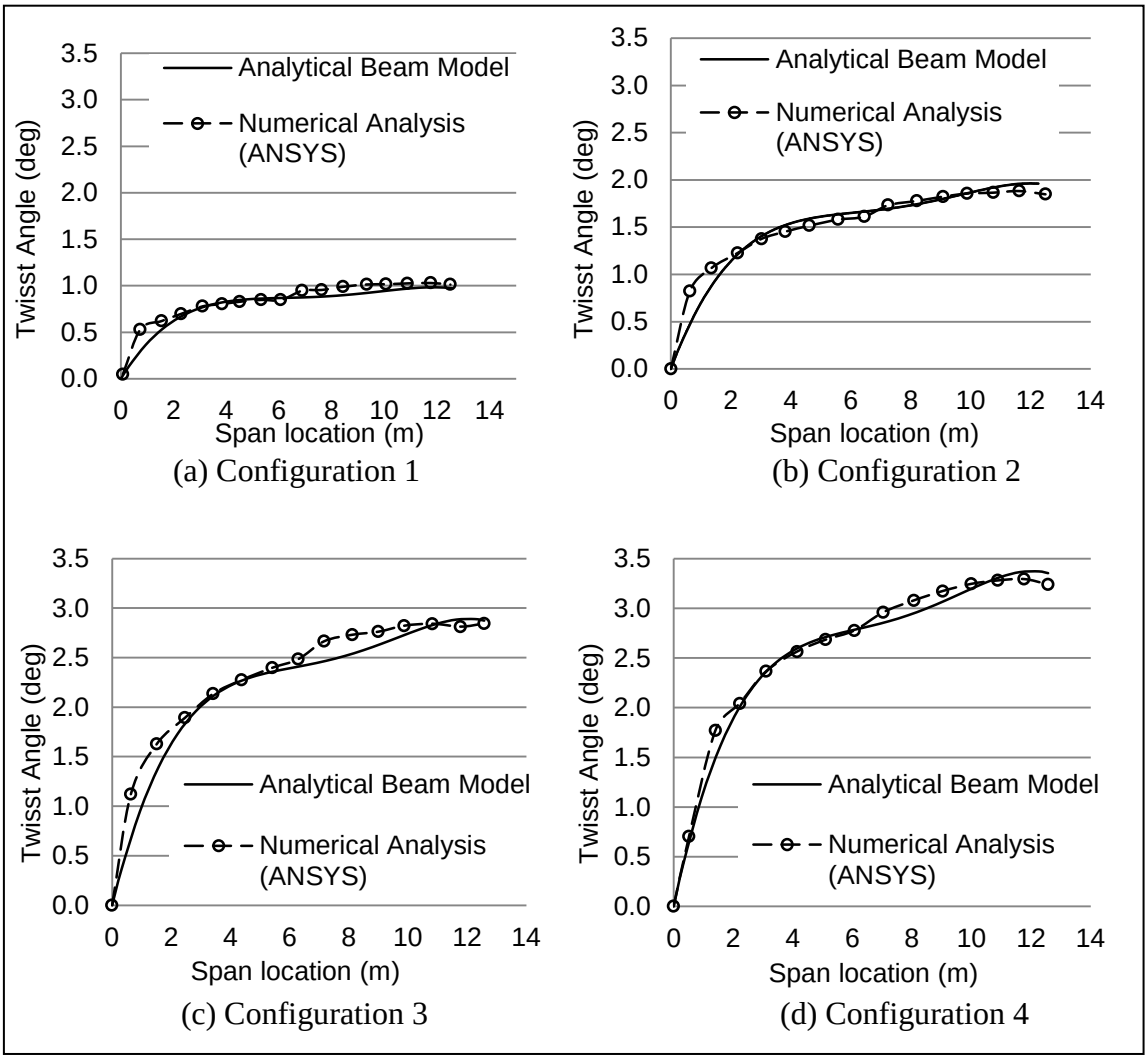

Figure 2.20-Twist angle distribution: layup configurations 1-4 (no web)

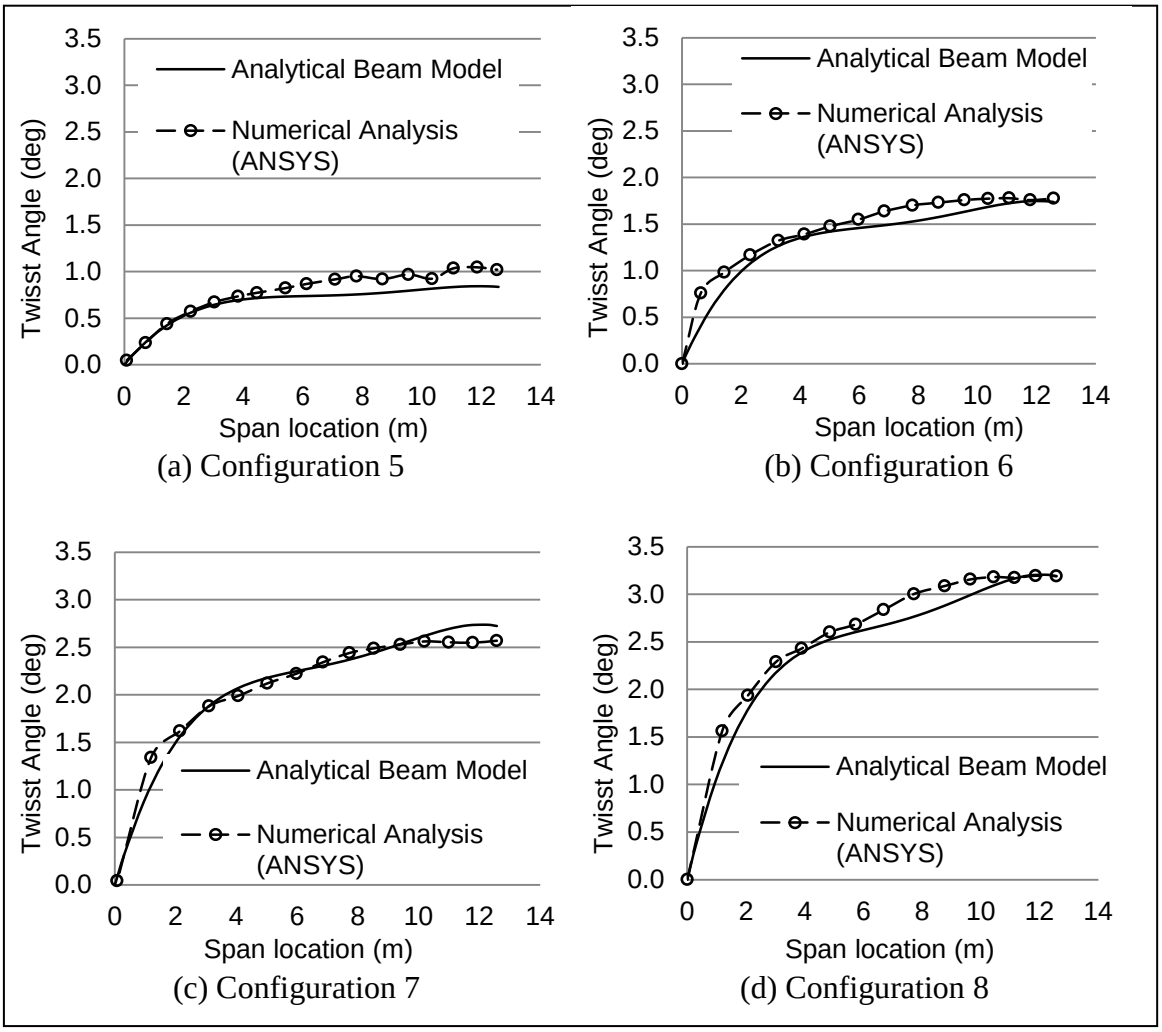

Figure 2.21- Twist angle distribution: layup configurations 5-8 (one web)

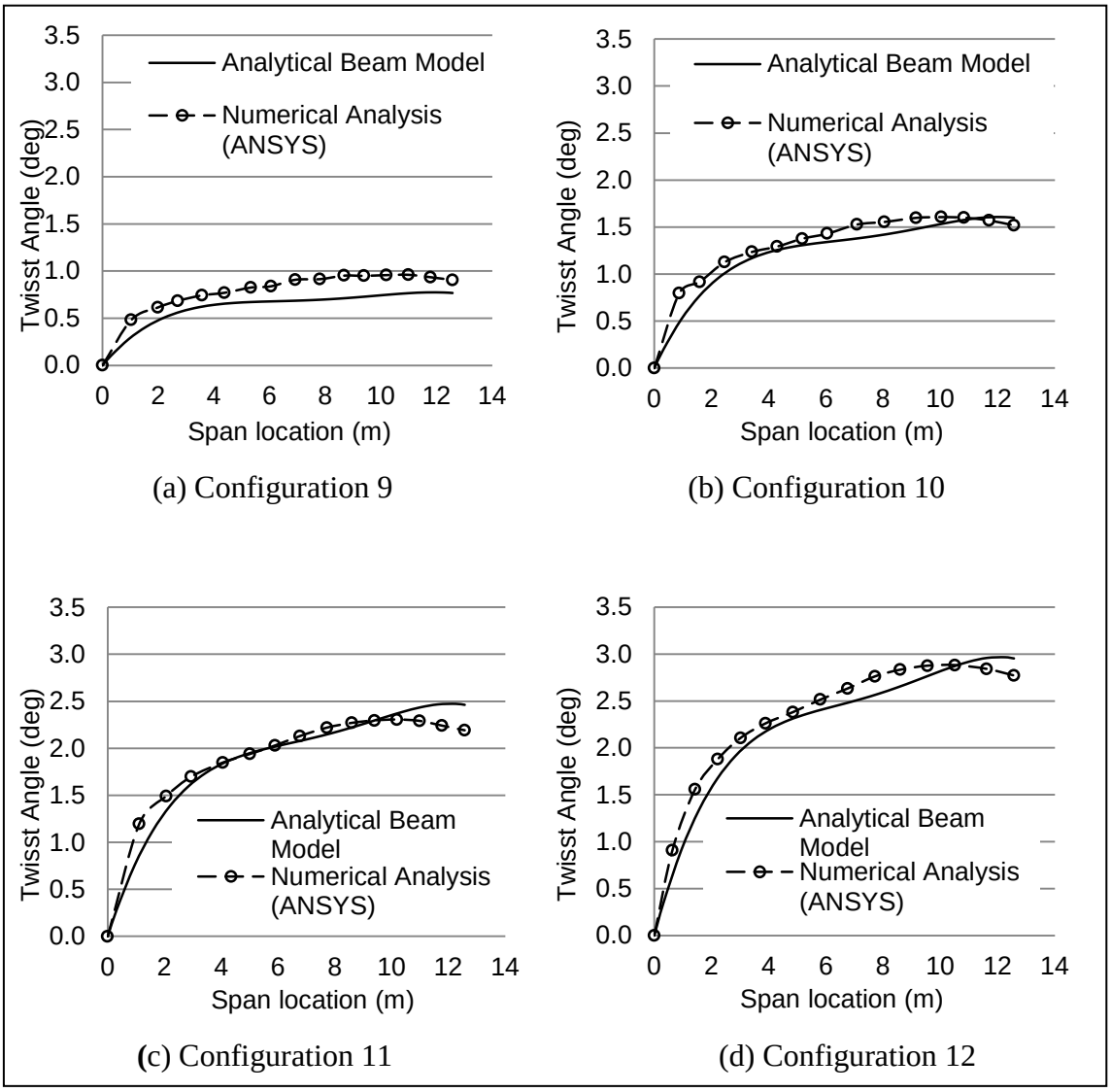

(a) Configuration 9

(b) Configuration 10

(c) Configuration 11

(d) Configuration 12

Figure 2.22- Twist angle distribution: layup configurations 9-12 (two webs)

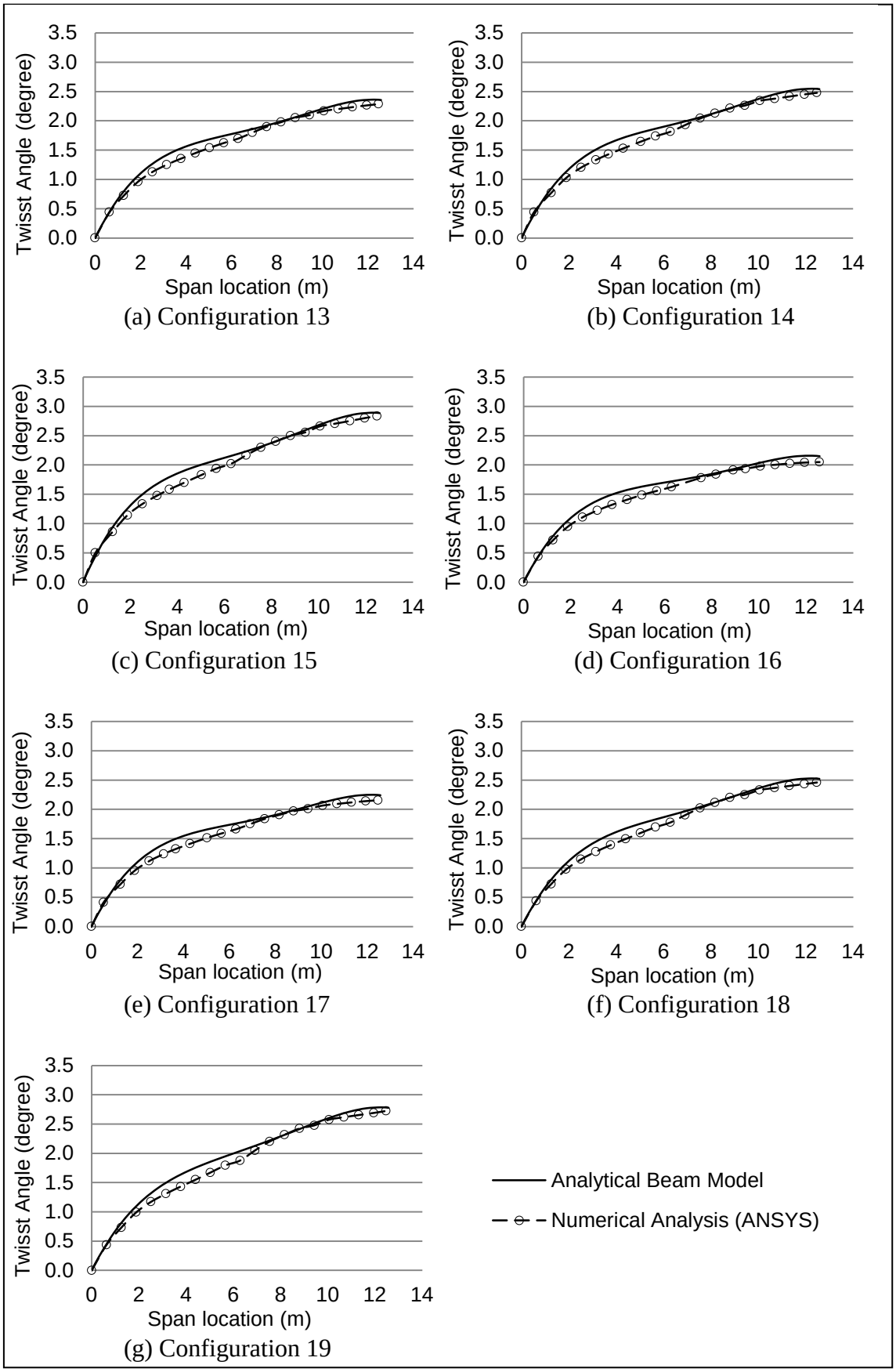

Figure 2.23- Twist angle distribution: layup configurations 13-19 (no web)

As it can be observed from Figures (2.20) to (2.23), the predicted induced twists are in good agreement with FEA based numerical results for most of the configurations. The maximum differences between the analytical and numerical results correspond to the layup configuration 5 and 9 with a ply angle of 20 degrees. However, this layup configuration generates a small-induced twist only. In case of configurations 1 to 12, a large deviation between the analytical and numerical results can be observed close to the root of the blade, this is because the developed analytical model ignores the warping effects at restrained root of the blade. It should be noted that since the inner parts of the blades have minor effects on the overall aerodynamic performance of wind turbines, this deviation has negligible effect on the predicted aerodynamic performance of the adaptive blade.

2.7 Summary

A general geometrically linear beam model is developed. This model is capable of predicting the induced twist due to elastic coupling for closed multi-cell thin-walled composite beams with span wise variable cross-sectional properties and non-uniform shell thickness distribution under various types of loads.

The performance of the developed model for various beams under various loading scenarios is investigated. Single-, two- and three-cell wind turbine blades with constant thickness are investigated under various layup configurations. Single-cell blades with variable thickness distributions along the blade longitudinal axis are also investigated. The results for all cases show a good agreement with analytical, experimental and numerical results, highlighting the accuracy of the results at required level for simulation and design of wind turbine adaptive blades.

3 Coupled Aero-Structure Simulation of Wind Turbines with Adaptive Blade

3.1 Introduction

As briefly mentioned in Chapter 1, simulation of adaptive blades is quite different from the simulation of ordinary wind turbine blades. For conventional blades, the twist angle of the blade is a combination of known parameters of pre-twist and pitch angle whilst the elastic torsional deformation is assumed negligible. In the case of wind turbines with adaptive blades, even by neglecting the torsion due to pitch moment, the angle of attack is still under the influence of elastic torsional deformation generated by bend-twist elastic coupling. Figure (3.1) showed the schematic diagram of WTAB, the software tool for aero-structure analysis of wind turbines with adaptive blades (Maheri, 2006c, 2006e). The aim of this chapter is to replace the box "Blade FEA" in Figure (3.1) by some software with a more efficient structural analyser based on the beam model developed in Chapter 2 of this thesis. Employing an analytical beam model as a part of a design objective evaluator rather than a FEA based structural analyser makes the aerodynamic objective evaluation more efficient and convenient.

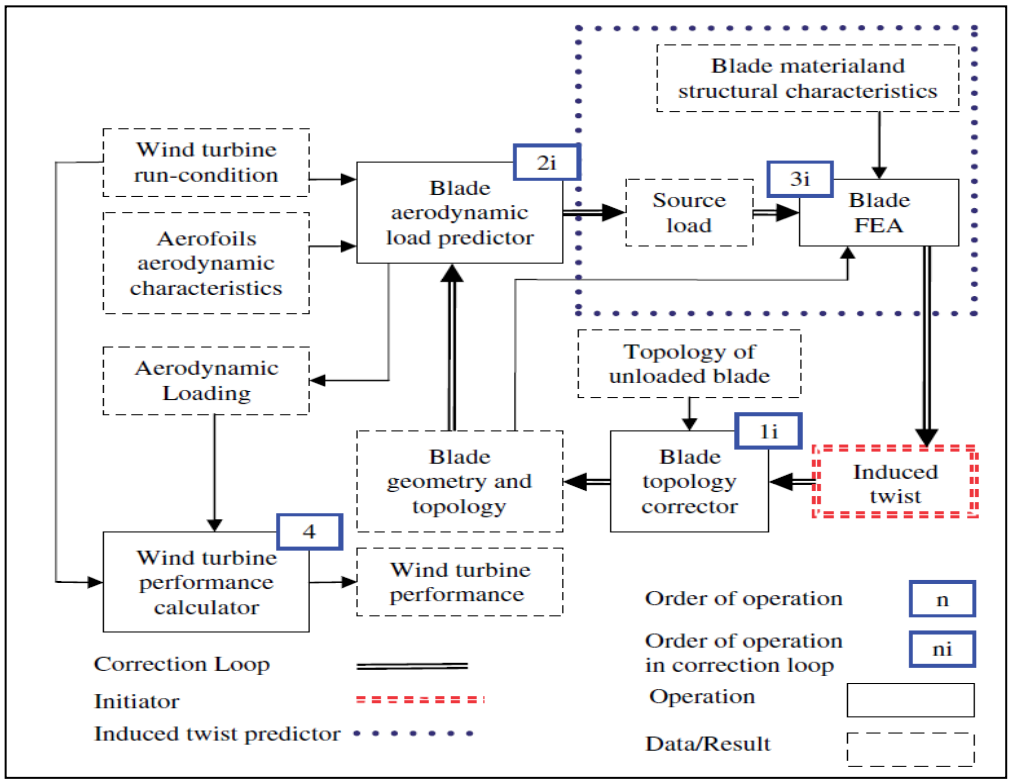

Figure 3.1- Coupled aero-structure simulation of a wind turbine with bend–twist adaptive blades (Maheri, 2006e)

To replace the FEA-based structural analyser with the beam model of Chapter 2, new interfaces needs to be developed for material and structural characteristics definitions. This chapter elaborates on these interfaces and necessary codes for calculating sectional properties for the blade.

3.2 Material Definition

A unidirectional fibre reinforced composite is made of parallel fibres arranged in a matrix. This type of material forms the basic configuration of fibre composite materials. An elementary cell of such a material can be approximately simulated as a fibre embedded in a cylinder of the matrix with circular base or a hexagonal base. This cell has an axis, called longitudinal direction and denoted, as the L-axis of revolution whose direction parallel to the fibres. Every direction normal to the fibres is called a transverse direction and the composite is treated as being transversely isotropic. The two orthogonal transverse directions are described by T and T'. The mechanical behaviour of a unidirectional composite is characterised by five independent quantities namely E_L, E_T, v_{LT}, G_{LT} and $G_{TT'}$; where, E_L and E_T denote Young's modulus in longitudinal and transverse directions respectively, v_{LT} denotes Poisson's ratio measured and G_{LT} and $G_{TT'}$ denote shear modulus in longitudinal and transverse directions respectively. The mechanical properties for the fibre and the matrix will be featured by their engineering constants such as Yong's modulus and Poisson ratio denoted by E_f, v_f, E_m, v_m respectively.

Longitudinal modulus E_L is predicted by the law of mixtures for Young's modulus in the direction of the fibres by Equation (3.1).

$$E_L = E_f V_f + E_m(1-V_f) \tag{3.1}$$

The variation of the modulus E_L is linear between the values E_m of the modulus of the matrix and E_f of the modulus of the fibres, when the fibre volume fraction V_f, varies from zero to one.

Longitudinal Poison's ratio is predicted by the law of mixtures and expressed by Equation (3.2)

$$v_{LT} = v_f V_f + v_m(1-V_f) \tag{3.2}$$

Longitudinal shear modulus is expressed as Equation (3.3) proposed by Hill (1964) and Hashin (1966).

$$G_{LT} = G_m \frac{G_f(1+V_f)+G_m(1-V_f)}{G_f(1-V_f)+G_m(1+V_f)} \tag{3.3}$$

Parameter K_L , the hydrostatic compression modulus measured in a lateral hydrostatic compression without longitudinal deformation, it was proposed by Hill (1964) and Hashin (1966) and showed by Equation (3.4). K_L is related to the bulk modulus k_m, k_f and the shear modulus G_m, G_f of matrix and fibre, these quantities are also functions of the Yong's modulus and Poisson's ratio of the matrix and fibres expressed by Equations (3.5) through (3.7) proposed by Hill (1964) and Hashin (1966) as well.

$$K_L = K_m + \frac{V_f}{\dfrac{1}{k_f - k_m + \dfrac{1}{3}(G_f - G_m)} + \dfrac{1-V_f}{k_m + \dfrac{4}{3}G_m}} \tag{3.4}$$

$$K_i = k_i + \frac{G_i}{3} \qquad i = m, f \tag{3.5}$$

$$k_i = \frac{E_i}{3(1-2v_i)} \qquad i = m, f \tag{3.6}$$

$$G_i = \frac{E_i}{2(1+v_i)} \qquad i = m, f \tag{3.7}$$

Transverse shear modulus is expressed as Equation (3.8) developed by Christensen (1979) and Christensen and Lo (1979)

$$G_{TT'} = G_m \left\{ 1 + \frac{V_f}{\frac{G_m}{G_f - G_m} + \frac{k_m + \frac{7}{3}G_m}{2k_m + \frac{8}{3}G_m}(1 - V_f)} \right\} \tag{3.8}$$

Transverse Young's modulus E_T and Poison's ratio $v_{TT'}$ are obtained from the relations associated with other independent quantities and stated in Equations (3.9) and (3.10)

$$E_T = \frac{2}{\frac{1}{2K_L} + \frac{1}{2G_{TT'}} + 2\frac{v_{LT}^2}{E_L}} \tag{3.9}$$

$$v_{TT'} = \frac{E_T}{2G_{TT'}} - 1 \tag{3.10}$$

Equations (3.1) through (3.10) describe the theoretical approaches for evaluating engineering constants of unidirectional composite based on exact solutions. Thus, these equations are becoming fundamentals of "Composite Material Definition" graphical user interface (GUI) for producing new materials.

3.2.1 GUI for Composite Material Definition

Equations (3.1) through (3.10) are embedded in the "Composite Material Definition" GUI shown in Figure (3.2) for material properties calculation.

There are two types of data input available in this GUI controlled by radio buttons. The first radio button on the left side of GUI controls the data input for producing the new materials theoretically by entering volume ratios and engineering constants of both of the constituents of the matrix and fibre. The second radio button controls the data input for material whose mechanical properties are known. The mechanical properties of material can be saved to a MATLAB mat-file. Subsequently the name of material is displayed in the top list

box. When one selects a material from the top list box, the material properties will be displayed in the empty cells on the right side of GUI.

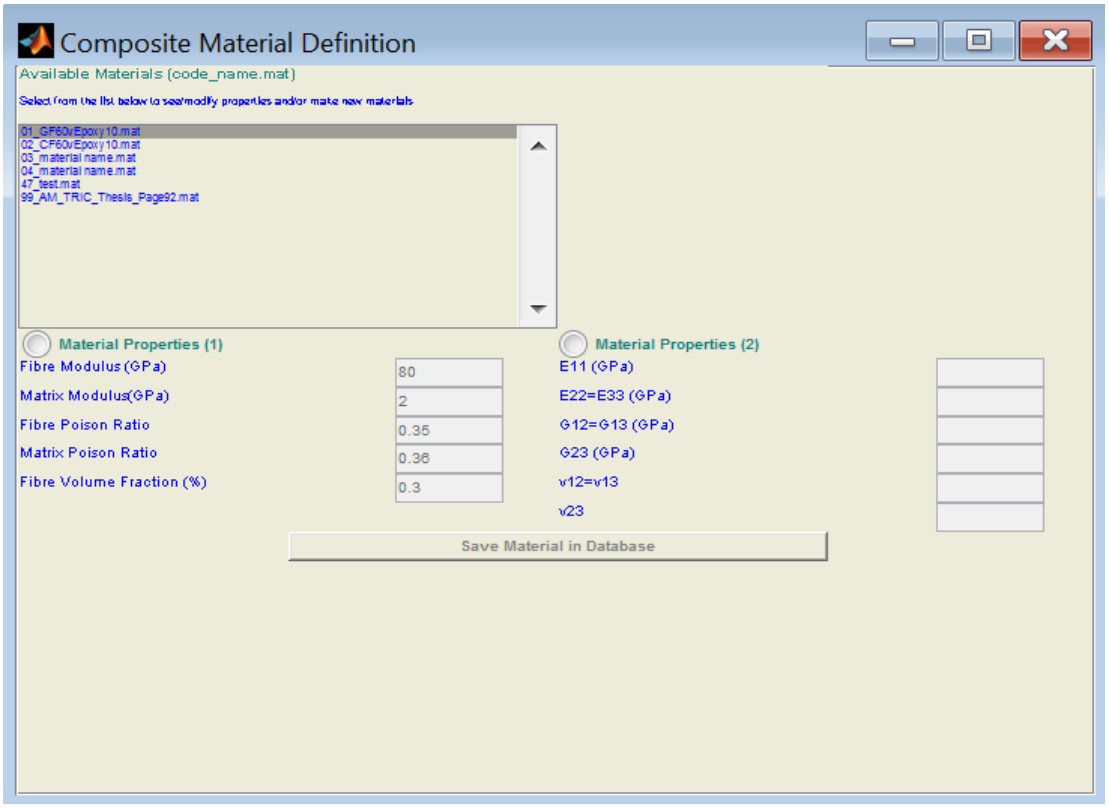

Figure 3.2-GUI of “Composite Material Definition”

3.3 Blade Structure Definition

Elastic coupling topology is as important as the blade material in producing the right elastic coupling in an adaptive blade. Designer needs to make various layup configurations and locate them on the blade wherever desired. In order to facilitate this, the blade is assumed to be made of basic components called “Patch”.

3.3.1 Shell Patches

In the developed software, blade structure is defined as a combination of shells called “Patch”. Each patch is a quadrilateral defined by the coordinates of its four corners. Patches are curved shell structures on the upper and lower surfaces of the blade and are flat on webs. In definition of patches on the upper and lower surfaces of the blade, firstly patch projection on the blade plane area is located in plane coordinates of system $(x_p - y_p - z_p)$ as shown in Figure (3.3).

As it can be seen from Figures (3.3.a) and (3.3.e), the coordinates x_p, y_p, z_p have their own specified origin. The origin of the spanwise coordinate z_p is located on the aerofoil plane at root of the blade pointing to the tip. Coordinate z_p is normalised by the length of the blade. At a general z_p-location, the origin of coordinate x_p is located at the leading edge (LE). The x_p coordinate is normalised by the chord length at z_p-location. For patches located on the upper or lower surface y_p coordinate is zero.

For patches located on webs, the four corners are defined by ($x_{p,w}, y_p, z_p$). Here, $x_{p,w}$ denotes the normalised x-coordinate of the web in plane system of coordinates. Coordinate y_p starts from the lower surface of the blade and is normal to the chord line. Coordinate y_p is normalised by the aerofoil thickness t at the web location $x_{p,w}$ and span location z_p.

The local coordinates of system $(x_l - y_l - z_l)$ for the corner of the patch is introduced as a transition system of coordinates by translating the origin of (x_p, y_p) to twist centre of blade showed in Figure (3.3.d). Thus, the coordinates of a corner under local system of coordinates can be expressed by Equations (3.11) to (3.13).

$$x_l = (x_p - x_{twist})c \tag{3.11}$$

$$y_l = \left(y_{lower\ surface}\right)_{x_{p,w}} + y_p t \tag{3.12}$$

$$z_l = z_p r_{span} \tag{3.13}$$

where c denotes the chord length at z_p location, r_{span} denotes the span of the blade, x_{twist} denotes distance between the leading edge and the twist centre of

aerofoil. Parameter $y_{lower\ surface}$ is the local coordinate of the lower surface at $x_{p,w}$ and z_p location.

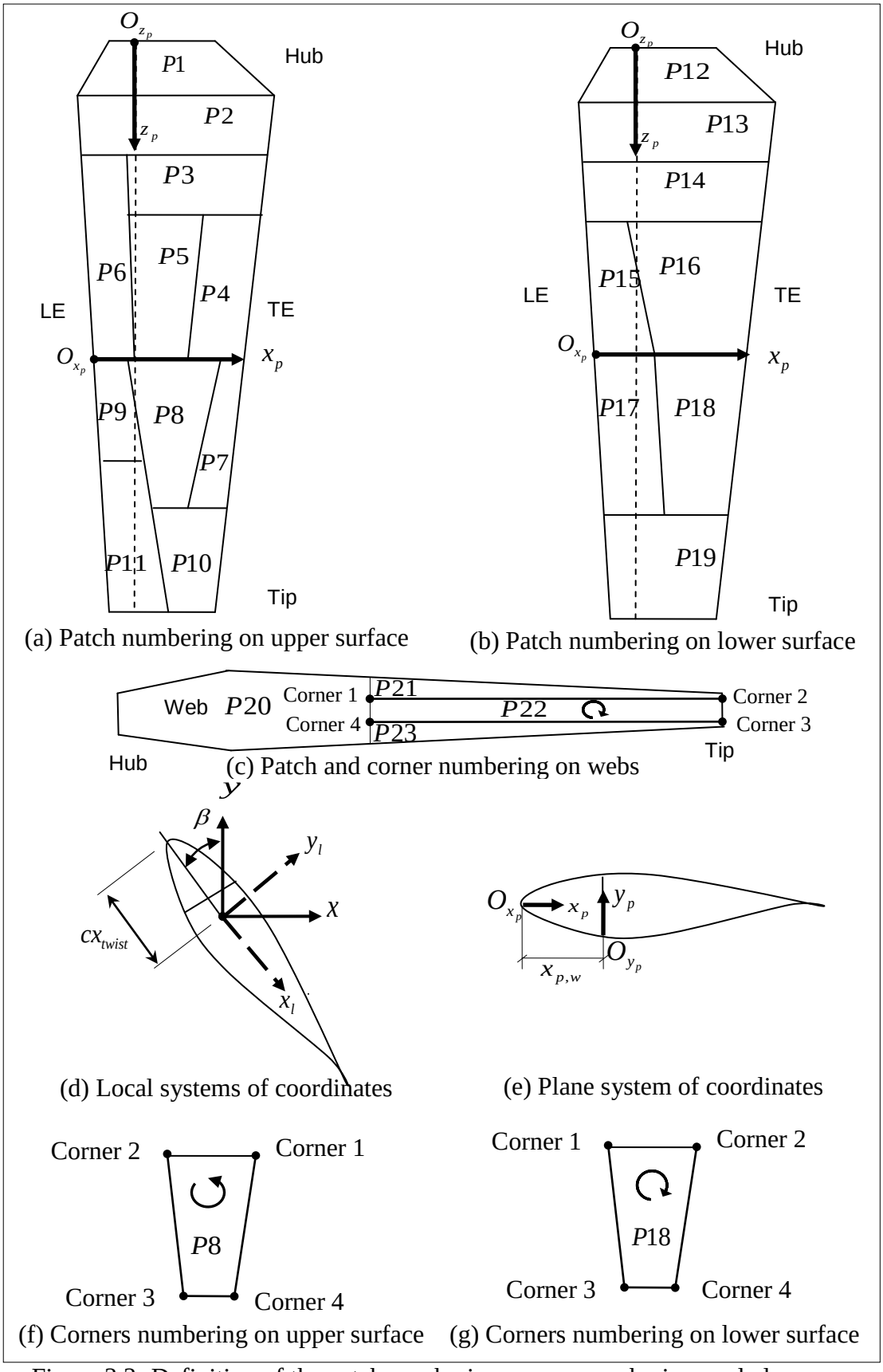

(a) Patch numbering on upper surface

(b) Patch numbering on lower surface

(c) Patch and corner numbering on webs

(d) Local systems of coordinates

(e) Plane system of coordinates

(f) Corners numbering on upper surface

(g) Corners numbering on lower surface

Figure 3.3- Definition of the patch numbering, corner numbering, and plane, global coordinates of system

The coordinates of a corner in global system of coordinates (x, y, z) can be expressed by Equations (3.14).

$$\begin{Bmatrix} x \\ y \\ z \end{Bmatrix}_k = \begin{bmatrix} x_l & y_l & 0 \\ y_l & -x_l & 0 \\ 0 & 0 & z_l \end{bmatrix}_k \begin{Bmatrix} \sin\beta \\ \cos\beta \\ 1 \end{Bmatrix}_k \tag{3.14}$$

where

$$\beta = \beta_o + pitch \tag{3.15}$$

in which, β and '$pitch$' stand for blade twist and blade pitch angle. Parameter β_0 denotes the pre-twist angle at z_l location of the blade.

In order to manipulate patch properties and locations in the coded software tool, specific rules for patch numbering and corner numbering should be introduced and employed.

3.3.1.1 Patch Numbering

When the beam model is used to calculate the coefficient matrix $[K_{ij}]$ for a cross-section of the blade, one needs consider the sequence of the patches around the section contour following s-coordinate. Thus sequencing the patch number by following s-direction in cross-section contour would make the calculation convenient. In order to be compatible with the $(s - z - n)$ coordinate of system of beam model the patch numbering follows the following set of rules (see also Figures (3.3.a) through (3.3.c)).

- On the upper surface, patch numbers starts from hub to tip and from trailing edge (TE) to leading edge (LE) viewed from top.
- On the lower surface, numbering of the patch is defined from hub to tip and from LE to TE viewed from the top.
- On webs, numbering of the patch starts from the web nearest to TE, and is defined from hub to tip and from upper surface (US) to lower surface (LS), viewed from LE.

3.3.1.2 Corner Numbering

In order to specify the location of the patch conveniently by four corners, it is also necessary to formulate the rules for numbering of four corners by the following rules (see also Figures (3.3.c), (3.3.f) and (3.3.g)).

- On the upper surface, corner numbering of a patch starts from the closest corner to hub and TE numbered counter clockwise and viewed from the top.
- On the lower surface, corner numbering of a patch starts from the closest corner to hub and LE numbered clockwise and viewed from top.
- On the web, corner numbering of a patch starts from the closest corner to hub and upper surface numbered clockwise and viewed from LE.

Figure (3.4) and Table (3.1) show an exemplar case using the rules explained above for patch and corner numbering.

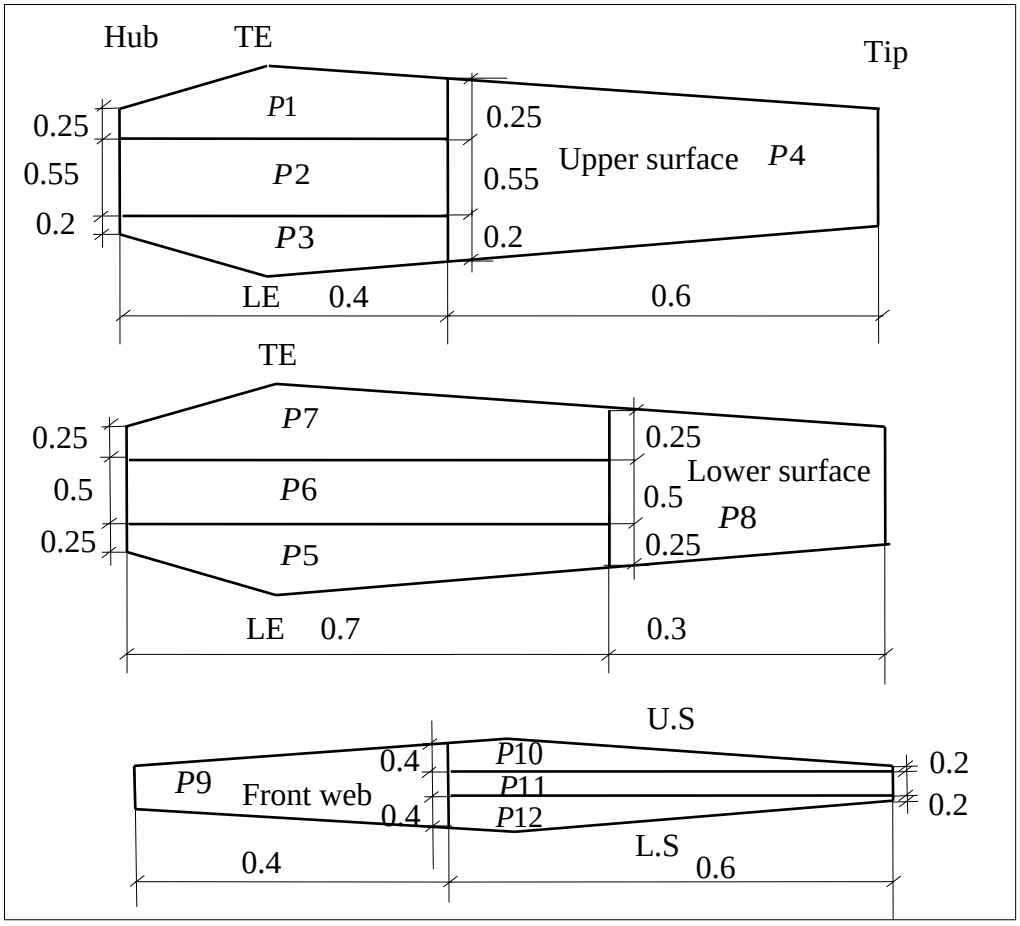

Figure 3.4-Definition of location of the patches

Table 3.1-Normalised coordinates of patches of the exemplar of Figure (3.4)

Patch	x_p	y_p	z_p	**Patch**	x_p	y_p	z_p	**Patch**	x_p	y_p	z_p	**Corner**
1	1	-	0	**2**	0.75	-	0	**3**	0.2	-	0	**1**
	0.75	-	0		0.2	-	0		0	-	0	**2**
	0.75	-	0.4		0.2	-	0.4		0	-	0.4	**3**
	1	-	0.4		0.75	-	0.4		0.2	-	0.4	**4**
4	1	-	0.4	**5**	0	-	0	**6**	0.25	-	0	**1**
	0	-	0.4		0.25	-	0		0.75	-	0	**2**
	0	-	1		0.25	-	0.7		0.75	-	0.7	**3**
	1	-	1		0	-	0.7		0.25	-	0.7	**4**
7	0.75	-	0	**8**	0		0.7	**9**	0.33	1	0	**1**
	1	-	0		1		0.7		0.33	1	0.4	**2**
	1	-	0.7		1		1		0.33	0	0.4	**3**
	0.75	-	0.7		0		1		0.33	0	0	**4**
10	0.33	1	0.4	**11**	0.33	0.6	0.4	**12**	0.33	0.4	0.4	**1**
	0.33	1	1		0.33	0.8	1		0.33	0.2	1	**2**
	0.33	0.8	1		0.33	0.2	1		0.33	0	1	**3**
	0.33	0.6	0.4		0.33	0.4	0.4		0.33	0	0.4	**4**

3.3.2 Patch Layup Configuration Definition

After defining and calculating the location of each patch, its layup configuration is also defined via setting:

- Number of layers
- Material of each lamina
- Fibre angle of each lamina

Different materials can be defined in Composite Material Definition GUI as explained in the previous section and are stored in a database.

For defining fibre orientations in layers, as mentioned in Chapter 2, the curvilinear coordinate of system $(s-z-n)$ used for strain and stress calculations, is employed here. Fibre angle θ is measured from the positive direction of the s-coordinate as shown in Figure (3.5).

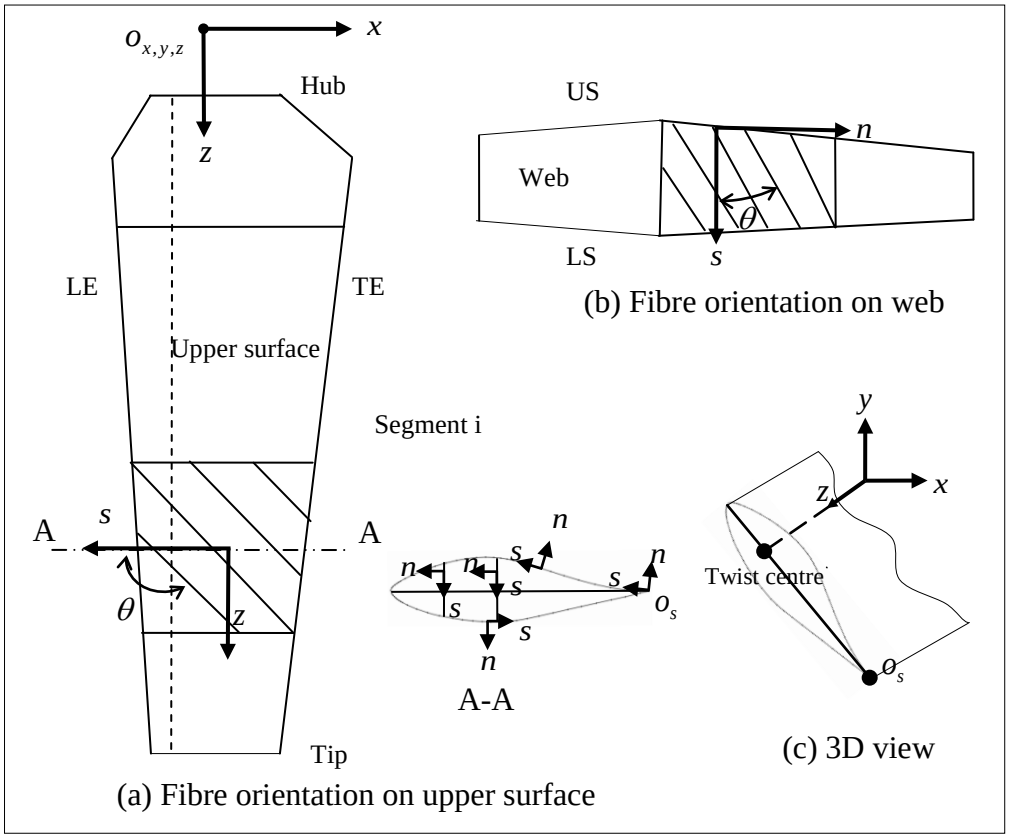

Figure 3.5-Definiton of the fibre orientation on blade surface and s-coordinate direction along contour

Figure (3.6) shows an example of the direction of n -coordinate, starting from the mid-line outward. The layer sequence, also shown in this figure, follows positive n-direction from the inner to the outer layer.

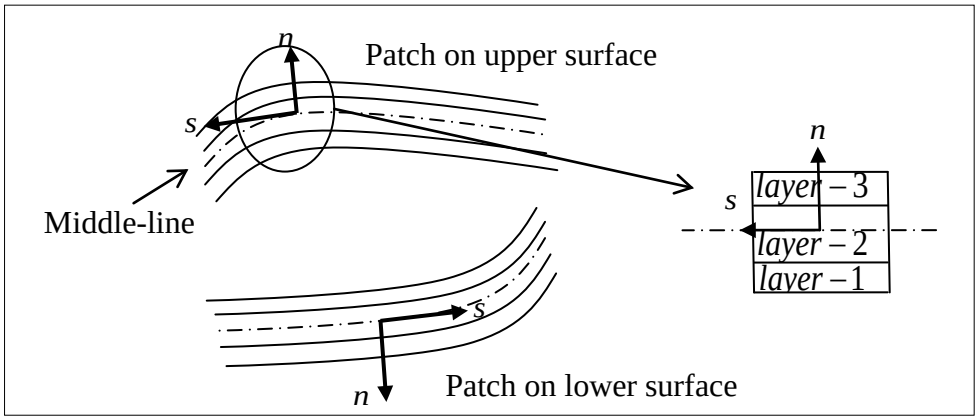

Figure 3.6-Layer stack sequence for a patch

3.3.3 GUI for Blade Structure Definitions

The "Blade Structure Definition" GUI shown in Figure (3.7) is developed in order to define various structural layups for adaptive blades. This GUI undertakes the

pre-processing of adaptive blades twist analysis. Structural characteristics of the blades are specified in this GUI by the following steps:

1) Set the number of patches on the upper and lower surfaces of the blades as well as webs.
2) For each patch:
    a. Set the location
    b. Set layup configuration (including number of layers and material, thickness and fibre orientation for each layer).
    c. Save the patch
3) Save the blade structure in the form of a mat-file.

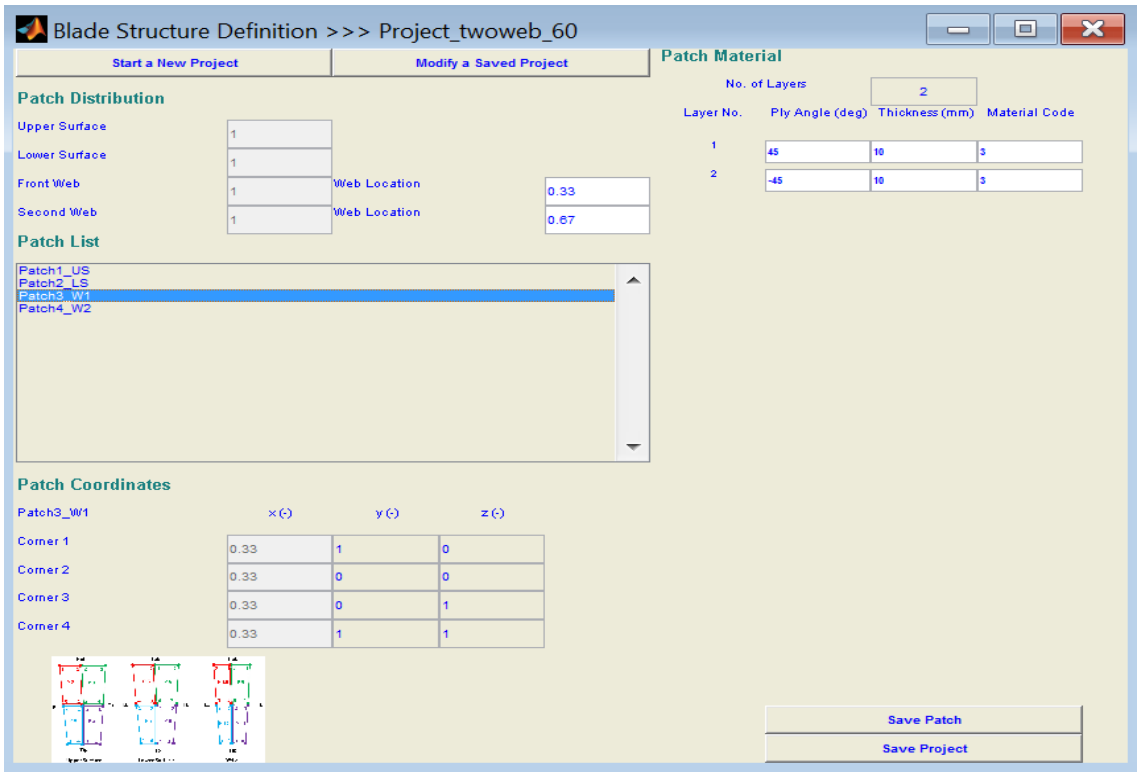

Figure 3.7- GUI of "Blade Structure Definition"

The blade structure file includes the following information:

- The number of the patches
- The location of each patch
- The number of layers in each patch
- Thickness of layers in each patch
- Fibre angle in each layer of the patch

- Material properties of each layer in the patch
- The shape of the cross-section (from aerofoil contour)

3.4 Induced Twist Calculation

As explained in Chapter 2, Equation (2.47) is used to find the blade deformations in various directions, including induced twist. The following steps are required for determination of the deformations:

1) Discretise the blade into *n* sections
2) Find internal forces at each section
3) For each section $i = 1,2,...,n$:
    a. Calculate the entries of the stiffness matrix $[K_{ij}]$ using Equations (B.1) to (B.42).
    b. Inverse stiffness matrix $[K_{ij}]$ and solve for rate of change of deformations $w_0^{'}(z), \theta_y^{'}(z), \theta_x^{'}(z), \phi^{'}(z)$ and $\theta_y + u_{pole}^{'}$, $\theta_x + v_{pole}^{'}$.
    c. Apply boundary conditions and find $w_0(z), \theta_x(z), \theta_y(z)$ and $\phi(z)$ via numerical integration at each section.
    d. Substitute back $\theta_x(z)$ and $\theta_y(z)$ obtained in previous step in $\theta_y + u_{pole}^{'}$ and $\theta_x + v_{pole}^{'}$ to find u'_{pole} and v'_{pole}.
    e. Apply boundary conditions to find u_{pole} and v_{pole} via numerical integration.

Figure (3.8) shows the GUI developed for deformation analysis of adaptive blades. In this GUI, deformation analysis starts by loading the blade structural mat-file from the “Project” list box on the top left of GUI. It then reads the internal forces at each section. The following background codes calculate required data for finding stiffness matrix:

- PatchCoordLocal.m- This code transforms coordinates of patches from plane system of coordinates to local system of coordinates.
- PatchCoordGlobal.m- Translate coordinates of patches from local system of coordinates to global system of coordinates.

- SectionProperties.m- This code extracts the structural/ material characteristics of each cross-section such as its contour, numbers of patches in it, number of layers in each patch in it, thickness of the layers in each patch, fibre angle in the layers of each patch, etc as required for calculating stiffness matrix entries.

Finally, the following codes calculate the entries of stiffness matrix for no-web, one-web and two-web cases:

- StifnessNoWeb.m
- StiffnessOneWeb.m
- StiffnessTwoWeb.m

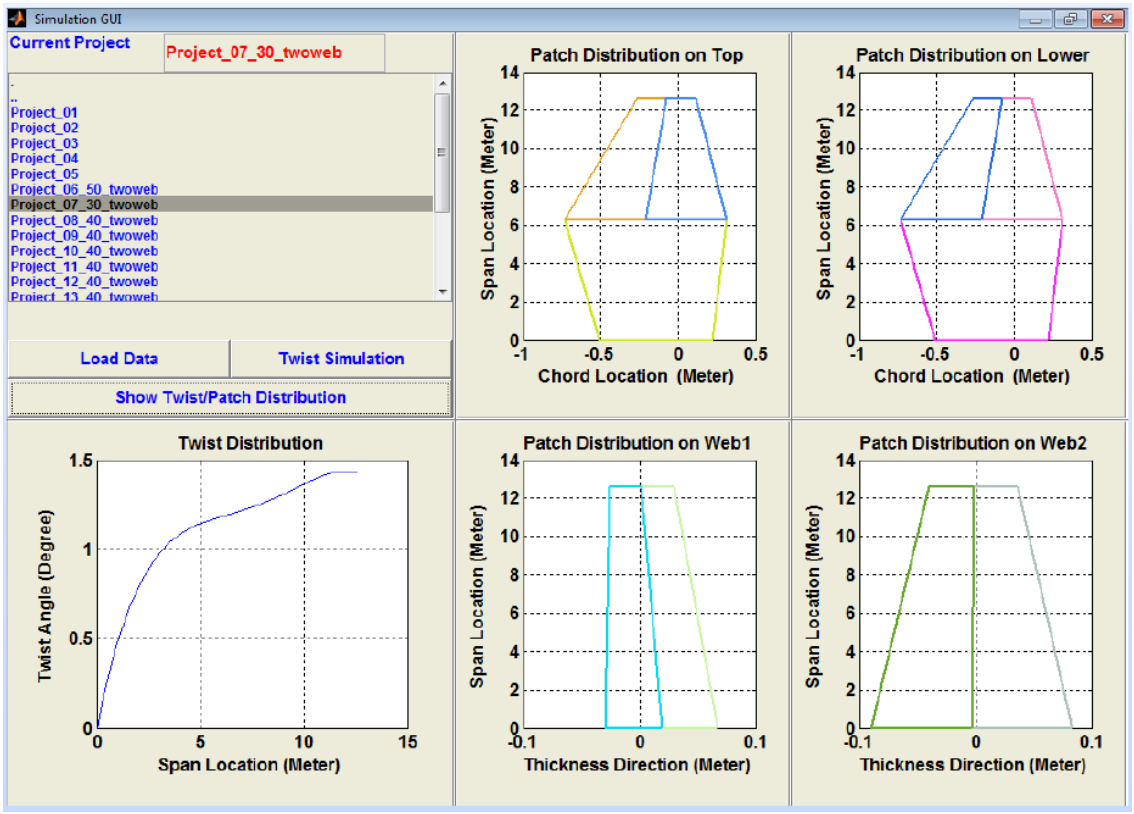

Figure 3.8-“Simulation GUI”

Figure (3.9) shows a typical cross-section of an adaptive blade with *n* different patches. In each patch, it can be made up of many layers. Then the fibre angle of layers, thickness of layers, material properties of layers and total number of layers can be defined separately by using defined GUI-“Blade Structure Definition”.

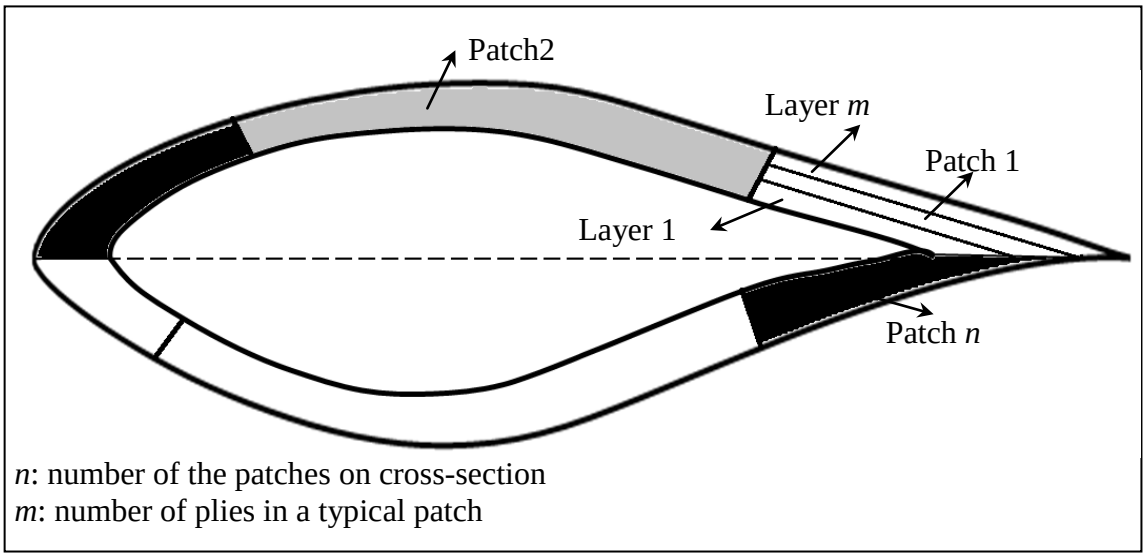

Figure 3.9-A typical cross-section of an adaptive blade with *n* patches

3.5 Aero-structure Simulation

Wind turbine aerodynamic simulation tool WTAero (Maheri, 2006a, 2006e) is integrated to the induced twist calculator explained above to find the aerodynamic force distributions along the blade. WTAero also calculates the internal forces at each cross-section (resultant forces shown in Equation (2.47)). The integrated software takes the following steps to evaluate the performance of a wind turbine utilising adaptive blades:

Given:

- Wind turbine specifications (e.g. wind turbine type, number of blades, rotor diameter, hub elevation, cone angle, blade pitch angle, etc)
- Wind turbine run condition (wind speed and rotor speed)
- Project name (the name of saved adaptive blade structure file produced by "Blade Structure Definition" GUI)
- Number of sections for blade discretisation

Step 1. Set initial elastic twist $\phi(z) = 0$

Step 2. Load the adaptive blade structure file.

Step 3. Compute the entries of stiffness matrix $[K_{ij}]$ for each section.

Step 4. Inverse stiffness matrix $[K_{ij}]$ for each section

Step 5. While convergence criterion has not been achieved do:

5.1. Calculate aerodynamic loads and internal forces at each section.

5.2. Solve Equation (2.47) for rate of change of deformations, of particular interest, $\phi'(z)$.

5.3. Apply boundary conditions to find $\phi(z)$ via numerical integration.

5.4. Compute the total twist distribution of adaptive blades $\beta(z) = \phi(z) + \beta_0(z)$ again considering elastic coupling induced twist.

5.5. Go to Step 5.1.

The convergence criterion can be defined on induced twist or rotor mechanical power.

The process of aero structure simulation is illustrated here by an adaptive blade AWT-27 without web that is the same as that in Chapter 2. The elastic coupling specified for this blade is by CAS $[50]_{10}$ with a constant thickness (10mm). Applying the convergence criterion on the rotor mechanical power $\left|(P_{new} - P_{old})/P_{old}\right| \le 1\%$, the results of iteration are shown in Figures (3.10) and (3.11). It is assumed that the wind turbine is operating at a steady wind speed of 10 m/s with a rotor speed of 53.3 rpm.

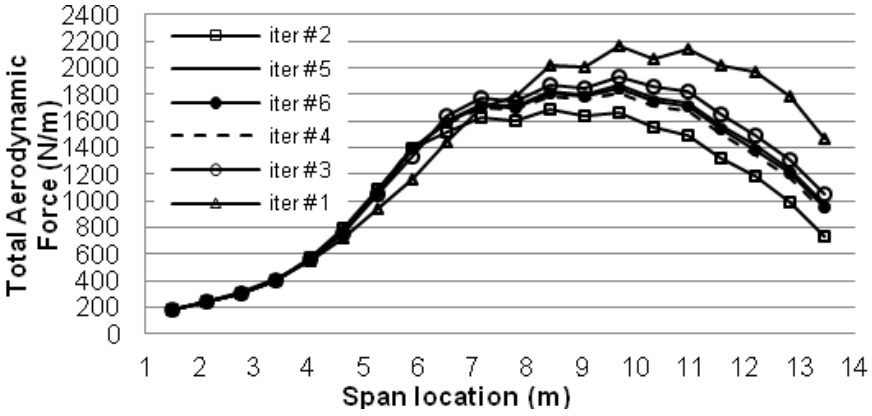

Figure 3.10 Span wise distribution of total aerodynamic force

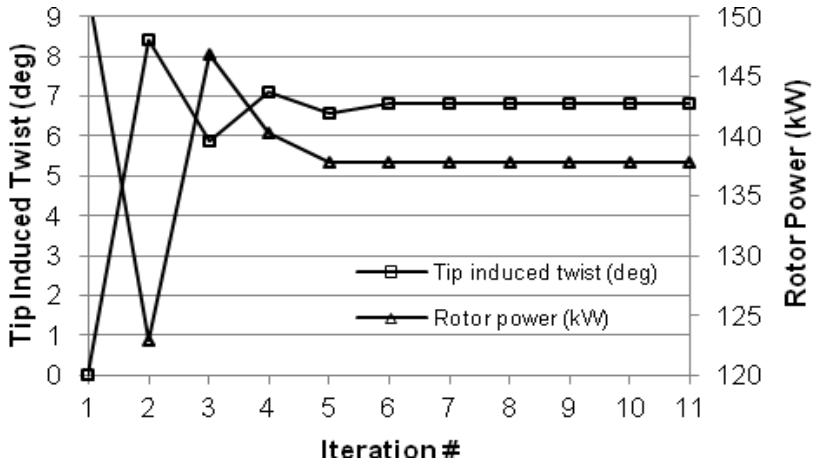

Figure 3.11 Aerodynamic performance of the wind turbine utilising adaptive blades

It can be seen from the Figures (3.10) through (3.11) that, the aerodynamic loads, tip induced twist and rotor power are not constant at first few iterations as adaptive blades simulation is aero-structure coupled process. A few iterations later, the aerodynamic loads, the induced twist and the rotor power reach their converged values.

3.6 Summary

In this chapter, three MATLAB® based GUIs are developed to implement the analytical beam model developed in Chapter 2 in an aero-structure simulation tool. The beam model takes the place of FEA coupled aero-structure analysis of adaptive blades.

The "Composite Material Definition GUI" allows the user to produce material properties by entering volume ratios and engineering constants of constituents, the matrix and fibre, for new materials. This GUI also can be used to save known materials by entering their material properties directly. The "Blade Structure Definition GUI" undertakes the pre-processing of adaptive blades simulation by constructing the structure of adaptive blades with the flexibility of having several different types of layup configurations at various locations. The "Simulation GUI" carries out the twist analysis of adaptive blades.

4 Extended Decoupled Design Method

4.1 Introduction

As explained in previous Chapter 3, the induced twist in a bend-twist adaptive blade depends on the following sets of parameters:

- Aerodynamic characteristics.
- Wind turbine run-conditions (wind speed, rotor speed and blade pitch angle).
- Material and structural properties of the blade (mechanical properties of the blade material, ply angle, shell thickness, etc.).
- Material and structural configurations of the blade (span wise variations of mechanical properties of the blade material, ply angle, shell thickness, etc.).

This makes the wind turbine aerodynamic performance evaluation an iterative coupled-aero-structure simulation and consequently the design of adaptive blades integrated in nature.

Maheri et al (2007a, 2008) proposed a decoupled design method applicable to bend-twist adaptive blades based on the concept of variable state design parameter (VSDP). Figure (4.1) describe this method schematically.

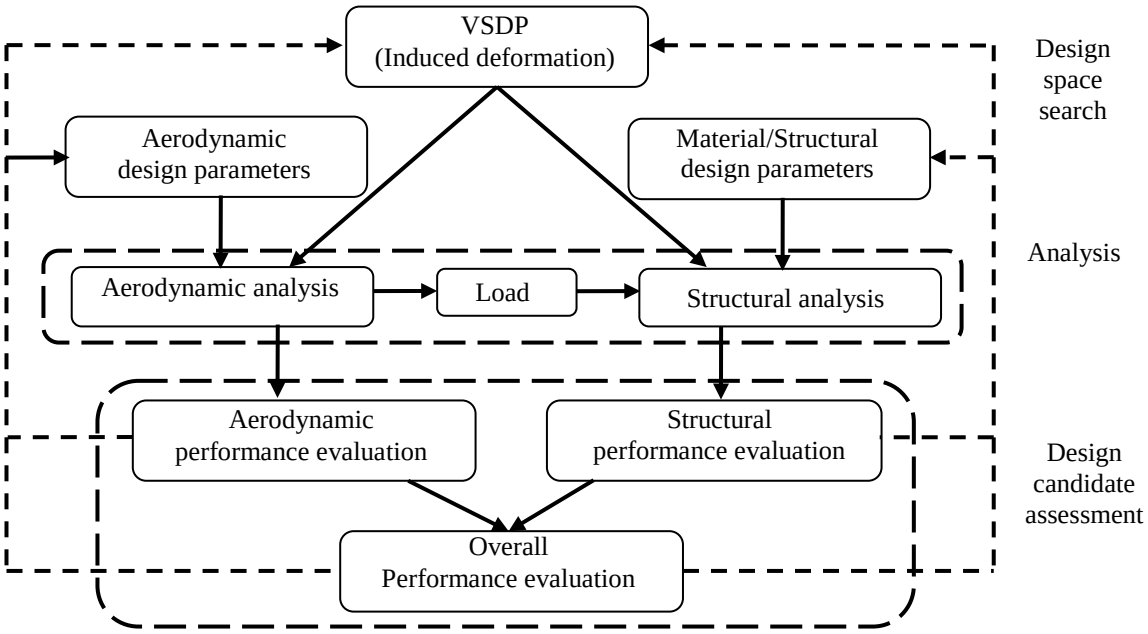

Figure 4.1-Decoupled design by VSDP (Maheri et al, 2008)

The main advantage of this method is the significant reduction in the aerodynamic evaluation time by avoiding running a time consuming structural analysis for each aerodynamic performance evaluation. In this method, the induced twist caused by bend-twist coupling is treated as an aerodynamic design parameter while its dependency on the structural characteristics of the blade is taken into account by imposing a proper constraint on the structure design. However, by use of decoupled method, in structure design side, the material and structural configurations selection must meet the requirements of generating the induced twist as planned in the aerodynamic design process. That is, planning an induced twist, as a design parameter must be realistic and achievable (Maheri et al, 2007a).

4.2 Decoupled Design Method: Background Theory

Maheri et al (2007c) started with the force-displacement relations for bend-twist coupled thin-/thick-walled composite beams of Equations (4.1) and (4.2) as proposed by Kim and White (1997), and then applied the following two basic assumptions:

- The contribution of the internal torque due to the off-axis aerodynamic loading of the blade is negligible.
- The edge-wise slope of the blade is negligible.

$$\begin{Bmatrix} F \\ V_y \\ V_z \end{Bmatrix}_i = \begin{bmatrix} k_{11} & k_{12} & k_{13} \\ k_{21} & k_{22} & 0 \\ k_{31} & 0 & k_{33} \end{bmatrix} \begin{Bmatrix} u_0' \\ v_0' - \theta_z \\ w_0' - \theta_y \end{Bmatrix} \tag{4.1}$$

$$\begin{Bmatrix} T \\ M_y \\ M_z \end{Bmatrix}_i = \begin{bmatrix} k_{44} & k_{45} & k_{46} \\ k_{54} & k_{55} & 0 \\ k_{64} & 0 & k_{66} \end{bmatrix} \begin{Bmatrix} \beta' \\ \theta_y' \\ \theta_z' \end{Bmatrix} \tag{4.2}$$

In case of the coordinate system of beam model adopted by Kim and White (1997), the F , V_y , V_z , T , M_y and M_z have the same meanings of Equation (2.47) by adopting a different coordinate system. In Equation (4.2), M_y , θ_y and β are internal flap-wise bending moment of cross-section (or resultant moment of

cross-section about *y*-axis), flap-wise rotation about *y*-axis and elastic coupling induced twist respectively. The first assumption reduces Equation (4.2) into the following form.

$$\begin{Bmatrix} 0 \\ M_y \end{Bmatrix} = \begin{bmatrix} k_{44} & k_{45} \\ k_{54} & k_{55} \end{bmatrix} \begin{Bmatrix} \beta' \\ \theta_y' \end{Bmatrix} \tag{4.3}$$

Applying the second assumption on Equation (4.3) leads to:

$$M_y = M_{flap} = K\partial\beta / \partial x \tag{4.4}$$

where

$$K = \frac{k_{44}k_{55} - k_{45}k_{54}}{k_{55} - k_{45}} \tag{4.5}$$

Using normalised flap bending moment M^*, normalised effective stiffness K^* and normalised radial location r^*, they showed that Equation (4.4) could be re-written as

$$\beta(r^*) = \frac{M_{hub}}{K_{\max}} \int_0^{r^*} \frac{M^*(r^*)}{K^*(r^*)} dr^* \tag{4.6}$$

in which:

$$M^* = \frac{M}{M_{hub}} \tag{4.7}$$

$$K^* = \frac{K}{K_{\max}} \tag{4.8}$$

$$r^* = \frac{r - R_{hub}}{R - R_{hub}} \tag{4.9}$$

In the above equations M_{hub} is the flap bending at the hub, $K_{\max}$ is the maximum effective stiffness of the blade, R and R_{hub} are rotor and hub radius respectively.

M and K are the flap bending-moment and the effective stiffness at span location r respectively.

Then, they also proved that the normalised bending moment M^* is independent of the wind turbine run-condition as can be seen in Figure (4.2). This figure denotes the normalised flap-bending moment for a variety of AWT-27 wind turbine run-conditions.

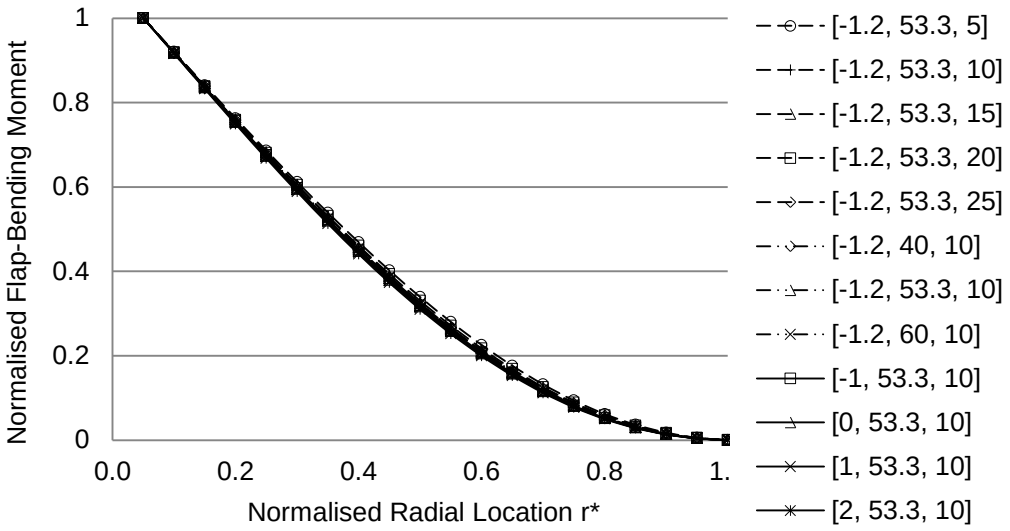

Figure 4.2- Variation of normalised flap-bending moment versus various run conditions [pitch angle (deg), Ω (rpm), V (m/s)]

They also argued that since the distribution of the effective stiffness K depends on the structural characteristics of the blade only and not the wind turbine run-condition, once the effective stiffness K is calculated at a wind turbine run-condition (through an analytical model or a FEA) it can be used for other run-conditions as well.

Having M^* and K^* independent of wind turbine run-condition, the term $\int_0^{r^*} \frac{M^*(r^*)}{K^*(r^*)} dr^*$ in Equation (4.6) becomes invariant to the wind turbine run-conditions. This leads to Equation (4.10), relating the induced twist distribution at a general run-condition $\beta(r^*)$ to the induced twist at a reference run-condition $\beta(r^*)_{ref}$.

$$\beta(r^*) = M_{hub} \frac{\beta(r^*)_{ref}}{M_{hub,ref}} \tag{4.10}$$

Equation (4.10) is the base of decoupled design method and variable state design parameter proposed by Maheri et al (2007a, 2008), as explained below.

Normalising the induced twist distribution by its maximum value occurring at the tip of the blade β_T and substitution from Equation (4.6) leads to:

$$\beta^*(r^*) = \frac{\beta(r^*)}{\beta_T} = \frac{\int_0^{r^*} \frac{M^*(r^*)}{K^*(r^*)} dr^*}{\int_0^1 \frac{M^*(r^*)}{K^*(r^*)} dr^*} \tag{4.11}$$

Combining Equations (4.10) and (4.11) leads to:

$$\beta_T = M_{hub} \frac{\beta_{T,ref}}{M_{hub,ref}} \tag{4.12}$$

In decoupled design $\beta_{T,ref}$ is treated as an independent design parameter, which needs to be obtained such that the aerodynamic performance of wind turbine is optimised. Having optimised $\beta_{T,ref}$ for aerodynamic performance, the elastic coupling in the blade should be implemented such that it produces the exact amount of tip-induced twist at reference run-condition.

Assigning a value to the reference tip induced twist $\beta_{T,ref}$, the tip induced twist at other run-conditions β_T can be found via Equation (4.12). To simulate the wind turbine with adaptive blade the actual distribution of induced twist is needed. In order to find the non-normalised induced twist at each run-condition the normalised induced twist β^* is also required:

$$\beta = \beta^* \beta_T \tag{4.13}$$

Normalised induced twist can be calculated by an analytical model or by employing a FEA.

Maheri et al (2007 a) proposed an analytical model for predicting the normalised induced twist for special case of constant layup configuration and shell thickness through span of the blade:

$$\beta^*(r^*) = \frac{\int_0^{r^*} \frac{M^*(r^*)}{t_{\max}^3(r^*)} dr^*}{\int_0^1 \frac{M^*(r^*)}{t_{\max}^3(r^*)} dr^*} \tag{4.14}$$

in which $t_{\max}$ is the maximum aerofoil thickness.

The rest of this chapter aims at proposing a more general equation for normalised induced twist.

4.3 Normalised Induced Twist Analytical Model

In order to investigate the effects of spanwise variation of shell thickness and layup configuration on the normalised induced twist of adaptive blades, different combinations of layup configurations and shell thickness are investigated. Tables (4.1) and (4.2) show different layup configurations and different shell thickness distributions. Table (4.1) shows three types of layup configurations, namely, (i) uniform (cases 1to 7), (ii) linear variation (cases 8 to 12) and (iii) partial elastic coupling (cases 13 to 17). The four types of thickness distributions are: (i) linear variation (cases 1 to 5 in Table (4.2)), (ii) quadratic variations (case 6), (iii) third degree variation (case 7), and (iv) uniform (cases 8 to 11). Figure (4.3) shows normalised thickness distributions for comparison. Using the developed software explained in Chapter 3, the induced twist of an AWT-27 blade made of thicknesses and layups shown in Tables (4.1) and (4.2) are examined. This blade is running at a wind speed of 10m/s and a rotor speed of 53.3 rpm.

The results are shown in Figures (4.5) to (4.11), (4.13) and (4.14). For convenience, each blade is represented by its corresponding [layup, thickness]

case. For example [2, 3] refers to an adaptive blade made of the layup configuration 2 and thickness distribution 3.

Table 4.1- Layup configurations

Case	Layup Configuration
1	$[20]_{20}$ mirror and uniform through span
2	$[30]_{20}$ mirror and uniform through span
3	$[40]_{20}$ mirror and uniform through span
4	$[50]_{20}$ mirror and uniform through span
5	$[60]_{20}$ mirror and uniform through span
6	$[70]_{20}$ mirror and uniform through span
7	$[80]_{20}$ mirror and uniform through span
8	20 identical layers; ply angle variable linearly from 10° at hub to 40° at tip
9	20 identical layers; ply angle variable linearly from 20° at hub to 50° at tip
10	20 identical layers; ply angle variable linearly from 30° at hub to 60° at tip
11	20 identical layers; ply angle variable linearly from 40° at hub to 70° at tip
12	20 identical layers; ply angle variable linearly from 50° at hub to 80° at tip
13	$[20]_{20}$ mirror for one fourth of span, $[\pm 20]_{10}$ rest of span
14	$[30]_{20}$ mirror for one fourth of span, $[\pm 30]_{10}$ rest of span
15	$[40]_{20}$ mirror for one fourth of span, $[\pm 40]_{10}$ rest of span
16	$[50]_{20}$ mirror for one fourth of span, $[\pm 50]_{10}$ rest of span
17	$[60]_{20}$ mirror for one fourth of span, $[\pm 60]_{10}$ rest of span

Table 4.2- Shell thickness distribution

Case	Variation type	Thickness [from to] (mm)	Normalised thickness distributions
1	Linear	34 to 15	$t^* = -0.574r^* + 1$
2		32 to 13	$t^* = -0.609r^* + 1$
3		29 to 10	$t^* = -0.672r^* + 1$
4		34 to 24.5	$t^* = -0.287r^* + 1$
5		34 to 19.75	$t^* = -0.430r^* + 1$
6	Quadratic	34 to 15.3	$t^* = 0.433r^{*2} - 1.009r^* + 1$
7	Third degree	34 to 15	$t^* = -0.004r^{*3} + 0.884r^{*2} - 1.479r^* + 1$
8	Uniform	10	$t^* = 1$

9		15	$t^*=1$
10		20	$t^*=1$
11		34	$t^*=1$

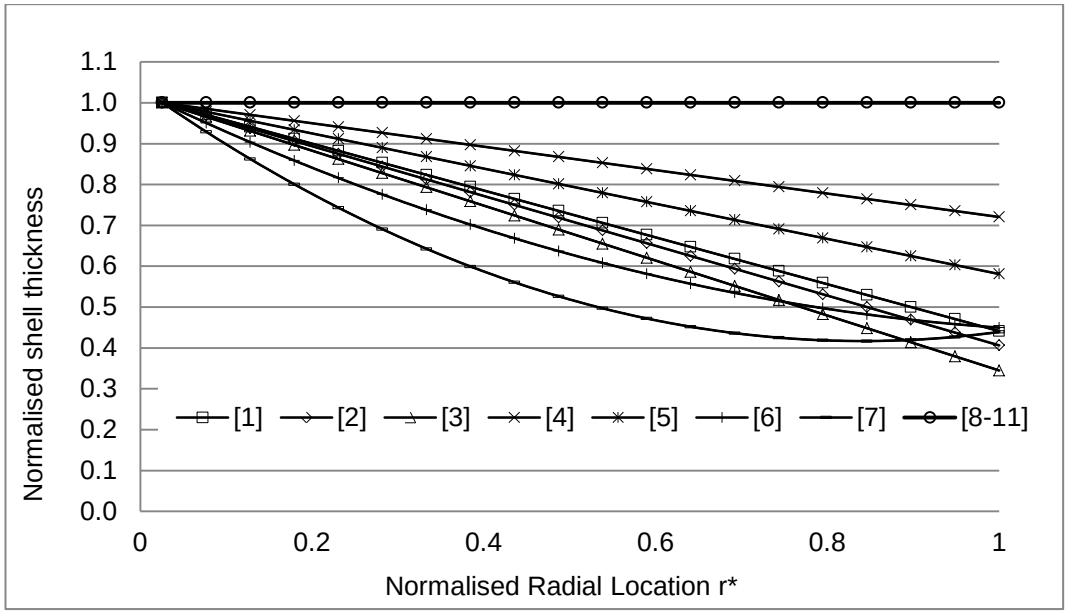

Figure 4.3-Normalised shell thickness distributions of Table (4.2)

In analysis, the continuous variations of shell thickness and layup configurations are replaced by stepwise variations using 20 segments shown in Figure (4.4).

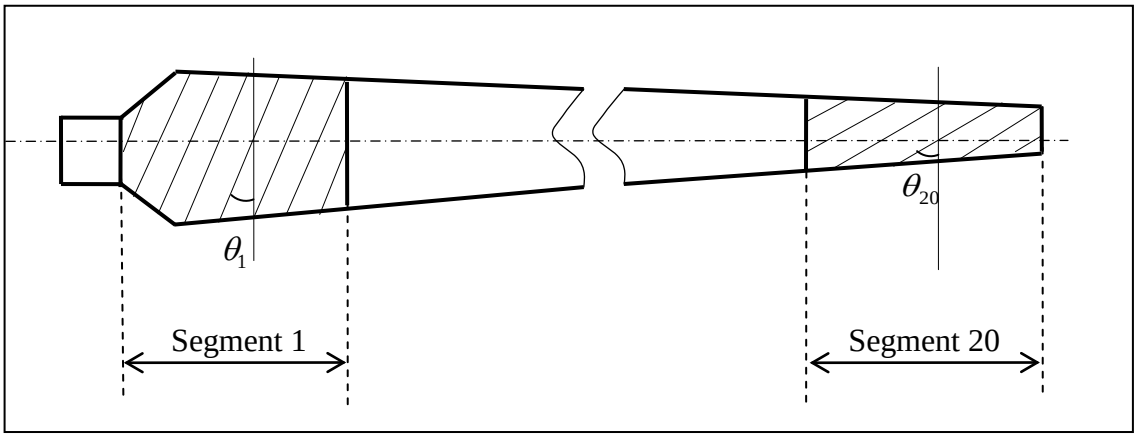

Figure 4.4-Variation of layups by a stepwise variation over 20 segments

4.3.1 Effect of Shell Thickness and Ply Angle on β^* for Uniform Shell Thickness and Constant Layup Configurations

The first case study is carried out by using various uniform shell thickness distributions and uniform layup configurations in the structure of the blades

[1/3/5/7, 8/9/10/11]. Figure (4.5) shows that normalised induced twist is independent of fibre angle or the actual value of shell thickness as long as the layup configuration and thickness remain constant spanwise.

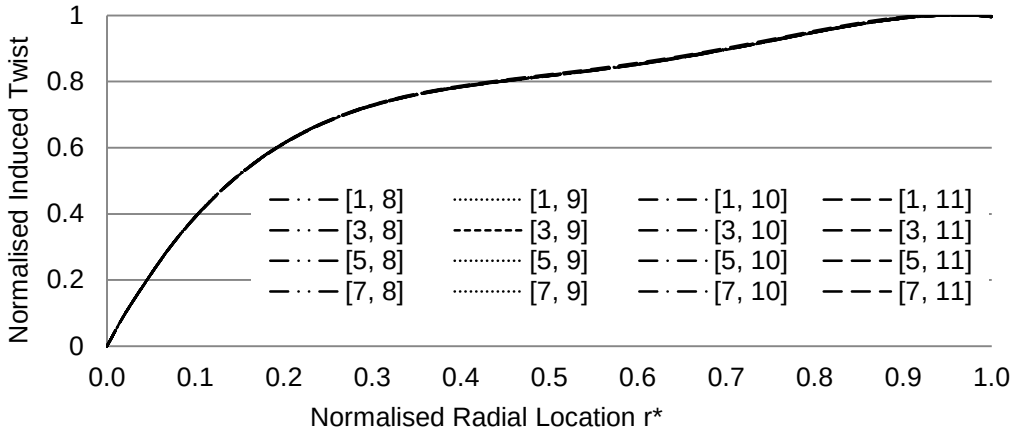

Figure 4.5-Effect of shell thickness and ply angle on β^* in case of uniform shell thickness and constant layup configuration

4.3.2 Effect of the Variation of Shell Thickness on β^* for Constant Layup Configurations

The second case study is carried out by using uniform layup configurations but spanwise variable shell thickness distributions in the structure of the blades [1/3, 1/2/3/4/5/6/7]. Figures (4.6) and (4.7) show the spanwise variation of normalised induced twist. In the first glance, one may conclude that the actual value of the thickness affects the form of normalised induced twist. However, with reference shown in Figures (4.3) and (4.8) (showing normalised shell thickness combinations [1/3, 1/2/3//6]) one notices that the trend of normalised induced twist is in fact a function of the slope of the variation of thickness rather than its actual value. Thickness cases 1, 2, 3 and 6 all have very close slopes (see Figure (4.3)).

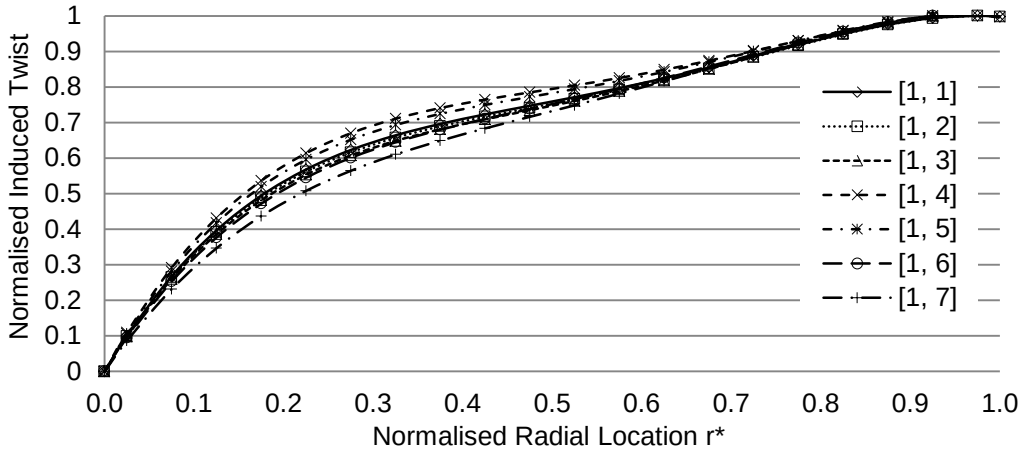

Figure 4.6-Effect of shell thickness variation on β^* in case of constant layup configuration [1, 1/2/3/4/5/6/7]

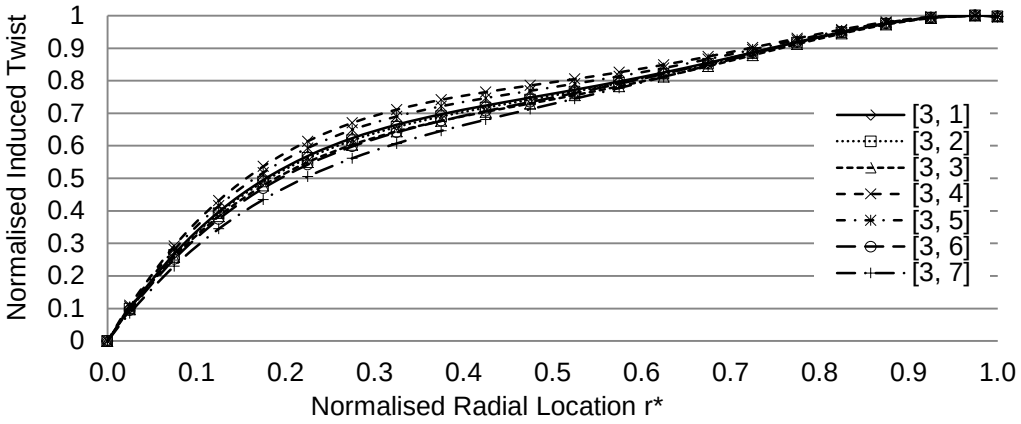

Figure 4.7-Effect of shell thickness variation on β^* in case of constant layup configuration [3, 1/2/3/4/5/6/7]

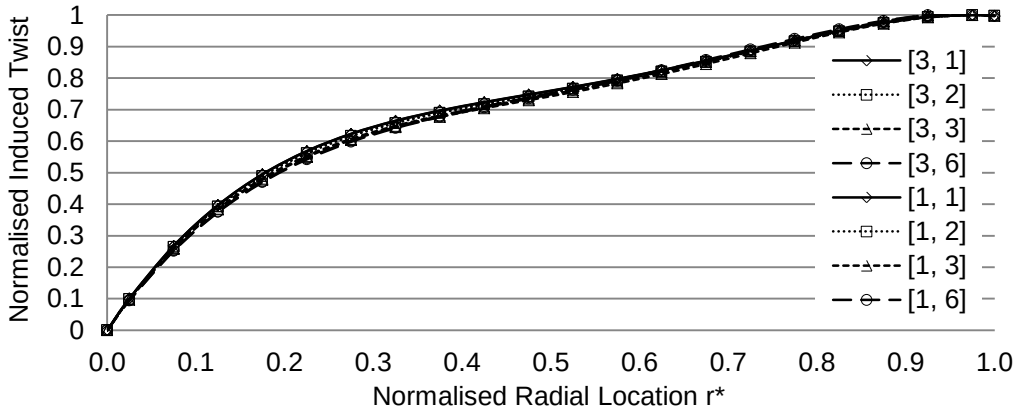

Figure 4.8- Effect of the slope of shell thickness variation on β^* in case of constant layup configuration [3, 1/2/3/6]

4.3.3 Effect of the Rate of the Variation of Thickness on β^*

The fourth case study is carried out by using uniform layup configurations but spanwise variable shell thickness distributions in the structure of the blades [1/3/5, 1/6/7]. Thickness cases 1, 6 and 7 all start from 34 mm at the hub and vary to about 15 mm at the tip, linearly (case 1), quadratic (case 6) and following a third degree variation (case 7). Figure (4.8) shows that the normalised induced twist depends on the form of the variation of thickness. This actually confirms the conclusion of the previous section, emphasising the fact that it is in fact the rate of variation of thickness that dictates the behaviour of the induced twist not the actual value.

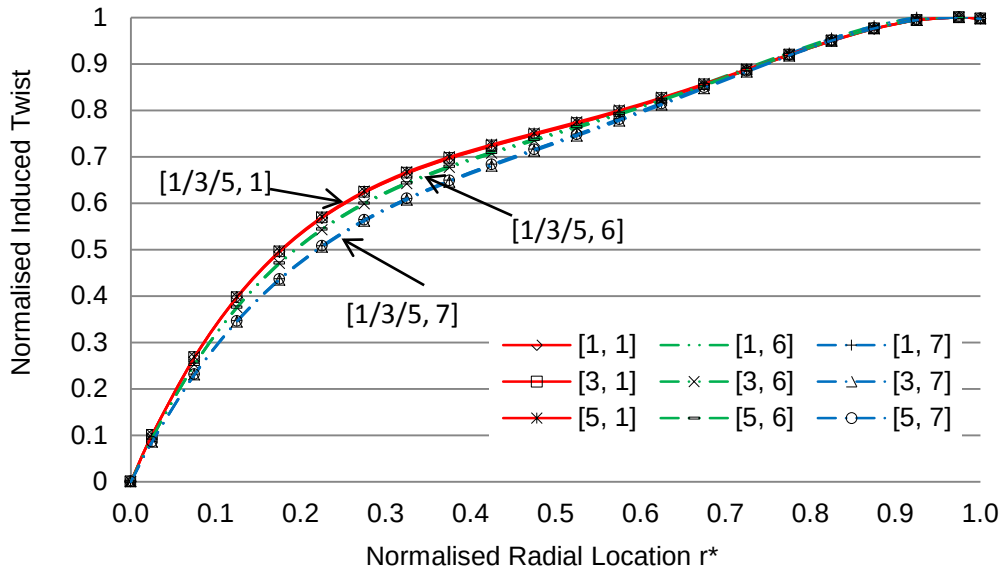

Figure 4.9- Effect of the form of the variation of thickness on normalised induced twist

4.3.4 Effect of Spanwise Variation of Fibre Angle on β^*

It was shown that the spanwise behaviour of the normalised induced twist is independent of the fibre angle as long as it remains constant along the span of the blade (see Figures (4.5) and (4.9)). In this section, adaptive blades with variable fibre angle along their span are analysed to investigate the effect of spanwise variation of fibre angle on β^*. The results for combinations [8/9/10/11/12, 8] are shown in Figure (4.10). It can be seen that the variation of fibre angle along the

span of the blade has the highest effect on the normalised induced twist. This was expected as the amount of elastic coupling highly depends on the fibre angle.

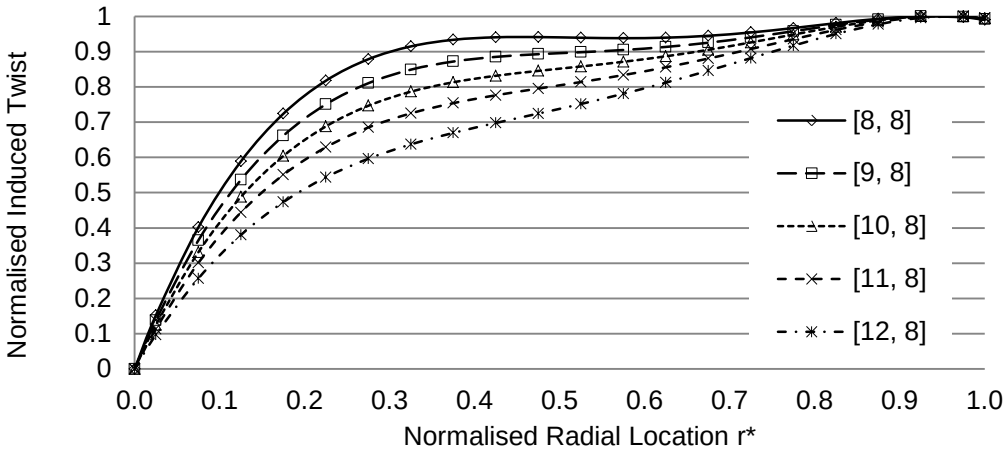

Figure 4.10 - Effect of spanwise variation of fibre angle on β^*

Another interesting result can be seen from the results shown on this figure by comparing combinations [8, 8] corresponding to fibre angle variation from 10 to 40 degrees and [12, 8] corresponding to fibre angle variation from 50 to 80 degrees. One can observe that combination [8, 8] produces induced twists as high of 90% of the maximum value for almost 70% of the blade span. In case of combination [12, 8] only 20% of the blade experience an induced twist above 90% of the tip induced twist.

Figure (4.11) shows the actual values of induced twist for cases [1 to 12, 8]. It can be observed that combinations with linearly variable fibre angles produce larger induced twists. Combination [10, 8] corresponding to fibre angle varying linearly from 30° at hub to 60° at tip, produces the highest values of induced twist at the tip of the blade. On the other hand, combinations [8, 8], corresponding to fibre angle varying linearly from 10° at hub to 40° at tip, produces more uniform induced twist through the blade span.

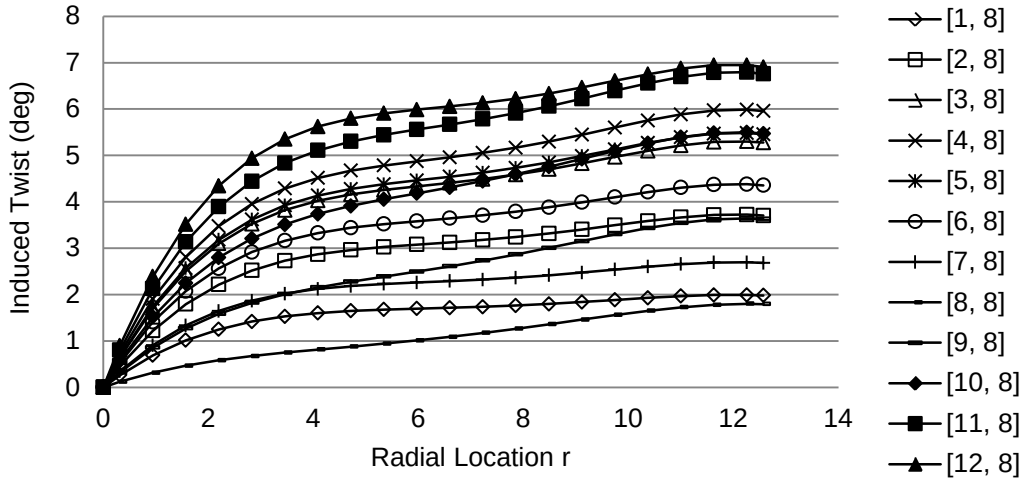

Figure 4.11- Induced twist distribution for cases [1 to 12, 8]

4.3.5 Effect of Combined Unbalanced-Balanced Layup on β^*

An adaptive blade with combined unbalanced-balanced layup is shown in Figure (4.12). In this blade, 25% of the span of the blade is made up of unbalanced layups, while the rest 75% is made of balanced layup. The layup configurations [13/14/15/16/17, 11] are used for analysis of this blade. The predicted induced twists are shown in Figure (4.13). It can be seen that the induced twist reaches its maximum value at the end of section with unbalanced layup and then remains almost constant for the rest of the blade. Deviation of induced twist curves from horizontal line after reaching their maximum values at about quarter of the blade is due to elastic twist produced by aerodynamic pitching moment, which in our case here is in the opposite direction of the induced twist produced by elastic coupling.

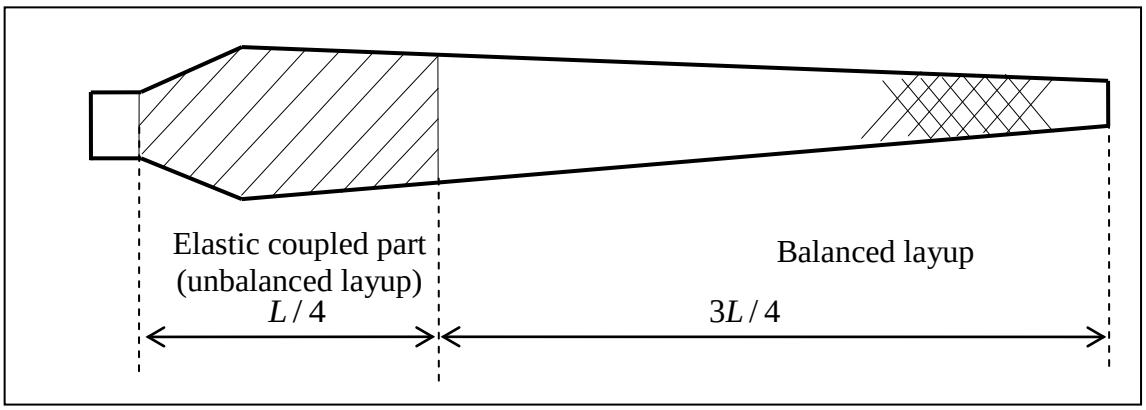

Figure 4.12-Adaptive blade with combined unbalanced-balanced layup

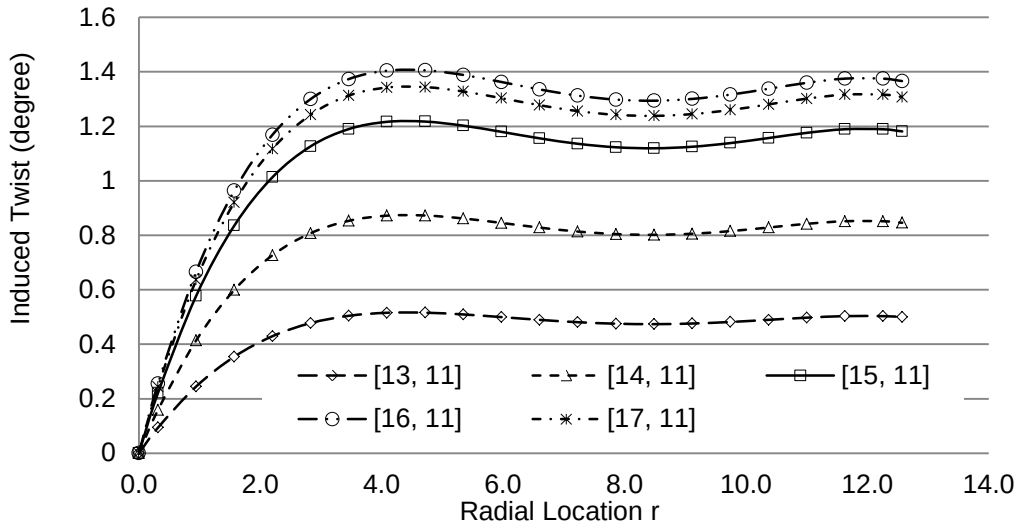

Figure 4.13-Induced twist in blades with combined unbalanced-balanced layup

Figure (4.14) shows the normalised induced twist for all cases. As expected, since the thickness is uniform and the layup configuration in the unbalanced segment is constant, the normalised induced twist is identical for all cases.

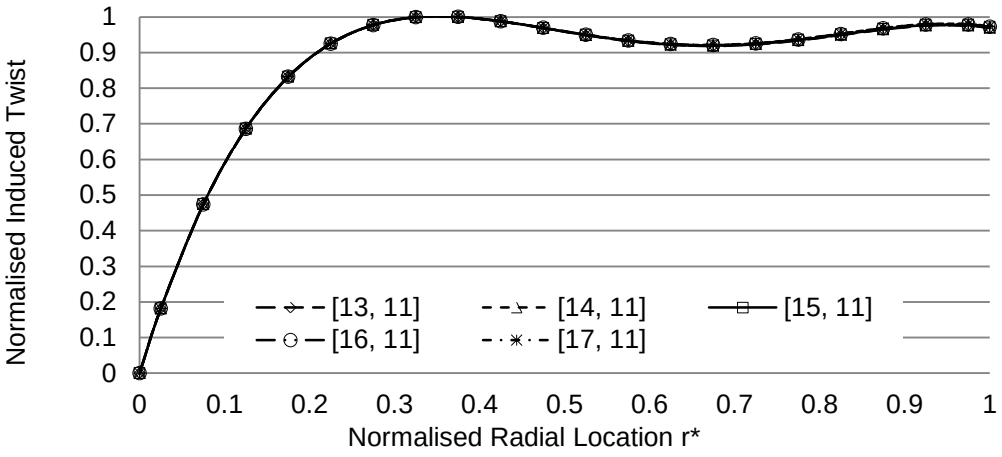

Figure 4.14-Normalised induced twist in blades with combined unbalanced-balanced layup

4.3.6 Extended Analytical Model for Normalised Induced Twist

Using the data generated in previous sections, the analytical model of Equation (4.15) is proposed for predicting normalised induced twist in adaptive blades with spanwise variable thickness distributions with constant layup configurations. This model is based on the old model proposed by Maheri et al (2007a) (see Equation (4.14)) which is only valid for the blades with uniform thickness and constant layup configurations.

$$\beta^*(r^*) = \frac{\int_0^{r^*} \frac{M^*(r^*)}{t_{\max}^3(r^*)t_s^*(r^*)} dr^*}{\int_0^1 \frac{M^*(r^*)}{t_{\max}^3(r^*)t_s^*(r^*)} dr^*} \tag{4.15}$$

In this equation, t_s^* stands for the normalised shell thickness defined as:

$$t_s^* = t_s / t_{s,\max} \tag{4.16}$$

In order to investigate the performance of the proposed model of Equation (4.15), the normalised induced twist predicted by this model has been compared with the numerical results obtained by ANSYS® for three sets of no-web, one-web and two-web adaptive blades with configurations [5, 1/2/3/4/5/6/7]. Results are shown in Figures (4.15) through (4.17). It can be seen that in all cases there is a good agreement between the results predicted by the proposed analytical model and the numerical results.

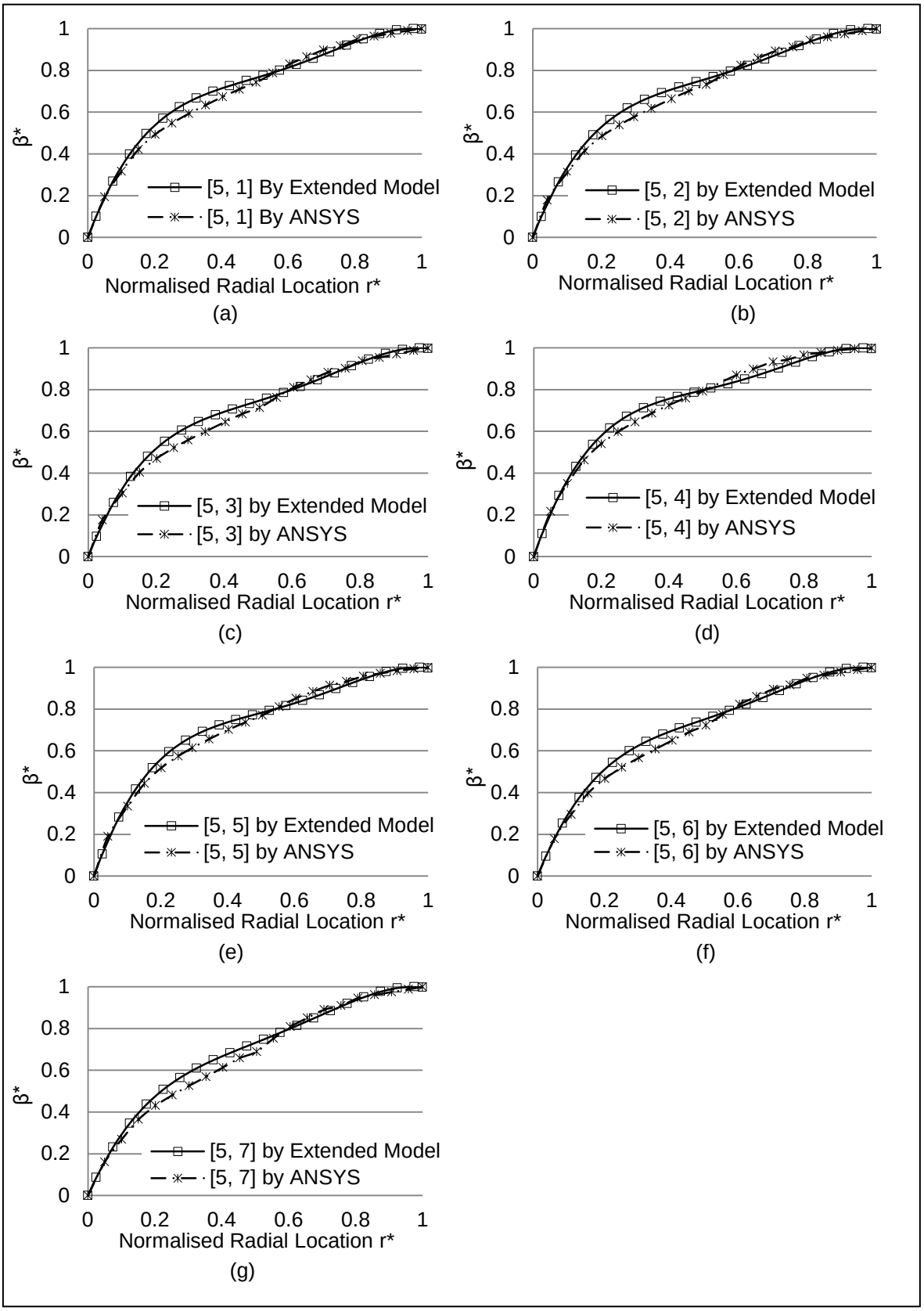

Figure 4.15-Predicted $\beta*$ by Eq. (4.15) and ANSYS in adaptive blades [5, 1/2/3/4/5/6/7] without web

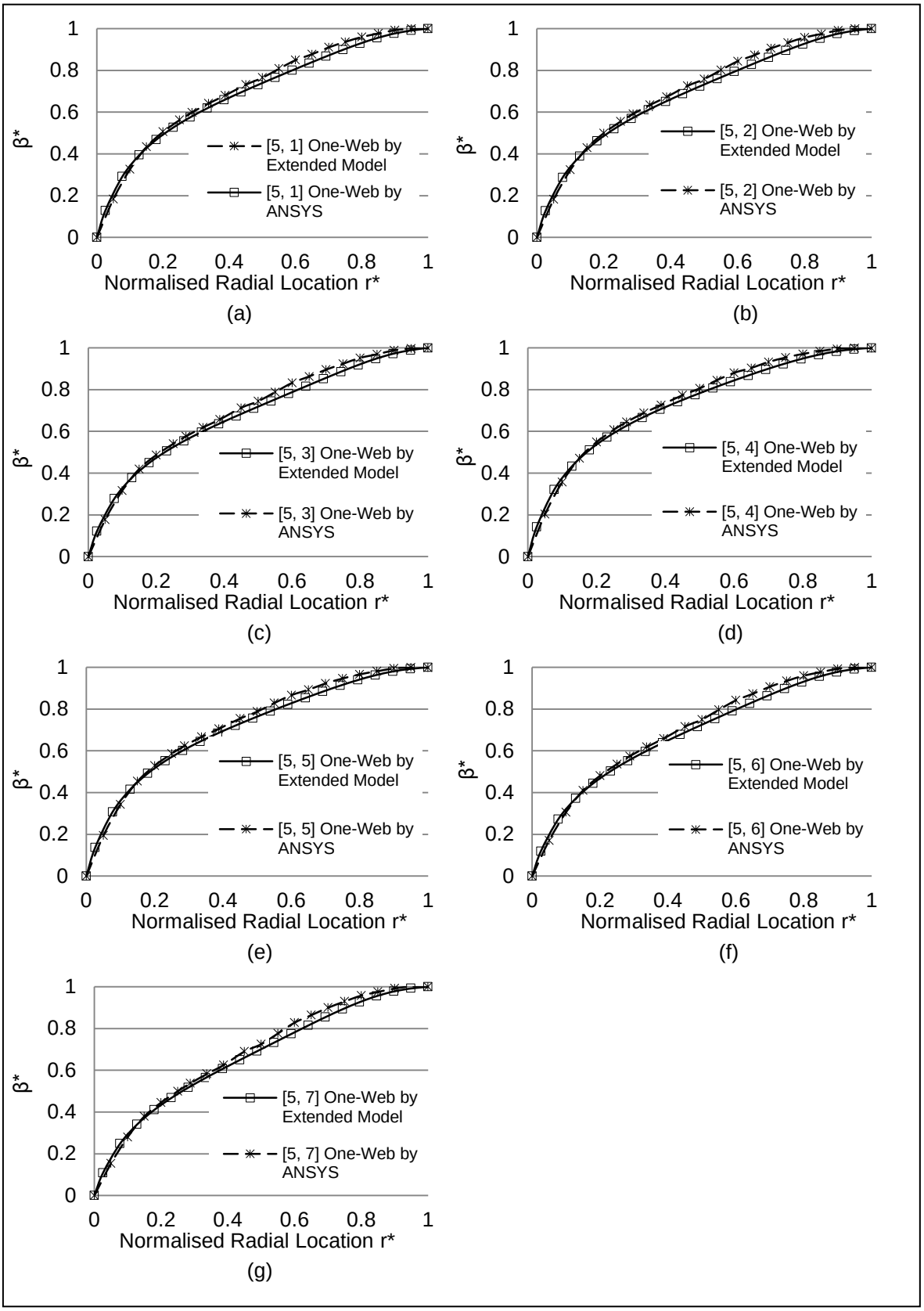

Figure 4.16 - Predicted $\beta*$ by Eq. (4.15) and ANSYS in adaptive blades [5, 1/2/3/4/5/6/7] with one web located at 33% of the chord from LE

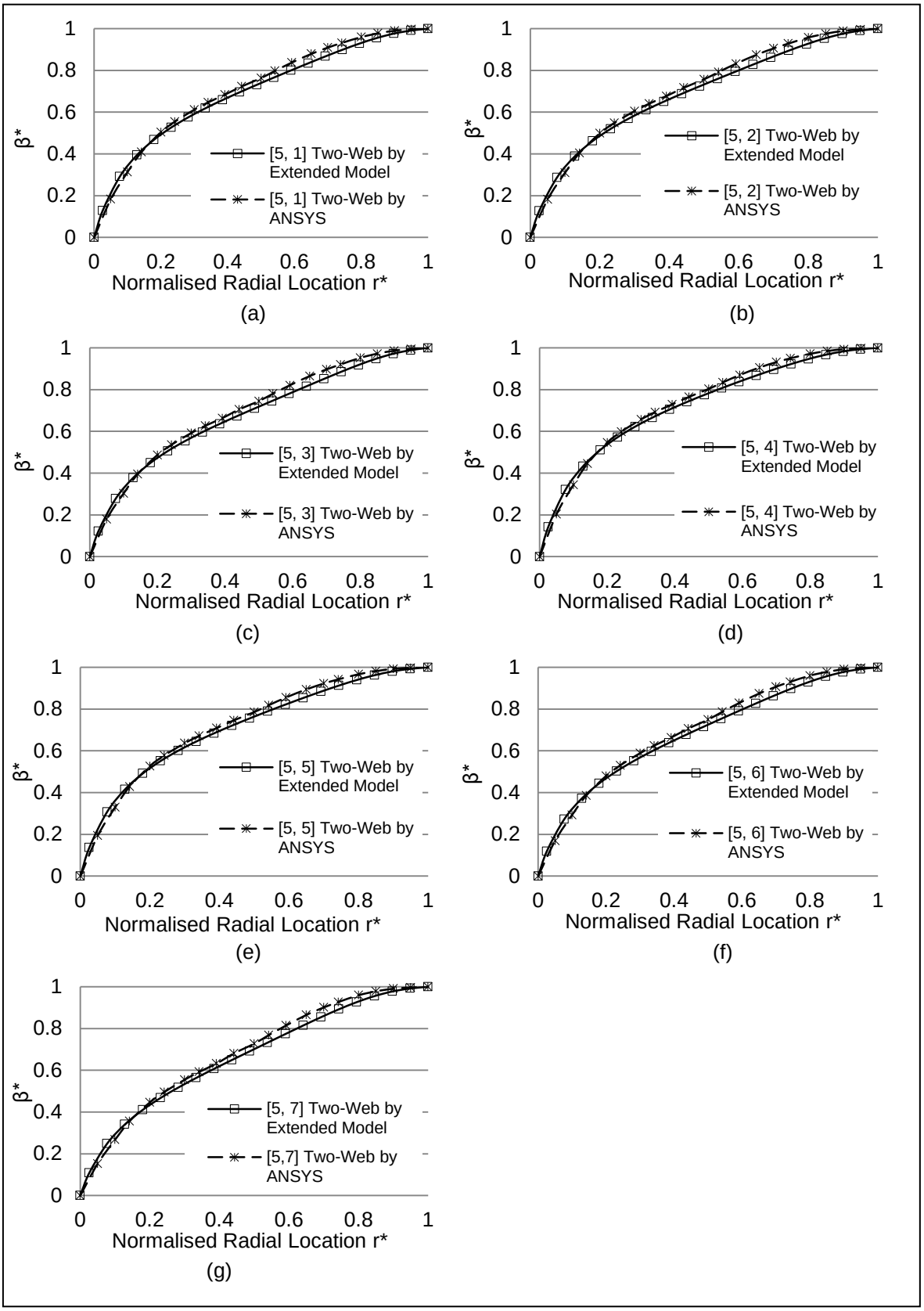

Figure 4.17- Predicted $\beta*$ by Eq. (4.15) and ANSYS in adaptive blades [5, 1/2/3/4/5/6/7] with two webs located at 33% and 67% of the chord from LE

4.4 Summary

In this chapter, using the software tools developed in Chapter 3, firstly, the behaviour of normalised induced twist for various combinations of shell thickness and layup configuration is investigated and then an analytical model for predicting the normalised induced twist in adaptive blades with variable shell thickness is introduced. Comparing the numerical results obtained by ANSYS® and those obtained by the proposed model shows that the model is capable of predicting normalised elastic twist for blade with variation of thickness with a good accuracy.

The following conclusions can be drawn from the results obtained in this chapter:

- Normalised induced twist is independent of fibre angle and the actual value of the shell thickness as long as the layup configuration and thickness remain constant spanwise.
- For constant layup configurations but spanwise variable shell thickness distributions, the trend of normalised induced twist is a function of the slope of the variation of thickness rather than its actual value. In other words, it is the rate of the variation of thickness that dictates the trend of the induced twist not the actual value.
- The variation of fibre angle along the span of the blade has the highest effect on the form of normalised induced twist.
- For adaptive blades with combined unbalanced-balanced layup configurations, the induced twist reaches its maximum value at the end of the section with unbalanced layup and then remains almost constant for the rest of the blade.
- For linearly variable layup configurations, with average fibre angle between 20 to 40 degrees, most of the blade span experiences an induced twist above 90% of the tip-induced twist.

5 Conclusion

5.1 Summary

Wind turbines are designed to extract energy with the highest efficiency. One of the basic requirements for wind turbines is to have a control mechanism in place to ensure that the rotors do not produce power excess to the rated value for a safe operation of the generator, and that the aerodynamic loads on the blade do not exceed the design load. Power and load control systems used in wind turbines can be classified as conventional and non-conventional. Among non-conventional control approaches, adaptive blade is the topic of investigated in this thesis.

In adaptive blades, a controlled and limited torsional deformation is produced as a result of the implanted elastic coupling (bend-twist) in the structure of the blade in response to the changes of rotor run condition. The earlier investigation on adaptive blades has shown great potentials for this kind of blades in increasing annual average power of wind turbines as well as load alleviation capabilities. However, comparing to conventional blades, simulation of wind turbines utilising adaptive blades and design of adaptive blades is more complicated. The main reason is the dependency of the aerodynamic performance of an adaptive blade to its structural characteristics.

Simulation of wind turbines utilising adaptive blades is an iterative coupled-aero-structure process. For aerodynamic simulation of wind turbine, the induced deformation due to elastic coupling needs to be known. Therefore, structural characteristics of the blade must be also known. Moreover, a sophisticated structural analyser with high accuracy is required to predict the induced deformation accurately (i.e. the order of a fraction degree for induced twist). Running finite element based structural analysis is highly time-consuming in an iterative process.

The traditional design methods for conventional blades are not applicable to the design of adaptive blades. The aerodynamic design of ordinary blades can be performed without direct participation of the material properties and structure configurations of the blade. The aerodynamic and structural design phases of traditional wind turbine blades take place sequentially. In case of adaptive blades,

the aerodynamic and structural design phases are integrated in nature. Two approaches could make a design process efficient and practical:

Running an integrated design process by employing an efficient and robust structural analysis tools. As mentioned previously, using FEA-based structural analysers makes the integrated optimal design of adaptive blades very time-consuming and therefore inefficient. Using analytical beam models instead of FEA-based analysis saves time and makes the analysis computationally efficient. However, none of the available beam models have been claimed or shown to be accurate enough for our purpose here. In order to make integrated design of adaptive blades practical, a robust structural analysis tool based on an accurate beam model for thin-walled, multi-cell, non-uniform composite beams is required.

Decoupling the coupled aero-structure design. Although decoupled design method has been shown to be highly efficient in design of adaptive blades, more investigation must be carried out to develop models in which the effect of the spanwise variations of the shell thickness and fibre angle are taken into account.

Aeroelastic stability is another major issue for elastically tailored aero-structures such as adaptive blades. While there have been many detailed research work carried out towards investigating the effect of specific layup configuration on natural frequencies of adaptive blades, no general guidance has been given yet. This is mainly due to not having an easy-to-run structural analyser capable of delivering modal analysis.

In view of the above, this project aimed at the development of efficient and robust tools and methods for optimal design of wind turbine adaptive blades.

5.2 Achievements and Original Contribution

The main achievements are listed as follows

- A general thin-walled composite beam model suitable for deformation analysis of elastically coupled multi-cell thin-walled beams with general cross-section was developed. This beam model is capable of predicting the induced twist due to elastic coupling for thin-walled closed multi-cell

composite beams with spanwise variable cross-sectional properties and non-uniform shell thickness distribution under various types of loads. The performance of the developed model for various beams under various loading scenarios was investigated. Single-, two- and three-cell wind turbine blades with constant thickness were investigated under various layup configurations. Single-cell blades with variable thickness distributions along the blade longitudinal axis were also investigated. The results for all cases show a good agreement with analytical experimental and numerical results, highlighting the accuracy of the results at required level for simulation and design of wind turbine adaptive blades.

- A software tool was developed for implementing the beam models, allowing for a robust and efficient iterative-coupled aero-structural analysis. Three graphical user interfaces were developed to code and link the analytical beam models with an aerodynamic analysis programme. The efficient and accurate beam model takes the place of FEA in the coupled aero-structure analysis of adaptive blades. This package allows the user to produce material properties and then define the blade structure efficiently. The method used for the definition of the structure of an adaptive blade is highly flexible, allowing defining adaptive blades with a wide range of elastic-coupling topologies and material configurations.
- The decoupled design method was extended by proposing and validating an analytical model for normalised induced twist variation for general case of spanwise variable thickness. Using the developed software as a search platform firstly, the behaviour of normalised induced twist for various combinations of shell thickness and uniform layup configuration was investigated and then an analytical model for predicting the normalised induced twist for adaptive blades with variable shell thickness was introduced. Comparing the numerical results obtained by ANSYS and those obtained by the analytical model proposed in this chapter shows that the analytical model is capable of predicting normalised elastic twist for blade with variation of thickness with a good accuracy.

- Further analysis was carried out towards investigation the effect of spanwise variation of layup configuration on the normalised induced twist. It was found that the variation of fibre angle along the span of the blade has the highest effect on the form of normalised induced twist and that it is possible to achieve uniform induced twists along the majority of the span of the blade by using a linearly variable fibre angle.

5.3 Critical Appraisal and Future Work

In coding the thin-walled composite beam model of Chapter 2, the aerofoil contour of the outer surface is assumed to be the middle-line of the blade shell to make the calculations over the cross-section easier. The real middle-line contour is a stepped curve for chord-wise variable shell thickness. This assumption makes the cross-section of the blade slightly bigger than the actual cross-section. However, considering the blade cross-section as a thin-walled structure, this assumption is expected to produce some but small amount error.

In all simulated and structurally analysed adaptive blades in this project, the mass of the blades is neglected. Mass of the blade is the source of blade axial forces due to gravity and inertia. In other words, in all simulated and structurally analysed adaptive blades the axial force is neglected. As a future work, the weight of the blade should be also considered in order to perform simulations that are more realistic.

Despite the assumptions described above, the analytical beam model is still capable of predicting the induced twist for bend-twist coupled adaptive blade efficiently without involving complicated beam theories and calculations.

The extended model for calculating normalised induced twist is superior to the original model proposed by Maheri et al (2007a), as it can incorporate the effect of spanwise thickness variation. However, this model is applicable to constant layup configurations only. This model needs to be modified to incorporate the effect of layup configuration variation as well as the shell thickness variation.

In theory, the developed beam models and the software tool can be used for stretch-twist adaptive blades as well. These models and the performance of the software tool needs to be investigated for stretch-twist adaptive blades in the future.

References

- ADAMS/SOLVER Reference Manual (1994) Version 8.0, Mechanical Dynamics, Inc., Ann Arbor, November 15.
- *ADAMS/WT User's Guide* (1997) Version 1.50, Mechanical Dynamics, Inc., Ann Arbor, February.
- Andersen P. B., Gaunaa . M. et al (2006) Load alleviation on wind turbine blades using variable airfoil geometry. In*: Proceedings of European Wind Energy Conference and Exhibition2006, Athens.*
- Ardoso, J. E. B., Benedito, N. M. B. & Valido, A. J. J. (2009) Finite element analysis of thin-walled composite laminated beams with geometrically nonlinear behaviour including warping deformation. *Thin-Walled Structures*, 47, 1363-1372.
- Ashwill, T. (2010) *Sweep-twist adaptive rotor blade: final project report.* Knight & Carver Wind Group. Report number: Sand2009-8037.
- Back, S.Y. & Will, K. M. (2008) Shear-flexible thin-walled element for composite I-beams. *Eng Struct*, 30, 1447-1458.
- Baker, J. P., Standish, K. J. & van Dam, C. P. (2005) Two-dimensional wind tunnel and computational investigation of a microtab modified S809 airfoil, *AIAA 2005-1186. In: Proceedings of the 43rd AIAA/ASME, Reno, NV, USA.*
- Barlas, T. & Van Kuik, G. M. (2010) Review of state of the art in smart rotor control research for wind turbines. *Aerospace Sciences*, 46, 1-27.
- Bertholet, J. M. Composite materials (1999) *Mechanical behaviour and structural analysis*, New York, Springer.
- Bir, G. S., Chopra, I. & Nguyen, K. (1990) Development of UMARC (University of Maryland advanced Rotor Code), In: *Proc. of the 46th Annual National Forum of the AHS, Washington, D.C., May.*
- Bir, G. S. & Chopra, I. (1994) Aeromechanical stability of rotorcraft with advanced geometry blades. *Mathematical and Computer Modelling*, 19, 159-191.

- Bhaskar, K. & Librescu, L. A (1995) Geometrically non-linear theory for laminated anisotropic thin-walled beams. *Int J Eng Sci*, 33(9), 1331–1344.
- Bossanyi, E. (2000) The design of closed loop controllers for wind turbine. *Wind Energy*, 3, 149–163.
- Bossanyi, E. (2003a) Individual blade pitch control for load reduction. *Wind Energy*, 6, 119–128.
- Bossanyi, E. (2003b) Wind turbine control for load reduction. *Wind Energy*, 6, 229–244.
- Bossanyi, E. (2005) Further load reduction with Individual pitch control. *Wind Energy*, 8, 481–485.
- Buhl, T. & Gaunaa, M. (2005) Potential load reduction using airfoils with variable trailing edge geometry. *Journal of Solar Energy Engineering*, 127, 503-516.
- Buhl, J. M. L. (2005) *A new empirical relationship between thrust coefficient and induction factor for the turbulent windmill state*. National Renewable Energy Laboratory. Report number: NREL/TP-500-36834.
- Burton, T., Sharpe, D., Jenkins, N. & Bossanyi, E. (2002) *Wind energy handbook*. John Wiley & Son Inc.
- Burton, T. (2011) *Wind energy handbook.* Chichester, West Sussex Wiley.
- Büter, A. & Breitbach, E. (2000) Adaptive blade twist calculations and experimental results. *Aerosp. Sci. Technol*, 4(5), 309–319.
- Caselitz, P., Kleinkauf, W., Krueger, W., Petschenka, J., Reichardt, M., & Stoerzel K. (1997). Reduction of fatigue loads on wind energy converters by advanced control methods. In*: European Wind Energy Conference, Dublin. Pages 555–558*.
- Cardoso, J. E. B., Benedito, N. M. B. & Valido, A. J. J. (2009). Finite element analysis of thin-walled composite laminated beams with geometrically nonlinear behaviour including warping deformation. *Thin-Walled Structures*, 47**,** 1363-1372.
- Cesnik, C. E. S. & Hodges, D. H. (1997) VABS: a new concept for composite rotor blade cross-sectional modelling. *Journal of the American Helicopter Society*, 42 (1), 27–38.

- Chandra, R. & Chopra, I. (1991) Experimental and Theoretical Analysis of Composite I-Beams with Elastic Couplings. *AIAA Journal*, 29(12).
- Chandra, R. & Chopra, I. (1992) Structural Behaviour of Two-Cell Composite Rotor Blades with Elastic Couplings. *AIAA Journal*, 30(12), 2914–2921.
- Chandra, R., Stemple, A. D. & Chopra, I. (1990) Thin-walled composite beams under bending, torsional, and extensional loads. *Aircraft*, 27(47), 619-626.
- Chow, R. & van Dam, C.P. (2007) Computational investigations of deploying load control microtabs on a wind turbine airfoil. In*: Proceedings of the 45th AIAA/ASME, Reno, NV, USA.*
- Christensen, R. M. & Lo, K. H. (1979) Solutions for effective shear properties in three phase sphere and cylinder models. *J. Mech. Phys. Solids, 27(4).*
- Currin, H. (1981) North wind 4kW Passive Control System Design, In: *Proceedings Wind Turbine Dynamics, NASA Pub. 2185, DOE Pub. CONF-810226, Cleveland, OH.*
- DOE (2005) Variable length wind turbine blade. DE-FG36-03GO13171.
- Don, W., Lobitz, et al (2001). The Use of Twist-Coupled Blades to Enhance the Performance of Horizontal Axis Wind Turbines. SAND 2001-1303.
- Eisler, G. R. & Veers, P. S. (1998) Parameter Optimization Applied to Use of Adaptive Blade on a Variable-Speed Wind Turbine. Sandia National Laboratories SAND98-2668.
- Enenkl, B., Klopper, V. et al. (2002) Full scale rotor with piezoelectric actuated blade flaps. In: *28th European Rotorcraft Forum*.
- Farhan, G. & Phuriwat, A. I. (2008) Skin design studies for variable camber morphing airfoils. *IOPP'S Journal*.
- Fatmi, R. E. & Ghazouani, N. (2011) Higher order composite beam theory built on Saint-Venant's solution. Part-I: Theoretical developments. *Composite Structures*, 93, 557-566.

- Ferrero, J. F., Barrau, J. J., Segura, J. M., Sudre, M. & Castanie, B. (2001a) Analytical theory for an approach calculation of non-balanced composite box beams. *Thin-Walled Struct*, 39, 709–729.
- Ferrero, J. F., Barrau, J. J., Segura, J. M., Castanie, B. & Sudre, M. (2001b) Torsion of thin-walled composite beams with midplane symmetry. *Comp Struct*, 54(1),111–120.
- Floros, M. W. & Smith, E. C. (1997) Finite element modelling of open-section composite beams with warping restraint effects. *AIAA J*, 35,1341–1347.
- Friedmann, P. P. & Shanthakumaran, P. (1982) Optimum Design of Rotor Blades for Vibration Reduction in Forward Flight. In: *Proc. of the 39th Annual Forum of the AHS.*
- Friedmann, P. P. & Shanthakumaran, P. (1983) Aeroelastic Tailoring of Rotor Blades for vibration Reduction in Forward Flight. *Journal of the AHS*, 29(4), 70-80.
- Friedmann, P. P., Venkatesan, C., & Yuan, K. (1992) Development of a Structural Optimization Capability for the Aeroelastic Tailoring of Composite Rotor Blades with Straight and Swept Tips. In: *4th AIAA Symp. on Multidisciplinary Analysis and Optimizations, Cleveland, Ohio, Sept. 1992*.
- Ganguli, R. & Chopra, I. (1993) Aeroelastic Optimization a Helicopter Rotor with Composite. *Journal of Aircraft*, 32(6), 1326-1334.
- Ganguli, R. & Chopra, I. (1994) Multi-Objective Optimization of a Composite Helicopter Rotor. In: *Presented at the 35th Structures, Structural Dynamics and Materials Conference and Adaptive tructures Forum, April 1994*.
- Ganguli, R. & Chopra, I. (1997) Aeroelastic Tailoring of Composite Couplings and Blade Geometry of a Helicopter Rotor Using Optimization Methods. *Journal of the AHS*, 42(3).
- GE Wind Energy LLC (2006) *Advanced wind turbine program next generation turbine development project*. NREL laboratory. Report number: NREL/SR-5000-38752.

- Gjelsvik, A. (1981)*The theory of thin-walled bars*. New York: Wiley.
- Hansen, C. (1998) *AeroDyn for ADAMS User's Guide*, Version 11.0, University of Utah, Salt Lake City.
- Hill, R. (1964) Theory of mechanical properties of fiber-strengthened materials: I. Elastic behaviour. *J.Mech.Phys.Solids*, 12, 199.
- Hohenemser, K. H. & Swift, A. H. P. (1981) Dynamics of an experimental two bladed horizontal axis wind turbine with blade cyclic pitch variation. NASA. Report number: NASA 82N23716.
- Hong, C. H. & Chopra, I. (1985) Aeroelastic stability of a composite blade. *Journal of the American Helicopter Society*, 30 (2), 57-67
- Jeon, S.M., Cho, M. H. & Lee I. (1998) Aeroelastic analysis of composite rotor blades in hover. *Comput Struct*, 66 (1), 59–67.
- Johnson, W. (1982) Self-Tuning regulators for Multicyclic Control of Helicopter vibration. NASA-TP-1996, March 1982.
- Johnson, E. R., Vasiliev, V. V. & Vasiliev, D. V.(2001) Anisotropic Thin-Walled Beams with Closed Cross-Sectional Contours. *AIAA Journal*, 39(12), 2389–2393.
- Johnson, S. J., van Dame, C. P. & Berg, D. E. (2008) *Active load control techniques for wind turbines*. SANDIA, Report number: SAND2008-4809.
- Jung, S. N., Nagaraj, V. T. & Chopra, I. (2002) Refined structural model for thin and thick-walled composite rotor blades. *AIAA J*, 40(1), 105–116.
- Jung, S. N. & Park, I. J. (2005a) Structural behaviour of thin- and thick-walled composite blades with multicell sections. *AIAA J*, 43(3), 572–581.
- Jung, S. N. & Park,I. J. (2005b) A simple mixed-based approach for thin-walled composite blades with two-cell sections. *J Mech Sci Technol* , 19, 2016-2024.
- Jung, S. N., Park, I. J. & Shin, E. S. (2007) Theory of thin-walled composite beams with single and double-cell sections. *Composites Part B: Engineering*, 38**,** 182-192.
- Karaolis, N. M., Mussgrove, P. J. & Jeronimidis, G. (1988) Active and passive aero-elastic power control using asymmetric fibre reinforced

laminates for wind turbine blades. In: *Proceedings of the 10th British Wind Energy Conference, London, 1988.*

- Karaolis, N. M., Jeronimidis, G. & Mussgrove, P. J. (1989) Composite wind turbine blades: coupling effects and rotor aerodynamic performance. In: *Proceedings of EWEC'89, European Wind Energy Conference, Glasgow, Scotland, 1989*.
- Kim, S. B. & Kim, M. Y. (2000) Improved formulation for spatial stability and free vibration of thin-walled tapered beams and space frames. *Eng Struct*, 22, 446-458.
- Kelley, N. D. (1993) Full-Vector (3-D) Inflow Simulation in Natural and Wind Farm Environments Using an Expanded Version of the SNLWIND (Veers) Turbulence Code. In: *Proceedings of the 12th ASME Wind Energy Symposium, Houston, 1993*.
- Kim, C. & White, S. R. (1996) Analysis of thick hollow composite beams under general loadings. *Compos Struct*, 34, 263-277.
- Kim, C. & White, S. R. (1997) Thick-walled composite beam theory including 3-d elastic effects and torsional warping. *International Journal of Solids and Structures,* 34(31–32), 4237-4259.
- Kim, N. I., KU, S. D. & Kim, M. Y. (2006) Exact solutions for thin-walled open-section composite beams with arbitrary lamination subjected to torsional moment. *Thin-Walled Structures,* 44**,** 638-654.
- Kim, N. I. & Shin, D. K. (2009)Torsional analysis of thin-walled composite beams with single- and double-celled sections. *Engineering Structures*, 31(7), 1509-1521.
- Klimas, P. C. (1984) *Tailored Airfoils for Vertical Axis Wind Turbines*. SAND84-1062, Sandia National Laboratories, Albuquerque, NM.
- Kooijman, H. J. T. (1996) *Bending-Torsion Coupling of a Wind Turbine Rotor Blade*, ECN-I 96- 060, Netherlands Energy Research Foundation ECN.
- Larsen, T., Madson, H. & Thomson, K. (2005) Active load reduction using individual pitch, based on local blade flow measurements. *Wind Energy*, 8, 67–80.

- Lee, J., Kim, S. E. & Hong, K. (2002) Lateral buckling of I-section composite beams. *Eng Struct*, 24, 955-964
- Lee, J. & Lee, S. H. (2004) Flexural–torsional behaviour of thin-walled composite beams. *Thin-Walled Structures*, 42(9), 1293-1305.
- Lee, J. (2005) Flexural analysis of thin-walled composite beams using shear-deformable beam theory. *Composite Structures*, 70, 212-222.
- Lee, J. (2006) Lateral buckling analysis of thin-walled laminated composite beams with monosymmetric sections. *Eng Struct*, 28, 1997-2009.
- Librescu, L. & Song, O. (1991) Behavior of Thin-Walled Beams Made of Advanced Composite Materials and Incorporating Non-Classical Effects. *Applied Mechanics Reviews*, 44(11), 174-180.
- Librescu, L. & Song, O. (1992) On the Static Aeroelastic Tailoring of Composite AircraftSwept Wings Modelled as Thin-Walled Beam Structures. *Composites Engineering*, 2, 497–512.
- Librescu, L., Song, O. and Rogers, C. A. (1993) Adaptive Vibrational Behavior of Cantilevered Structures Modeled as Composite Thin-Walled Beams. *International Journal of Engineering*, 31(5), 775-792.
- Librescu, L., Meirovitch, L. & Song, O. (1996) Refined Structural Modeling for Enhancing Vibrations and Aeroelastic Characteristics of Composite Aircraft Wings. *La RechercheAe´rospatiale*, 1, 23–35.
- Librescu, L., Meirovitch, L. & Song, O. (1996b) Integrated Structural Tailoring and Control Using Adaptive Materials for Advanced Aircraft Wings. *Journal of Aircraft*, 33(1), 203–213.
- Librescu, L., Meirovitch, L. & Na, S. S. (1997) Control of Cantilever Vibration via Structural Tailoring and Adaptive Materials. *AIAA Journal*, 35(8), 1309–1315.
- Librescu, L. and Na, S. S. (1998a) Dynamic Response Control of Thin-Walled Beams to Blast Pulses Using Structural Tailoring and Piezoelectric Actuation. *Journal of Applied Mechanics*. 65(2), 497-504.

- Librescu, L. & Na, S. S. (1998b) Dynamic Response of Cantilevered Thin-Walled Beams to Blast and Sonic-Boom Loadings. *Shock and Vibration*, 5, 23–33.
- Librescu, L. & Na, S. S. (1998c) Bending Vibration Control of Cantilevers via Boundary Moment and Combined Feedback Control Law. *Journal of Vibration and Controls*, 4(6), 733–746.
- Librescu, L. and Na, S. S. (1998d) Boundary Control of Free and Forced Oscillation of Shearable Thin-Walled Beam Cantilevers. *European Journal of Mechanics/A Solids*, 17(4), 687–700.
- Librescu, L., Na, S. S. & Park, S. (2000) Dynamics and Active Feedback Control of Wing-Type Structures Modelled as Thin-Walled Beams: Implication of Beam Cross-Section Non uniformity. *Journal of the Chinese Society of Mechanical Engineers*, 21(1), 87–96.
- Librescu, L. and Na, S. S. (2001) Active Vibration Control of Thin-Walled Tapered Beams Using Piezoelectric Strain Actuation. *Journal of Thin-Walled Structures*, 39(1), 65–82.
- Librescu, L., Qin, Z. & Ambur, D. R. (2003) Implications of Warping Restraint on Statics and Dynamics of Elastically Tailored Thin-Walled Composite Beams. *International Journal of Mechanical Sciences*, 45(8), 1247–1267.
- Librescu L. & Song O. (2006) Thin-walled composite beams theory and application. Berlin, springer.
- Liu, Z. & Young, Y. L. (2009) Utilization of bend–twist coupling for performance enhancement of composite marine propellers. *Journal of Fluids and Structures*, 25, 1102-1116.
- Lobitz, D. W., Veers, P. S., & Migliore, P. G. (1996) Enhanced Performance of HAWTs Using adaptive Blades. In: *Proc. Wind Energy '96, ASME Wind Energy Symposium, Houston, Jan. 29 - Feb. 2, 1996*.
- Lobitz, D. W. & Veers, P. S. (1998) Aeroelastic Behaviour of Twist-Coupled HAWT Blades. In: *Proceedings of the 1998 ASME Wind Energy Symposium, Reno, January*, 12-15.

- Lobitz, D. W. & Laino, D. J. (1999) *Load mitigation with twist-coupled hawt blades.* American Institute of Aeronautics and Astronautics .Report number: AIAA-99-0033.
- Lobitz, D. W., Veers, P. S., Eisler, G. R., Laino, D. J., Migliore, P. G. & Bir, G. (2001) *The Use of Twist- Coupled Blades to Enhance the Performance of Horizontal Axis Wind Turbines*. Sandia National Laboratories, Report SAND2001-1003, May 2001.
- Lovera, M., Colaneri, P., Malpica, C. & Celi, R. (2003) Closed-loop stability analysis of HHC and IBC, with application to a hinge less rotor helicopter. In: *29th European Rotorcraft Forum*.
- Lovera, M., Colaneri, P., Malpica, C. & Celi, R. (2004) Discrete-time, closed loop aeromechanical stability analysis of helicopters with higher harmonic control. In: *60th Annual forum of the American Helicopter Society*.
- Loughlan, J. & Ata, M. (1995) The restrained torsional response of open section carbon fibre composite beams. *Composite Struct*, 32, 13–31.
- Loughlan, J. & Ata, M. (1997a) The constrained torsional characteristics of some carbon fibre composite box-beams. *Thin-Walled Struct*, 28, 233–52.
- Loughlan, J. & Ata, M. (1997b) The behaviour of open and closed section carbon fibre composite beams subjected to constrained torsion. *Comp Struct*, 38, 631–47.
- Loughlan, J. & Ata, M. (1998a) Variable twist torsion tests on carbon fibre composite beams. *Comp Struct*, 42, 307–327.
- Loughlan, J. & Ata, M. (1998b) The analysis of carbon fibre composite box beams subjected to torsion with variable twist. *Comput Meth Appl Mech Eng*, 152, 373–391.
- Maddur, S. S. & Chaturvedi, S. K. (1999) Laminated composite open profile sections: first order shear deformation theory. *Comp Struct*, 45,105–114.

- Maddur, S. S. & Chaturvedi, S. K. (2000) Laminated composite open profile sections: non-uniform torsion of I-sections. *Comp Struct*, 50, 159–69.
- Maheri, A., Noroozi, S., Toomer, C. & Vinney, J. (2006a) Single step versus coupled aero-structure simulation of a wind turbine with bend-twist adaptive blades. In: *European Wind Energy Conference EWEC 2006, 27 February-2 March 2006, Athens, Greece*.
- Maheri, A., Noroozi, S., Toomer, C. & Vinney, J. (2006b) A Simple algorithm to modify an ordinary wind turbine blade to an adaptive one. In: *European Wind Energy Conference EWEC 2006, 27 February-2 March 2006, Athens, Greece*.
- Maheri, A., Noroozi, S., Toomer, C. & Vinney J. (2006c) WTAB, a Computer Program for Predicting the Performance of Horizontal Axis Wind Turbines with Adaptive Blades. *Renewable Energy*, 31(11), 1673-1685.
- Maheri, A., Noroozi, S., Toomer, C. & Vinney, J. (2006d) Damping the fluctuating behaviour and improving the convergence rate of the axial induction factor in the BEMT-based rotor aerodynamic codes. In: *European Wind Energy Conference EWEC 2006, 27 February-2 March 2006, Athens, Greece*.
- Maheri, A. (2006e) Aero-structure simulation and aerodynamic design of wind turbines utilising adaptive blades. University of West England-Bristol, PhD Thesis.
- Maheri, A., Noroozi, S. & Vinney, J. (2007a) Decoupled design of wind turbine adaptive blades. *Renewable Energy*, 32(10), 1753-1767.
- Maheri, A., Noroozi, S., Toomer, C. & Vinney, J. (2007b) Efficient meshing of a wind turbine blade using force adaptive mesh sizing functions. *Renewable Energy*, 32 (1), 95-104.
- Maheri, A., Noroozi, S. & Vinney, J. (2007c) Combined Analytical/FEA-based Coupled-Aero-Structure Simulation of Wind Turbines with Bend-Twist Adaptive Blades", *Renewable Energy*, 32(6), 916-930.

- Maheri, A., Noroozi, S. & Vinney, J. (2007d) Application of combined analytical/FEA coupled-aero-structure simulation in design of wind turbine adaptive blades. *Renewable Energy*, 32(12), 2011-2018.
- Maheri, A. & Isikveren, A. T. (2008) Variable-state design parameters in design of aero-structures made of intrinsically smart materials. In: de Wilde, W. P., Brebbia, C. A., Press, V. (eds.)*: High Performance Structures and Materials IV*. pp. 421-430.
- Maheri, A. & Isikveren, A. T. (2009) Design of wind turbine passive smart blades. In: *European Wind Energy Conference EWEC 2009, Marseille, France*.
- Maheri, A. & Isikveren, A. T. (2010) Performance prediction of wind turbines utilising passive smart blades: approaches and evaluation. *Wind Energy*, 3, 255-265.
- Maheri, A. (2012) A Finite Element Suite for Deformation Analysis of Composite Aeroelastic Structures Subjected to Operational Aerodynamic Loading. *Journal of Mechanical Science*, 226(8), 2062-2076.
- Mayda, E. A., van Dam, C. P., & Nakafuji, D. Y. (2005) Computational investigation of finite width microtabs for aerodynamic load control. *AIAA-2005-1185. In: Proceedings of the 43th AIAA/ASME, Reno, NV*.
- Migliore, P. G., Quandt, G. A., et al. (1995) *Wind turbine trailing edge aerodynamic brakes*. National Renewable Energy Laboratory. Report number: NREL/TP-441-7805.
- Milborrow, D. (ed.) (1998) *Wind power Monthly*. February Windtech Notes, 42-43.
- Nicholls-Lee, R. & Turnock, S. (2007) Enhancing performance of a horizontal axis tidal turbine using adaptive blades. In: *Oceans '07. Aberdeen, Scotland: IEEE; 2007.*
- Nicholls-Lee, R., Turnock, S. & Boyd, S. (2008) Performance prediction of a free stream tidal turbine with composite bend-twist coupled blades. In: *2nd international conference on ocean energy (ICOE 2008); 2008. Brest, France.*

- Nicholls-Lee, R. F., Turnock, S. R. & Boyd, S. W. (2013) Application of bend-twist coupled blades for horizontal axis tidal turbines. *Renewable Energy*, 50, 541-550.
- Nijssen, R. P. L. (2006) *Fatigue life prediction and strength degradation of wind turbine rotor blade composites*. Knowledge Centre Wind Turbine Materials and Constructions (KC-WMC), Netherland. Report number: ISBN-10: 90-9021221-3.
- Oh, S. Y. & Song, O. & Librescu, L. (2003) Effects of pretwist and presetting on coupled bending vibrations of rotating thin-walled composite beams. *International Journal of Solids and Structures*, 40,1203-1224.
- Panda, B. & Chopra, I. (1987) Dynamics of Composite Rotor Blades in Forward Flight. *Vertica*, 11, 1-2.
- Pasupulati, S. V., Wallace, J. & Dawson, M. (2005) *Variable Length Blades Wind Turbine.* Energy Unlimited Inc.
- Patil, M. J. & Johnson, E. R. (2005) Cross-sectional Analysis of Anisotropic, Thin-Walled, Closed-Section Beams with Embedded Strain Actuation. *AIAA*, 2005-2037
- Piovan, M. T. & Cortínez, V. H. (2007) Mechanics of shear deformable thin-walled beams made of composite materials. *Thin-Walled Structures*, 45, 37-62.
- Qin, Z. & Librescu, L. (2002) On a shear-deformable theory of anisotropic thin-walled beams: Further contribution and validation. *Journal of Composite Structures, 5*6, 345-358.
- Rand, O. (1998) Fundamental closed-form solutions for solid and thin-walled composite beams including a complete out-of-plane warping model. *Int J Solids Struct*, 35, 2775-2793.
- Rehfield, L. W., Atilgan, A. R. & Hodges, D. H. (1990) Nonclassical behaviour of thin-walled composite beams with closed cross-sections. J. *American Helicopter Society*, 35, 42-50.
- Salim, H. A. & Davalos, J. F. (2005) Torsion of open and closed thin-walled laminated composite sections. *J Compos Mater*, 39, 497-524.

- Sanderse, B., van der Pijl, S. P. & Koren, B. (2011) Review of computational fluid dynamics for wind turbine wake aerodynamics. *Wind Energy, 14, 799-819.*
- Shadmehri, F., Haddadpour, H. & Kouchakzadeh, M. A. (2007) Flexural–torsional behaviour of thin-walled composite beams with closed cross-section. *Thin-Walled Structures*, 45(7–8), 699-705.
- Shrama, R. N. & Madawala, U. (2007) The concepts of a smart wind turbine system. In*: Proceeding* of *16th Australian Fluid Mechanics Conference, ustralia*.
- Sim, S. K. (2006) Simulation of Wind Turbines Using Anisotropic Composite Blades by CFX / ANSYS. In: *2006 UK ANSYS Conference, The Belfry, Warwickshire, UK, 4-5 October 2006.*
- Smith, E. C. & Chopra, I. (1991) Formulation and evaluation of an analytical model for composite box-beams. *J Am Helicopter Soc*, 36(3), 23–35.
- Song, O., Librescu, L. & Jeong, N. H. (2001) Static response of thin-walled composite I-beams loaded at their free-end cross section: analytical solution. *Comp Struct*, 52, 55–65.
- Song, O. (1990) Modelling and response analysis of thin-walled beam structures constructed of advanced composite materials. PhD Thesis. Virginia Polytechnic Institute and State University, 1990.
- Song, O. and Librescu, L. (1993) Free Vibration of Anisotropic Composite Thin-Walled Beams of Closed Cross-Section Contour. *Journal of Sound and Vibration*, 16791, 129–147.
- Song, O. & Librescu, L. (1997) Structural modelling and free vibration analysis of rotating composite thin-walled beams. *J Am Helicopter Soc*, 42(4), 358–369.
- Song, O., Kim, J. B. & Librescu, L. (2001) Synergistic Implications of Tailoring and Adaptive Materials Technology on Vibration Control of Anisotropic Thin-Walled Beams. *International Journal of Engineering Science*, 39(1), 71–94.

- Snel, H. (1998) Review of the present status of rotor aerodynamics, *Wind Energy, 1, 46–69.*
- Snel, H. (2003) Review of aerodynamics for wind turbines, *Wind Energy, 6, 203–211*.
- Stemple, A. D. & Lee, S. W.(1988) Finite element model for composite beams with arbitrary cross-sectional warping. *AIAA J,* 26, 1512–20.
- Stoddard, F., Nelson, V., Starcher, K. & Andrews, B. (1989) *Determination of Elastic Twist in Horizontal Axis Wind Turbines (HAWTs)*. Alternative Energy Institute, West Texas State University, SERI Contract RL-6-06013, NREL, Golden, CO.
- Stuart, J. G., Wright, A. D. & Butterfield, C. P. (1996) Considerations for an integrated wind turbine controls capability at the national wind technology centre: an aileron control case study for power regulation and load mitigation. National Renewable Energy Laboratory, Technical Report NREL/TP-440-21335.
- Stuart, J. G., Wright, A. D., et al. (1997) Wind turbine control systems: dynamic model development using system identification and the fast structural dynamics code. In*: Proceedings 35th AIAA/ASME*.
- Stuart, J. G., Wright, A. D. & Butterfield, C. P. (1996) Considerations for an integrated wind turbine controls capability at the national wind technology centre: an aileron control case study for power regulation and load mitigation. National Renewable Energy Laboratory. Report number: NREL/TP-440-21335.
- Swanson, S. R. (1998) Torsion of Laminated Rectangular Rods. *Composite Structures, 42, 23-31*.
- Tangler, J. (1987) A Horizontal Axis Wind Turbine Performance Prediction Code for personal computers. Solar Energy Research Institute, Golden, CO.
- Tangler, J. & Somers, D. (1995) NREL Aerofoil Families for HAWTs. Proceedings of Windpower, Washington D. C.

- Toutanji, H. & Dempsey, S. (2001), Stress modelling of pipelines strengthened with advanced composites materials. *Thin-Walled Structures,* 39**,** 153-165.
- Troldborg, N. (2005) Computational study of the risø-b1-18 aerofoil with a hinged flap providing variable trailing edge geometry. *Wind Engineering*, 29(2), 89-113.
- Tsai, S. & Ong, C. H. (1998) *D-Spar Blade Design and Manufacture. unpublished contractor reports*. Sandia National Laboratories contract BB-6066 Stanford University.
- van Engelen, T. (2006) Design Model and Load Reduction Assessment for Multi-rotational Mode Individual Pitch Control (Higher Harmonics Control). In: *European Wind Energy Conference. Athens, Greece.*
- Veers, P., Bir, G. & Lobitz, D. (1998) Aeroelastic tailoring in wind turbine blade applications. In: *Windpower '98, American wind energy association meeting and exhibition. Bakersfield, California, USA: Sandia National Laboratories; 1998.*
- Vasilier, V. V. (1993) *Mechanics of Composite Structures*. Taylor and Francis Washington, DC.
- Vlasov, V. Z. (1961) *Thin walled elastic beams*. 2nd ed. Jerusalem, Israel Program for Scientific Transactions.
- Volovoi, V. V. & Hodges, D. H. (2000) Theory of anisotropic thin-walled beams. *Trans ASME: J Appl Mech*, 67, 453–9.
- Volovoi, V. V. & Hodges, D. H. (2002) Single- and multi-celled composite thinwalled beams. *AIAA J,* 40(5), 960–965.
- Vo, T. P. & Lee, J. (2007) Flexural-torsional behaviour of thin-walled closed-section composite box beams. *Eng Struct*, 29, 1774-1782.
- Vo, T. P. & Lee, J. (2008) Flexural–torsional behaviour of thin-walled composite box beams using shear-deformable beam theory. *Engineering Structures,* 30(7), 1958-1968.
- Vo, T. P. & Lee, J. (2009a) Flexural–torsional behaviour of thin-walled composite space frames. *International Journal of Mechanical Sciences,* 51, 837-845.

- Vo, T. P. & Lee, J. (2009b) Geometrically nonlinear analysis of thin-walled composite box beams. *Computers and Structures*, 87, 236-245.
- Vo, T. P. & Lee, J. (2010a) Geometrically nonlinear analysis of thin-walled open-section composite beams. *Computers and Structures*, 88, 347-356.
- Vo, T. P. & Lee, J. (2010b) Geometrically nonlinear theory of thin-walled composite box beams using shear-deformable beam theory. *International Journal of Mechanical Sciences*, 52, 65-74.
- Vo, T. P. & Thai H. T. (2011) Geometrical nonlinear analysis of thin-walled composite beams using finite element method based on first order shear deformation theory. *Arch Appl Mech*, 81, 419-435.
- Vo, T. P. & Thai, H. T. (2012) Static behaviour of composite beams using various refined shear deformation theories. *Composite Structures*, 94, 2513-2522.
- Wu, X. X. & Sun, C. T. (1992) Simplified theory for composite thin-walled beams. *AIAA J*, 30(12), 2945–2951.
- Wu, Y., Zhu, Y., Lai, Y., Zhang, X. & Liu, S. (2002) Analysis of thin-walled composite box beam under torsional load without external restraint. *Thin-Walled Structure*, 40, 385-397.
- Yu, W., Hodges, D. H., Volovoi, V. V. & Cesnik, C. E. S. (2002) On Timoshenko-like modelling of initially curved and twisted composite beams. *International Journal of Solids and Structures*. 39 (19), 5101–5121.
- Yu, W., Volovoi, V. V., Hodges, D. H., & Hong, X. (2002) Validation of the variational asymptotic beam sectional analysis. *AIAA Journal*, 40, 2105-2112
- Yu, W., Hodges, D. H., Volovoi, V. V., & Fuchs, E. D (2005) A generalized Vlasov theory of composite beams. *Thin-Walled Structures*, 43, 1493-1511.

Appendix A

Stiffness constant of an orthotropic material:

$$C_{12} = (\nu_{12} + \nu_{32}\nu_{13})/(E_2E_3\Delta) \quad \text{(A.1)}$$

$$C_{13} = (\nu_{13} + \nu_{12}\nu_{23})/(E_1E_2\Delta) \quad \text{(A.2)}$$

$$C_{22} = (1 - \nu_{13}\nu_{31})/(E_1E_3\Delta) \quad \text{(A.3)}$$

$$C_{23} = (\nu_{23} + \nu_{21}\nu_{13})/(E_1E_2\Delta) \quad \text{(A.4)}$$

$$C_{33} = (1 - \nu_{12}\nu_{21})/(E_1E_2\Delta) \quad \text{(A.5)}$$

$$C_{44} = G_{23} \quad \text{(A.6)}$$

$$C_{55} = G_{13} \quad \text{(A.7)}$$

$$C_{66} = G_{12} \quad \text{(A.8)}$$

$$\Delta = (1 - \nu_{12}\nu_{21} - \nu_{23}\nu_{32} - \nu_{31}\nu_{13} - 2\nu_{21}\nu_{32}\nu_{13})/(E_1E_2E_3) \quad \text{(A.9)}$$

Stiffness constant of an orthotropic material (see Figure A1 for angle θ):

$$\overline{C}_{11} = C_{11}\cos^4\theta + C_{22}sin^4\theta + 2(C_{12} + 2C_{66})sin^2\theta\cos^2\theta \quad \text{(A.10)}$$

$$\overline{C}_{12} = (C_{11} + C_{22} - 4C_{66})sin^2\theta\cos^2\theta + C_{12}(\sin^4\theta + cos^4\theta) \quad \text{(A.11)}$$

$$\overline{C}_{13} = C_{13}\cos^2\theta + C_{23}\sin^2\theta \quad \text{(A.12)}$$

$$\overline{C}_{14} = 0 \quad \text{(A.13)}$$

$$C'_{15} = 0 \quad \text{(A.14)}$$

$$\overline{C}_{16} = (C_{11} - C_{12} - 2C_{66})sin\theta\cos^3\theta + (C_{12} - C_{22} + 2C_{66})\sin^3\theta\, cos\theta \quad \text{(A.15)}$$

$$\overline{C}_{22} = C_{11}\sin^4\theta + 2(C_{12} + 2C_{66})sin^2\theta\cos^2\theta + C_{22}cos^4\theta) \quad \text{(A.16)}$$

$$\overline{C}_{23} = C_{13}\sin^2\theta + C_{23}cos^2\theta) \quad \text{(A.17)}$$

$$\overline{C}_{24} = 0 \quad \text{(A.18)}$$

$$\overline{C}_{25} = 0 \quad \text{(A.19)}$$

$$\overline{C}_{26} = (C_{11} - C_{12} - 2C_{66})sin^3\theta\cos\theta + (C_{12} - C_{22} + 2C_{66})\sin\theta\, cos^3\theta \quad \text{(A.20)}$$

$$\overline{C}_{33} = C_{33} \quad \overline{C}_{34} = 0 \quad \overline{C}_{35} = 0 \quad \text{(A.21)}$$

$$\overline{C}_{36} = (C_{13} - C_{23})sin\theta\cos\theta \quad \text{(A.22)}$$

$$\overline{C}_{44} = C_{44}\cos^2\theta + C_{55}sin^2\theta \quad \text{(A.23)}$$

$$\overline{C}_{45} = (C_{55} - C_{44})sin\theta\cos\theta \quad \text{(A.24)}$$

$$\overline{C}_{46} = 0 \quad \text{(A.25)}$$

$$\overline{C}_{55} = C_{44}sin^2\theta + C_{55}\cos^2\theta \quad \text{(A.26)}$$

$$\overline{C}_{56} = 0 \quad \text{(A.27)}$$

$$\overline{C}_{66} = [C_{11} + C_{22} - 2(C_{12} + C_{66})]sin^2\theta\cos^2\theta + C_{66}(\sin^4\theta + c\cos^4\theta) \quad \text{(A.28)}$$

Reduced stiffness constants of an orthotropic material:

$$\tilde{C}_{11} = \overline{C}_{22} + (\overline{C}_{23}^2\overline{C}_{11} + \overline{C}_{12}^2\overline{C}_{33} - 2\overline{C}_{13}\overline{C}_{12}\overline{C}_{23})/(\overline{C}_{13}^2 - \overline{C}_{33}\overline{C}_{11}) \quad \text{(A.29)}$$

$$\tilde{C}_{12} = \overline{C}_{26} + (-\overline{C}_{12}\overline{C}_{13}\overline{C}_{36} + \overline{C}_{12}\overline{C}_{16}\overline{C}_{33} - \overline{C}_{16}\overline{C}_{23}\overline{C}_{13} + \overline{C}_{11}\overline{C}_{36}\overline{C} \quad \text{(A.30)}$$

$$\tilde{C}_{21} = \tilde{C}_{12} \quad \text{(A.31)}$$

$$\tilde{C}_{22} = \overline{C}_{66} + (-\overline{C}_{16}\overline{C}_{13}\overline{C}_{36} + \overline{C}_{16}^2\overline{C}_{33} + \overline{C}_{36}^2\overline{C}_{11} - \overline{C}_{36}\overline{C}_{16}\overline{C}_{13})/(\overline{C}_{13}^2 - \overline{C}_{33}\overline{C}_{11}) \quad \text{(A.32)}$$

$$\tilde{C}_{33} = \overline{C}_{44} - \overline{C}_{45}^2/\overline{C}_{55} \quad \text{(A.33)}$$

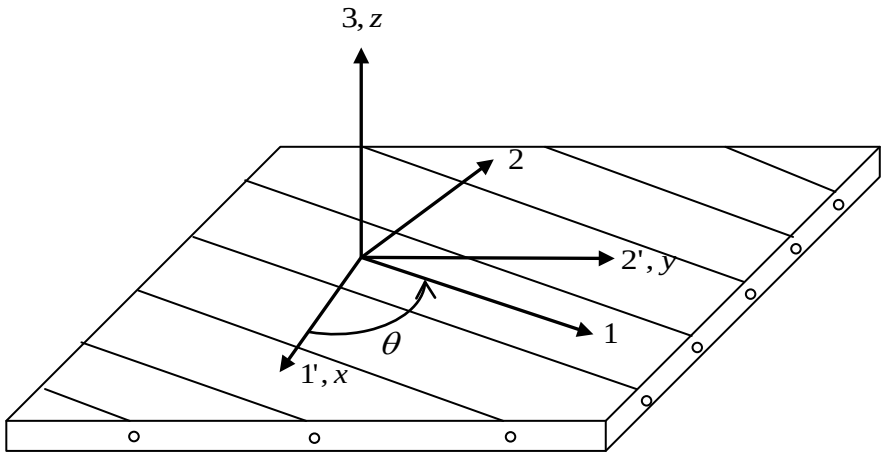

Figure A1-The principal directions (1, 2, 3) of a laminate layer, and the reference system $(1', 2', 3)$ or (x, y, z) of the laminate

Appendix B

Entries of $[K]$ matrix in force-deformation Equation (2.47):

$$K_{11} = \sum_{j=1}^{N} \left(\sum_{i=1}^{M} \iint \tilde{C}_{11}^{i} dnds \right) \tag{B.1}$$

$$K_{12} = \sum_{j=1}^{N} \left(\sum_{i=1}^{M} \iint \tilde{C}_{11}^{i} (x + n\frac{dy}{ds}) dnds \right) \tag{B.2}$$

$$K_{13} = \sum_{j=1}^{N} \left(\sum_{i=1}^{M} \iint \tilde{C}_{11}^{i} (y - n\frac{dx}{ds}) dnds \right) \tag{B.3}$$

$$K_{14} = \sum_{j=1}^{N} \left(\sum_{i=1}^{M} \iint \tilde{C}_{12}^{i} \frac{dx}{ds} dnds \right) \tag{B.4}$$

$$K_{15} = \sum_{j=1}^{N} \left(\sum_{i=1}^{M} \iint \tilde{C}_{12}^{i} \frac{dy}{ds} dnds \right) \tag{B.5}$$

$$K_{16} = \sum_{j=1}^{N} \left(\sum_{i=1}^{M} \iint \tilde{C}_{12}^{i} (\frac{2\Omega + 2n\beta_p}{h(s)G_{sz}(s)L}) dnds \right) \tag{B.6}$$

$$K_{16} = \sum_{j=1}^{N} \left(\sum_{i=1}^{M} \iint \tilde{C}_{12}^{i} \frac{\lambda^{i,j}}{(h(s)G_{sz}(s))_{i,j}} dnds \right) \text{(mutiple cell beam)} \tag{B.7}$$

$$K_{21} = \sum_{j=1}^{N} \left(\sum_{i=1}^{M} \iint \tilde{C}_{12}^{i} \frac{dx}{ds} dnds \right) \tag{B.8}$$

$$K_{22} = \sum_{j=1}^{N} \left(\sum_{i=1}^{M} \iint \tilde{C}_{12}^{i} (x + n\frac{dy}{ds}) \frac{dx}{ds} dnds \right) \tag{B.9}$$

$$K_{23} = \sum_{j=1}^{N} \left(\sum_{i=1}^{M} \iint \tilde{C}_{12}^{i} (y - n\frac{dx}{ds}) \frac{dx}{ds} dnds \right) \tag{B.10}$$

$$K_{24} = \sum_{j=1}^{N} \left(\sum_{i=1}^{M} \iint (\tilde{C}_{22}^{i} (\frac{dx}{ds})^2 + \tilde{C}_{33}^{i} (\frac{dy}{ds})^2) dnds \right) \tag{B.11}$$

$$K_{25} = \sum_{j=1}^{N} \left(\sum_{i=1}^{M} \iint (\tilde{C}_{22}^{i} \frac{dx}{ds}\frac{dy}{ds} - \tilde{C}_{33}^{i} \frac{dx}{ds}\frac{dy}{ds}) dnds \right) \tag{B.12}$$

$$K_{26} = \sum_{j=1}^{N} \left(\sum_{i=1}^{M} \iint \tilde{C}_{22}^{i} (\frac{2\Omega + 2n\beta_p}{h(s)G_{sz}(s)L}) \frac{dx}{ds} dnds \right) \tag{B.13}$$

$$K_{26} = \sum_{j=1}^{N} \left(\sum_{i=1}^{M} \iint \tilde{C}_{22}^{i} \frac{\lambda^{i,j}}{(h(s)G_{sz}(s))_{i,j}} \frac{dx}{ds} dnds \right) \text{(mutiple cell beam)} \tag{B.14}$$

$$K_{31}=\sum_{j=1}^{N}(\sum_{i=1}^{M}\iint \tilde{C}_{12}^{i}\frac{dy}{ds}dnds) \tag{B.15}$$

$$K_{32}=\sum_{j=1}^{N}(\sum_{i=1}^{M}\iint \tilde{C}_{12}^{i}(x+n\frac{dy}{ds})\frac{dy}{ds}dnds) \tag{B.16}$$

$$K_{33}=\sum_{j=1}^{N}(\sum_{i=1}^{M}\iint \tilde{C}_{12}^{i}(y-n\frac{dx}{ds})\frac{dy}{ds}dnds) \tag{B.17}$$

$$K_{34}=\sum_{j=1}^{N}(\sum_{i=1}^{M}\iint (\tilde{C}_{22}^{i}(\frac{dy}{ds}\frac{dx}{ds})-\tilde{C}^{i}{}_{33}(\frac{dy}{ds}\frac{dx}{ds}))dnds) \tag{B.18}$$

$$K_{35}=\sum_{j=1}^{N}(\sum_{i=1}^{M}\iint (\tilde{C}_{22}^{i}(\frac{dy}{ds})^{2}+\tilde{C}^{i}{}_{33}(\frac{dx}{ds})^{2})dnds) \tag{B.19}$$

$$K_{36}=\sum_{j=1}^{N}(\sum_{i=1}^{M}\iint \tilde{C}_{22}^{i}(\frac{2\Omega+2n\beta_{p}}{h(s)G_{sz}(s)L})\frac{dy}{ds}dnds) \tag{B.20}$$

$$K_{36}=\sum_{j=1}^{N}(\sum_{i=1}^{M}\iint \tilde{C}_{22}^{i}\frac{\lambda^{i,j}}{(h(s)G_{sz}(s))_{i,j}}\frac{dy}{ds}dnds)\ \text{(mutiple cell beam)} \tag{B.21}$$

$$K_{41}=\sum_{j=1}^{N}(\sum_{i=1}^{M}\iint \tilde{C}_{12}^{i}[\frac{dy}{ds}(x+n\frac{dy}{ds})-\frac{dx}{ds}(y-n\frac{dx}{ds})]dnds) \tag{B.22}$$

$$K_{42}=\sum_{j=1}^{N}(\sum_{i=1}^{M}\iint \tilde{C}_{12}^{i}[\frac{dy}{ds}(x+n\frac{dy}{ds})^{2}-\frac{dx}{ds}(x+n\frac{dy}{ds})(y-n\frac{dx}{ds})]dnds) \tag{B.23}$$

$$K_{43}=\sum_{j=1}^{N}(\sum_{i=1}^{M}\iint \tilde{C}_{12}^{i}[\frac{dy}{ds}(x+n\frac{dy}{ds})(y-n\frac{dx}{ds})-\frac{dx}{ds}(y-n\frac{dx}{ds})^{2}]dnds) \tag{B.24}$$

$$K_{44}=\sum_{j=1}^{N}\sum_{i=1}^{M}\iint [\tilde{C}_{22}^{i}(\frac{dx}{ds}\frac{dy}{ds}(x+n\frac{dy}{ds})-(\frac{dx}{ds})^{2}(y-n\frac{dx}{ds}))-\tilde{C}^{i}{}_{33}(\frac{dx}{ds}\frac{dy}{ds}(x+n\frac{dy}{ds})-(\frac{dy}{ds})^{2}(y-n\frac{dx}{ds}))]dnds \tag{B.25}$$

$$K_{45}=\sum_{j=1}^{N}(\sum_{i=1}^{M}\iint [\tilde{C}_{22}^{i}(\frac{dy}{ds}\frac{dy}{ds}(x+n\frac{dy}{ds})-\frac{dx}{ds}\frac{dy}{ds}(y-n\frac{dx}{ds}))+\tilde{C}^{i}{}_{33}(\frac{dx}{ds}\frac{dx}{ds}(x+n\frac{dy}{ds})+\frac{dx}{ds}\frac{dy}{ds}(y-n\frac{dx}{ds}))]dnds) \tag{B.26}$$

$$K_{46}=\sum_{j=1}^{N}(\sum_{i=1}^{M}\iint \tilde{C}_{22}^{i}(\frac{2\Omega+2n\beta_{p}}{h(s)G_{sz}(s)L})(\frac{dy}{ds}(x+n\frac{dy}{ds})-\frac{dx}{ds}(y-n\frac{dx}{ds}))dnds) \tag{B.27}$$

$$K_{46}=\sum_{j=1}^{N}(\sum_{i=1}^{M}\iint \tilde{C}_{22}^{i}\frac{\lambda^{i,j}}{(h(s)G_{sz}(s))_{i,j}}(\frac{dy}{ds}(x+n\frac{dy}{ds})-\frac{dx}{ds}(y-n\frac{dx}{ds}))dnds)\ \text{(mutiple cell beam)} \tag{B.28}$$

$$K_{51}=\sum_{j=1}^{N}(\sum_{i=1}^{M}\iint\widetilde{C}_{11}^{i}(y-n\frac{dx}{ds})dnds) \tag{B.29}$$

$$K_{52}=\sum_{j=1}^{N}(\sum_{i=1}^{M}\iint\widetilde{C}_{11}^{i}(x+n\frac{dy}{ds})(y-n\frac{dx}{ds})dnds) \tag{B.30}$$

$$K_{53}=\sum_{j=1}^{N}(\sum_{i=1}^{M}\iint\widetilde{C}_{11}^{i}(y-n\frac{dx}{ds})^{2}dnds) \tag{B.31}$$

$$K_{54}=\sum_{j=1}^{N}(\sum_{i=1}^{M}\iint\widetilde{C}_{12}^{i}\frac{dx}{ds}(y-n\frac{dx}{ds})dnds) \tag{B.32}$$

$$K_{55}=\sum_{j=1}^{N}(\sum_{i=1}^{M}\iint\widetilde{C}_{12}^{i}\frac{dy}{ds}(y-n\frac{dx}{ds})dnds) \tag{B.33}$$

$$K_{56}=\sum_{j=1}^{N}(\sum_{i=1}^{M}\iint\widetilde{C}_{12}^{i}(\frac{2\Omega+2n\beta_{p}}{h(s)G_{sz}(s)L})(y-n\frac{dx}{ds})dnds) \tag{B.34}$$

$$K_{56}=\sum_{j=1}^{N}(\sum_{i=1}^{M}\iint\widetilde{C}_{12}^{i}\frac{\lambda^{i,j}}{(h(s)G_{sz}(s))_{i,j}}(y-n\frac{dx}{ds})dnds)\ (\text{mutiple cell beam}) \tag{B.35}$$

$$K_{61}=\sum_{j=1}^{N}(\sum_{i=1}^{M}-\iint\widetilde{C}_{11}^{i}(x+n\frac{dy}{ds})dnds) \tag{B.36}$$

$$K_{62}=\sum_{j=1}^{N}(\sum_{i=1}^{M}-\iint\widetilde{C}_{11}^{i}(x+n\frac{dy}{ds})^{2}dnds) \tag{B.37}$$

$$K_{63}=\sum_{j=1}^{N}(\sum_{i=1}^{M}-\iint\widetilde{C}_{11}^{i}(y-n\frac{dx}{ds})(x+n\frac{dy}{ds})dnds) \tag{B.38}$$

$$K_{64}=\sum_{j=1}^{N}(\sum_{i=1}^{M}-\iint\widetilde{C}_{12}^{i}\frac{dx}{ds}(x+n\frac{dy}{ds})dnds) \tag{B.39}$$

$$K_{65}=\sum_{j=1}^{N}(\sum_{i=1}^{M}-\iint\widetilde{C}_{12}^{i}\frac{dy}{ds}(x+n\frac{dy}{ds})dnds) \tag{B.40}$$

$$K_{66}=\sum_{j=1}^{N}(\sum_{i=1}^{M}-\iint\widetilde{C}_{12}^{i}(\frac{2\Omega+2n\beta_{p}}{h(s)G_{sz}(s)L})(x+n\frac{dy}{ds})dnds) \tag{B.41}$$

$$K_{66}=\sum_{j=1}^{N}(\sum_{i=1}^{M}-\iint\widetilde{C}_{12}^{i}\frac{\lambda^{i,j}}{(h(s)G_{sz}(s))_{i,j}}(x+n\frac{dy}{ds})dnds)\ (\text{mutiple cell beam}) \tag{B.42}$$

(M denotes the number of the patches on the cross-section, N denotes the number of layers in the patch)

Appendix C

Publications

1. Zhang, H., Maheri, A., Daadbin, A. & Hackney, P. (2012) An analytical model for frequency analysis of composite wind turbine adaptive blades. In: *Proceedings of the 2012 2nd International Symposium On Environment Friendly Energies And Applications. IEEE, Piscataway, pp. 415-420. ISBN 9781467329095*
2. Zhang, H., Maheri, A., Daadbin, A. & Hackney, P. (2012) Effect of laminate configuration and shell-thickness variation on the induced twist distribution in wind turbine adaptive blades. In: *Proceedings of the 2012 2nd International Symposium on Environment Friendly Energies and Applications. IEEE, Piscataway, pp. 406-411. ISBN 9781467329095*
3. Zhang, H., Maheri, A., Daadbin, A. & Hackney, P. (2012) An analytical model for deformation analysis of wind turbine adaptive blades. In: High Performance Structure and Materials VI. WIT transactions on the built environment, 124 . WIT Press, Southampton, UK, pp. 13-25. ISBN 9781845645960
4. Rahul, B., Zhang, H., Maheri, A. (2013) Effect of different bend-twist coupling topologies on induced twist and cost of wind turbine adaptive blades. In: *International Conference on Engineering of Tarumanagara (ICET 2013) Faculty of Engineering, TarumanagaraUniversity, Jakarta-Indonesia, October, 2-3, 2013*
5. Maheri, A., Zhang, H., An extended decoupled design method for elasticly tailored wind trubine blades. Submitted to *Materials & Design*
6. Zhang, H., Maheri, A., Structural analysis of wind turbine adaptive blades using a linear beam model. Submitted to *Computers & Structures*